

STRUCTURAL BASIS FOR REGULATED
INHIBITION AND SUBSTRATE SELECTION
IN YEAST GLYCOGEN SYNTHASE

Krishna Kishore Mahalingan

Submitted to the faculty of the University Graduate School
in partial fulfillment of the requirements
for the degree
Doctor of Philosophy
in the Department of Biochemistry and Molecular Biology,
Indiana University

February 2017

Accepted by the Graduate Faculty, Indiana University, in partial fulfillment of the requirements for the degree of Doctor of Philosophy.

Thomas D. Hurley, Ph.D., Chair

Jeffrey Elmendorf, Ph.D.

Doctoral committee

Millie M. Georgiadis, Ph.D.

December 8, 2016

Peter J. Roach, Ph.D.

DEDICATION

I would like to dedicate this work to my appa and amma, J. Mahalingan and Neelavathy Mahalingan, for their constant love, support and inspiration. They have dedicated their lives to me, so it is an honor to dedicate this work to them.

This work is also dedicated to my sister, Priyadharshini Mahalingan and her son/ my nephew, Shravan (“Pintu”).

Finally, to my late grandmother (ethai), Ruckiammal, for her love, inspiration and blessings.

ACKNOWLEDGEMENTS

First and foremost, I would to thank my advisor, Dr. Thomas D. Hurley for his support, guidance and scientific mentorship throughout my graduate thesis research work. I came into his lab with an engineering background and very little research experience; yet, he took me into his lab and provided me with all the freedom to venture into the field of X-ray crystallography. I am very grateful for his patience, support and the efforts he took to teach me everything that I have learned in these five years.

I would also like to thank Drs. Peter J Roach and Anna Depaoli-Roach for their constant support and encouragement. They have given me invaluable advice on my project that helped it move forward. I would like to express my sincere gratitude to Dr. Millie M. Georgiadis, who introduced me into the field of structural biology and also provided me with valuable suggestions that helped me carry my project forward. I would also like to thank Dr. Jeffrey Elmendorf for his time, support and helpful suggestions during my committee meetings.

I am very thankful to my past and present lab members; Dr. Vimbai M. Chiwana, Dr. Sulochanadevi Baskaran, Lanmin Zhai, Dr. May Khanna, Dr. Bibek Parajuli, Dr. Cindy A. Morgan, Dr. Cameron Buchman, Dr. Ann Kimble-Hill, Buyun Tang, Mikail Chtcherbinine for creating a stimulating and fun environment in the lab. I am especially grateful to Dr. Vimbai M. Chikwana and Lanmin Zhai for teaching me the basics of biochemistry and molecular biology during my first year in the lab. I am also grateful to my colleagues Dr. Qiuja Chen, Dr. Hongzhen He, Dr. Isha Singh, Dyann Segvich, Christopher Contreras, Dr.

Alexandra V. Skurat, Dr. Punitee Garyali, Dr. Jose Irimia-Dominguez, Chandra Karthick, for their friendship and support. It was a pleasure coming to work every day and interacting with you guys.

I would like to thank the Biochemistry office staff for their timely help and assistance. I would like to extend my thanks to Drs. Quyen Hoang and Yuichiro Takagi for letting me use their lab resources for the completion of my project. I would also like to thank the beamline scientists at the SBC-CAT and GM/CA-CAT stations at the Advanced Photon Source, Chicago for their scientific assistance.

I would like to extend my gratitude to my landlord, Donna Sanders who was more like a guardian to me for the past five years. I would like to thank Ms. Deepika Raghu for her constant support and encouragement during my under graduation in India. I would also like to thank all my friends in and around Indianapolis for their friendship and memories, especially my friends in speedway with whom I played football (soccer) all these years. I am going to miss you all dearly.

Last but not least, my family, especially my parents. Without them none of these would be possible.

Krishna Kishore Mahalingan

STRUCTURAL BASIS FOR REGULATED INHIBITION AND SUBSTRATE
SELECTION IN YEAST GLYCOGEN SYNTHASE

Glycogen synthase (GS) is the rate limiting enzyme in the synthesis of glycogen. Eukaryotic GS catalyzes the transfer of glucose from UDP-glucose to the non-reducing ends of glycogen and its activity is negatively regulated by phosphorylation and allosterically activated by glucose-6-phosphate (G6P). A highly conserved cluster of six arginine residues on the C-terminal domain controls the responses toward these opposing signals. Previous studies had shown that tetrameric enzyme exists in three conformational states which are linked to specific structural changes in the regulatory helices that carry the cluster of arginines. These helices are found opposite and anti-parallel to one another at one of the subunit interfaces. The binding of G6P beneath the regulatory helices induces large scale conformational changes which open up the catalytic cleft for better substrate access. We solved the crystal structure of the enzyme in its inhibited state and found that the tetrameric and regulatory interfaces are more compacted compared to other states. The structural consequence of the tighter interfaces within the inhibited state of the tetramer is to lower the ability of glycogen chains to access to the catalytic cleft. Based on these observations, we developed a novel regulatory feature in yeast GS by substituting two of its conserved arginine residues on the regulatory helix with cysteines that permits its

activity to be controlled by reversible oxidation/reduction of the cysteine residues which mimics the effects of reversible phosphorylation. In addition to defining the structural changes that give rise to the inhibited states, we also used X-ray crystallography to define the mechanism by which the enzyme discriminates between different UDP-sugar donors to be used as substrates in the catalytic mechanism of yeast GS. We found that only donor substrates can adopt the catalytically favorable bent conformation for donor transfer to a growing glycogen chain.

Thomas D. Hurley, Ph.D., Chair

TABLE OF CONTENTS

LIST OF TABLES.....	xii
LIST OF FIGURES	xiii
LIST OF ABBREVIATIONS.....	xvi
INTRODUCTION	1
1.Glycogen.....	1
1.A. Structure of Glycogen	3
1.B. Glycogen synthesis and degradation.....	5
2.Hormonal regulation of glycogen metabolism	8
2. A. Insulin	9
2 .B. Glucagon and epinephrine.....	11
3.Glycogen metabolism and regulation in yeast.....	12
4.Glycogen Synthase	14
4. A. Naturally occurring mutation of the glycogen synthase gene.....	15
i. Glycogen storage disease type 0	15
ii. Polysaccharide storage myopathy (PSSM)	16
4.B. Covalent regulation of eukaryotic glycogen synthase	17
4.C. Regulation by Cellular translocations	21
5.Allosteric regulation of GS and kinetic model.....	22
6.Structural studies on eukaryotic glycogen synthase	24
7. Role of the regulatory arginines	30
8.Donor binding at the catalytic site	32
9. Proposed catalytic mechanism	34
RATIONALE AND OVERVIEW OF THE THESIS RESEARCH	36
EXPERIMENTAL PROCEDURES	38

1.Site directed mutagenesis.....	38
2.Expression and purification of yGsy2.....	39
3.Non-reducing SDS PAGE	41
4.Gel filtration.....	41
5.Crystallization.....	42
5. A. yGsy2 R589A/R592A mutant.....	42
5. B. UDP-glucose analogues in the activated state	43
6.Hydrolysis of UDP-glucose analogues by yGsy2	44
7.X-ray diffraction, data Collection, processing, structure determination and refinement.....	45
7. A. Data collection	45
7. B. Structure determination, model building and refinement.....	45
8. Structural alignments and domain motion measurements	47
9. Glycogen synthase activity measurements	47
9.A. Glycogen treatment	47
9.B. Glycogen synthase assays	48
i. Standard condition	48
ii. Activity ratio	49
iii. Reducing agent titrations	50
iv. G-6-P titrations	50
v. UDP-glucose titrations.....	50
vi. UDP-sugar donor titrations.....	50
10. Kinetic data analysis	51
RESULTS	52
1.Expression and purification of yGsy2.....	52

2. Crystallization of yGsy2-R589A/R592A.....	53
3. Structure determination and refinement	54
4. Overall structure of yGsy2R589A/R592A.....	57
5. Structural comparisons with the basal state structure	62
6. Redox regulation of yGsy2.....	66
7. Non-reducing SDS-PAGE analysis	67
8. Gel filtration.....	69
9. Specific activity measurements.....	70
10. Glucose-6-Phosphate titrations.....	71
11. Reducing agent titrations	72
12. UDPG titrations	73
13. Analysis of yGsy2 activity towards UDP-glucose analogues.....	75
14. Inhibition by nucleotide sugars.....	77
15. Substrate binding in yGsy2 active site	78
15. A. UDP-Glucosamine	79
15. B. UDP-2-fluro-2-deoxy-glucose (UDP-FDG).....	83
16. Non-substrate binding to the yGsy2 active site	85
16.A. UDP-galactose	85
16.B. UDP-N-acetylglucosamine (UDP-GlucNac).....	89
16.C. UDP-Xylose.....	92
DISCUSSION.....	95
1. Substrate selection in yeast Gsy2.....	95
2. Catalytic mechanism of yGsy2.....	103
3. Role of the regulatory helix in the inhibition of GS	107
4. Redox regulation of yeast Gsy2	111

CONCLUSION	117
REFERENCES	119
CURRICULUM VITAE	

LIST OF TABLES

Table 1. Known glycogen storage diseases and its effects.	2
Table 2. Data collection statistics.	55
Table 3. Refinement statistics.....	56
Table 4. Specific activity measurements.	71
Table 5. UDPG kinetics.	74

LIST OF FIGURES

Figure 1. Polymerization of glucose residues.	1
Figure 2. Structure of glycogen.....	4
Figure 3. Glycogen metabolism.	7
Figure 4. Hormonal regulation of GS.....	11
Figure 5. Glycogen regulation in yeast.....	13
Figure 6. Enzymatic function and classification of glycogen synthase (GS).	15
Figure 7. Naturally occurring GS mutations.	16
Figure 8. GS regulation by phosphorylation.	18
Figure 9. Three state kinetic model for yGsy2.	23
Figure 10. Crystal structures of yeast and Ce GS.	25
Figure 11. Multiple sequence alignment of various species of GS.	27
Figure 12. G6P mediated activation of GS.....	29
Figure 13. Role of the regulatory helix.....	31
Figure 14. UDP•G binding in yGsy2.....	33
Figure 15. Catalytic mechanism of GS.....	35
Figure 16. Representative SDS PAGE of ygsy2 purification.	52
Figure 17. Optimization of yGsy2-R589A/R592A crystals.	53
Figure 18. Crystal structure of yGsy2 inhibited state.	58
Figure 19. Nucleotide binding in the active site of yGsy2-R589A/R592A.	60
Figure 20. Dimer interface of the inhibited and active state of yGsy2.....	61
Figure 21. N-terminal domain closure of the inhibited state.....	63
Figure 22. Glycogen access to the inhibited state.	64

Figure 23. Regulatory interface of the three states of yGsy2.....	66
Figure 24. Redox regulation of ygsy2.	67
Figure 25. Inter-subunit di-sulfide bond formation.	68
Figure 26. Gel filtration analysis of the cysteine mutants.....	69
Figure 27. G-6-P activation of the yGsy2 mutants.	72
Figure 28. Effect of different reducing agents on the cysteine mutants.	73
Figure 29. Hydrolysis of different UDP-sugar donor.	76
Figure 30. UDP-sugar donor titrations.	77
Figure 31. UDP•glucosamine binding to the ygsy2 active site.	80
Figure 32. N-terminal domain closure induced by UDP•glucosamine.	81
Figure 33. Subunit interactions of UDP•glucosamine.	82
Figure 34. UDP-FDG binding to the yGsy2 active site.....	84
Figure 35. N-terminal domain closure induced by UDP-FDG.	85
Figure 36. UDP-galactose binding to the active site.	86
Figure 37. Structural conformation and subunit interactions made by UDP- galactose.	87
Figure 38. N-terminal domain closure induced by UDP-galactose.	88
Figure 39. UDP-GlucNac binding to the active site.....	90
Figure 40. N-terminal domain motions induced by UDP-GlucNac.....	91
Figure 41. UDP-xylose binding to the yGsy2 active site.	92
Figure 42. Subunit interactions made by UDP-xylose and the domain motions induced by it.....	94
Figure 43. Analysis of glucose and its analogues as potential substrates.	97

Figure 44. Structural basis for the observed UDP-galactose conformation in the active site of yGsy2.....	100
Figure 45. Structural basis for the observed UDP-GlucNac conformation in the active site of yGsy2.....	101
Figure 46. Structural basis for the observed UDP-Xylose conformation in the active site of yGsy2.	102
Figure 47. Molecular basis for UDP-glucose hydrolysis.	104
Figure 48. Catalytic role of N-terminal domain closure.....	106
Figure 49. Role of the regulatory interface in inhibiting GS.	109
Figure 50. N-terminal phosphorylation.....	110
Figure 51. Naturally occurring and rationally introduced cysteine residues in yGsy2.	112
Figure 52. Structural model for the inhibited state and redox regulation of yeast GS.....	115

LIST OF ABBREVIATIONS

AMP	Adenosine monophosphate
ATP	Adenosine triphosphate
BE	Branching enzyme
Bis-Tris	Bis (2-hydroxyethyl)iminotris(hydroxymethyl)-methane
BME	β -mercapto ethanol
<i>Ce</i>	<i>Caenorhadditis elegans</i>
CK2	Casein Kinase 2
DBE	Debranching enzyme
DNA	Deoxyribonucleic acid
DTT	Dithiothreitol
EDTA	Ethylenediaminetetraacetic acid
G6P	Glucose-6-phosphate
GAA	lysosomal acid- α -glucosidase
GFP	Green fluorescence protein
GK	Glucokinase
GLUT	Sodium independent glucose transporter
GPh	Glycogen phosphorylase
GS	Glycogen synthase
GSD	Glycogen storage disorder
GSK3	Glycogen synthase kinase 3
Gsy2	Glycogen synthase isoform 2

GT	Glycosyl transferase
IPTG	Isopropyl β -D-1-thiogalactopyranoside
K_M	Michaelis-Menten constant
LB	Luria-Bertani broth
$MgCl_2$	Magnesium Chloride
NaCl	Sodium Chloride
NADP	Nicotinamide adenine dinucleotide phosphate
NCS	Non-crystallographic symmetry
PCR	Polymerase chain reaction
PEG	Polyethylene glycol
PhK	Phosphorylase kinase
PKA	Protein Kinase A
PPP	Pentose Phosphate Pathway
rpm	revolutions per minute
R_{GL}	Regulatory targeting subunit
SDS-PAGE	Sodium dodecyl sulfate polyacrylamide gel electrophoresis
STRE	Stress response element
TCA	Tricarboxylic Acid cycle
TCEP	Tris-(2-carboxyethyl) phosphine
Tris	Tris (hydroxymethyl) aminomethane
UDP	Uridine diphosphate
UDP-FDG	Uridine diphosphate 2'-fluoro-2'-deoxy-glucose
UDPG	Uridine diphosphate glucose

UDP-gal	Uridine diphosphate galactose
UDP-GlucNac	Uridine diphosphate N-acetylglucosamine
V_{\max}	Maximum velocity
WT/wt	Wildtype

INTRODUCTION

1. Glycogen

In nature, glucose polymerization is a universally adapted mechanism to store glucose as a metabolic reserve during times of nutritional sufficiency, which can be rapidly mobilized when demand exceeds available resources (1). In plants, glucose is stored in the form of starch, which is composed of amylopectin (Figure 1B), a branched semi-crystalline polysaccharide, and amylose (Figure 1A), an unbranched polymer of glucose (2) (3). In bacteria, archaea and animals, glucose gets stored in the form of glycogen (Figure 1C), a highly branched osmotically inert polymer of glucose (1).

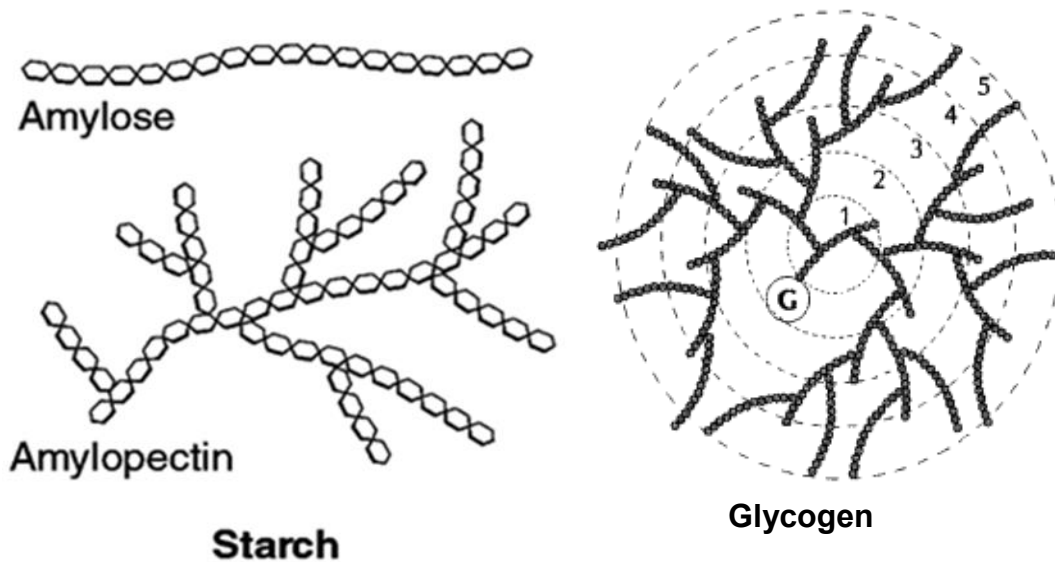


Figure 1. Polymerization of glucose residues.

In humans, the major sites of glycogen storage are skeletal muscle and liver, but several other tissue types like heart, brain and adipose are also capable of synthesizing the polysaccharide (1). Glycogen is an important energy source during times of nutritional depletion. In particular, liver glycogen is responsible for

maintaining blood glucose levels for tissues such as the brain, which depends mostly on glucose as an energy source. In contrast, skeletal muscle glycogen is limited to acting as an internal cellular energy reserve because muscle lacks the ability to export glucose derived from glycogen. Glycogen metabolism in the liver and skeletal muscle is highly regulated. Enzymatic defects in the processing of glycogen synthesis and breakdown result in a class of diseases called Glycogen Storage Disease (GSD) (1, 4). There are currently eleven known diseases (Table1) that fall under the GSD category affecting at least 1 in every 40,000 live births, worldwide (5-7).

GSD	Enzyme deficiency	Eponym	Development and prognosis
Type 0	Glycogen synthase		Occasional muscle cramping
Type I	Glucose-6-phosphatase	Von Gierke's disease	Growth failure
Type II	Acid α -glucosidase	Pompe's disease	Muscle weakness and death by age ~2
Type III	Glycogen debranching enzyme	Cori's disease	Myopathy
Type IV	Glycogen branching enzyme	Andersen disease	Failure to thrive, death at age ~5
Type V	Muscle glycogen phosphorylase	McArdle disease	Renal failure
Type VI	Liver glycogen Phosphorylase	Her's disease	Growth retardation
Type VII	Muscle phosphofructokinase	Tarui's disease	Growth retardation and anemia
Type IX	Phosphorylase kinase		Delayed motor development and growth retardation
Type XI	GLUT2	Fanconi-Bickel Syndrome	
Type XII	Aldolase A	Red cell aldolase Deficiency	Exercise intolerance

Table 1. Known glycogen storage diseases and its effects.

1. A. Structure of Glycogen

Glycogen synthesis can be characterized in two basic steps, polymerization and branching. Linear polymerization of glucose is catalyzed through α -1,4 glycosidic bonds with occasional α -1,6 glycosidic bonds as branch points spaced approximately 12-15 glucose residues apart along the linear chains (Figure 2B) (1). Glycogen obtained from biological sources is often heterogeneous in nature making it an extremely difficult candidate for structure determination using classical approaches of structural biology. However, extensive chemical analyses had shed light on the overall structure and chemistry of glycogen molecules. One widely accepted model (1, 8-11) for glycogen structure categorizes the outermost chains of glycogen as A-chains which are unbranched and the innermost chains as B-chains which are branched and typically contain two branch points per 13 residues. According to this model (Figure 2B), glycogen is made up of concentric tiers with the outermost tier containing ~50% of the total glucose residues and each tier containing approximately twice the number of glucose residues as the preceding one. Theoretically, a maximally sized glycogen molecule will be spherical in shape with 12 tiers containing approximately 55,000 glucose residues. Such an arrangement not only facilitates maximal storage of glucose molecules, but also rapid degradation and release of stored glucose upon depletion. In addition to glucose, glycogen also contains trace amounts of glucosamines (12, 13) and phosphates (14-16) with the later affecting the branching properties and the overall structure of glycogen as seen in the Lafora Disease (17, 18).

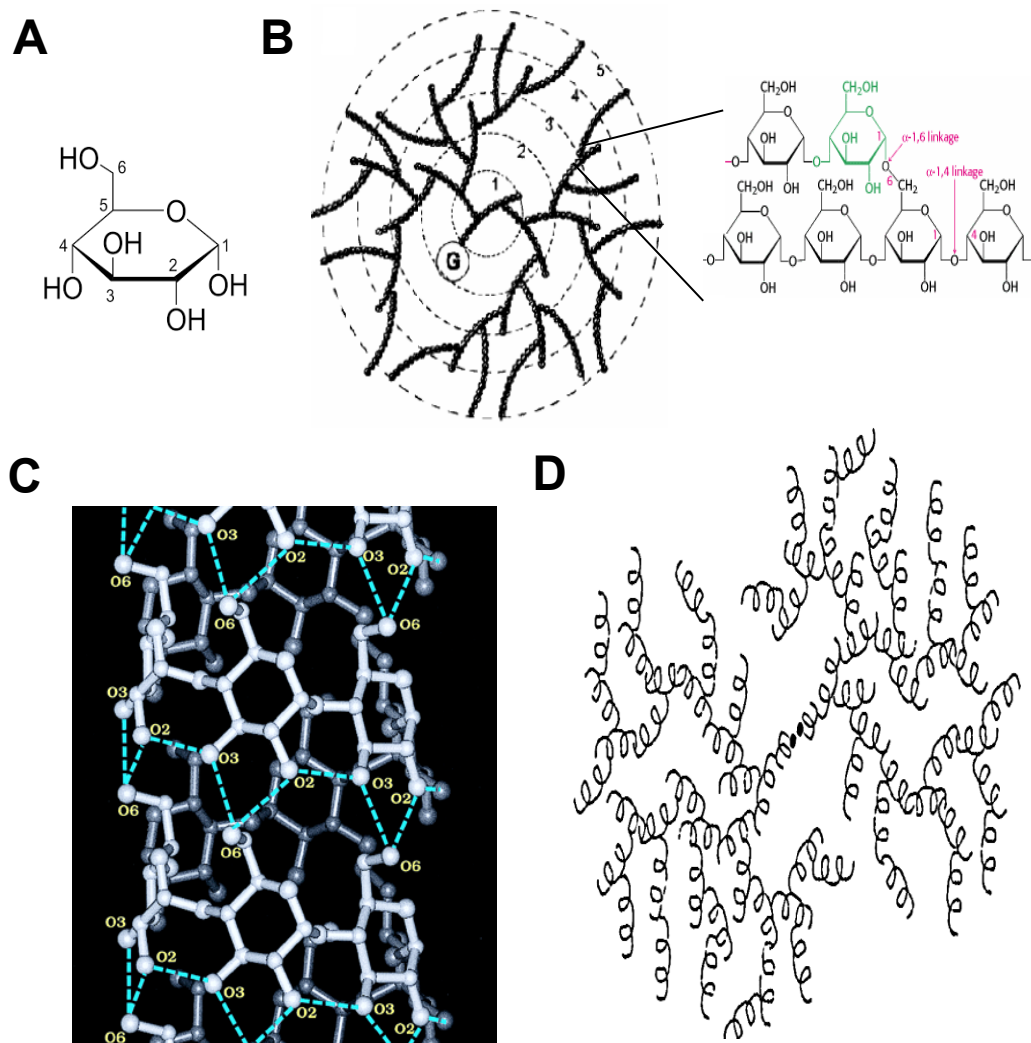


Figure 2. Structure of glycogen.

A. Glucose molecule with its carbon atoms numbered from 1-6. B. The tiered model showing glycogen molecule as made up of concentric tiers (tiers 1-5 are labelled). Glucose polymerization through an α -1,4 glycosidic linkages with occasional α -1,6 glycosidic linkage are shown. The G denotes Glycogenin. C. Atomic model of CA26 with the inter- and intra-molecular hydrogen bonds are shown in dotted lines. D. Glycogen molecule with its linear chains shown as helices. The two black circles denote the glycogenin dimer.

Unlike glycogen, amylose is an unbranched form of starch that can be crystallized. A crystal structure of cycloamylose (cyclized form of amylose) containing 26 glucose residues (CA26) was solved to a maximum resolution of

1.1 Å (Figure 2C) (19). In this structure, CA26 folds itself into two short left-handed helices in antiparallel arrangement. Thirteen glucose residues make up a helix with 6 glucose residues per turn. Intramolecular hydrogen bonds between the hydroxyl groups stabilize the helical structure. Every glycogen chain of 13-15 glucose residues can be considered to form a helix at which point branching occurs and the next helix starts (Figure 2D).

1. B. Glycogen synthesis and degradation

Glucose metabolism in the skeletal muscle starts with glucose entering the cell to be phosphorylated at the sixth position by hexokinase (HK) thus forming glucose-6-phosphate (G6P) (20). Once phosphorylated, the metabolic fate of G6P depends on the nutritional status of the cell (Figure 3). For instance, when nutrients are limiting, the majority of G6P is oxidized through the glycolytic pathway or enters the Pentose Phosphate Pathway (PPP) to form NADPH and other cellular building materials (21). In times of nutritional sufficiency, excess G6P is diverted to form glycogen. Glycogen synthesis (glycogenesis) starts with the enzymatic conversion of G6P to an activated nucleotide sugar donor, uridine diphosphate glucose (UDP-glucose) (4). G6P is first converted to glucose-1-phosphate (G1P) by phospho-glucomutase and then to UDP-glucose by UDP-glucose pyrophosphorylase. Once UDP-glucose is formed, glycogenin, an autocatalytic initiator of glycogen synthesis, transfers glucose to one of its conserved tyrosine residues, via a covalent O-glycosidic linkage (22). Glycogenin will continue to add an additional 10-12 glucose residues forming a linear chain, whereupon glycogen synthase (GS) and the glycogen branching enzyme (GBE)

complete the synthesis of glycogen. GS catalyzes the transfer of glucose from UDP-glucose to the non-reducing end of the acceptor chain. Glycogen synthase is responsible for the bulk of glycogen synthesis and is considered to be the rate limiting step in glycogenesis (1). Once the linear chain of glucose exceeds 12 residues, GBE catalyzes the formation of branches to the growing glycogen molecule by transferring 7-8 glucose residues from the terminal chain segment to the C6 hydroxyl group of a glucose residue on the same or another chain (1, 23). GS will now have two different acceptor chains to which glucose can be added. This combined action of both GS and GBE will lead to the synthesis of the spherical glycogen molecule.

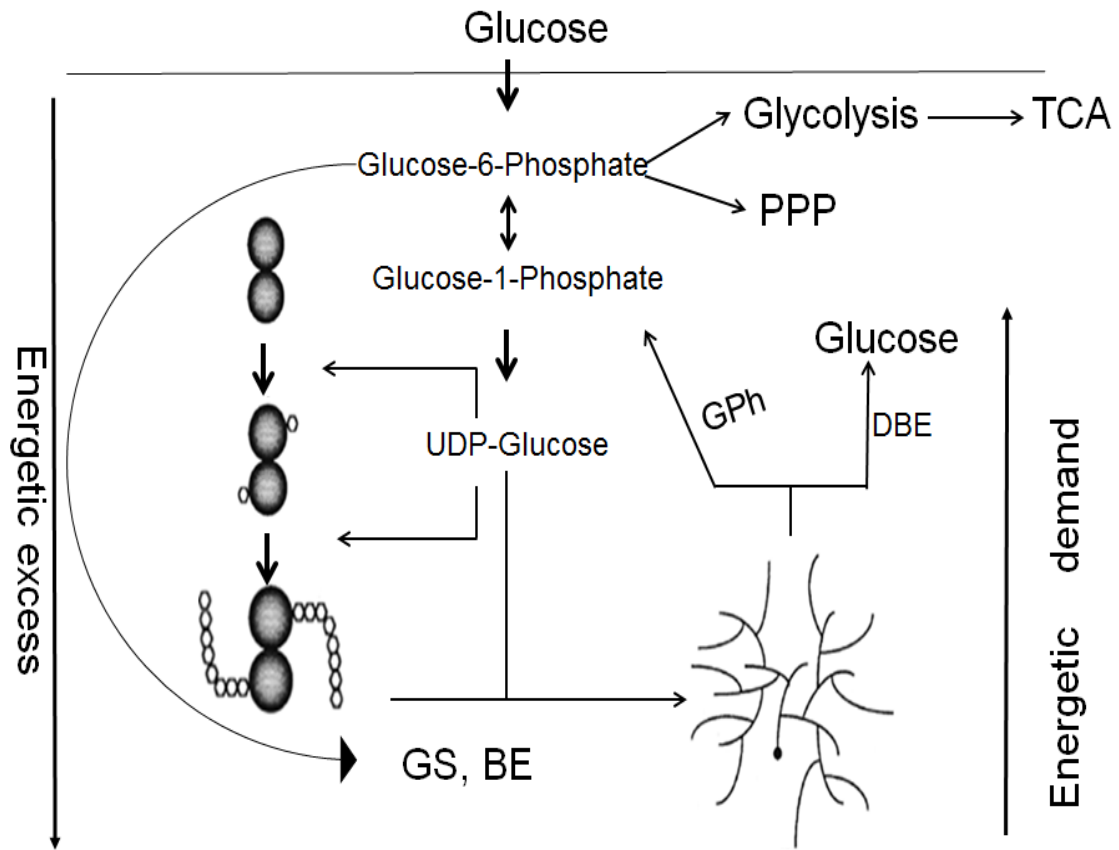


Figure 3. Glycogen metabolism.

Flow chart showing the pathway for glycogen biosynthesis and degradation. Synthesis of Glycogen involves Glycogenin, glycogen synthase and branching enzyme. Glycogen degradation is mediated by glycogen phosphorylase and debranching enzyme.

When the cellular demand for glucose exceeds exogenous supplies, glycogen is degraded to mobilize the stored glucose. Glycogen degradation (glycogenolysis) requires the combined action of glycogen phosphorylase (GPh) and the glycogen debranching enzyme (DBE) (Figure 3). GPh catalyzes the phosphorolysis of α -1,4-glycosidic bonds in glycogen_(n) producing glucose-1-phosphate and glycogen_(n-1). GPh uses pyridoxal phosphate as a co-factor (24). Phosphorylase can act only on linear chains of glycogen (α -1,4-glycosidic bonds)

and its action will come to a halt four residues away from an α -1,6-glycosidic branch point. To continue the breakdown, the debranching enzyme is necessary to remove the branch point. Glycogen debranching enzyme is a relatively large enzyme (165kDa) and is composed of two different functional domains with two distinct catalytic activities (25). The N-terminal domain of DBE and its associated α -1,4-transglycosylase activity will transfer three glucose residues from the four residue glycogen branch to the main chain (25). This exposes a single glucose residue joined to the main chain through an α -1,6-glycosidic linkage. The C-terminal domain of DBE will then hydrolyze the α -1,6 linkage giving free glucose as the hydrolysis product (25).

Reversible synthesis and degradation of glycogen can occur multiple times within the cytosol. However, a fraction of glycogen ends up in the lysosome where it is irreversibly degraded by a different enzyme, acid- α -glucosidase. Glycogen degradation in the lysosome is straight forward. Acid- α -glucosidase is capable of hydrolyzing both α -1,4 and α -1,6 glycosidic linkages to produce free glucose (26). The importance of this enzyme in glycogen metabolism can be seen in patients with Pompe disease where the absence or deficiency of the enzyme can lead to abnormal accumulation in lysosomal glycogen with severe phenotypes in heart and brain resulting in death within the first year of life (<https://ghr.nlm.nih.gov/condition/pompe-disease>).

2. Hormonal regulation of glycogen metabolism

In mammals, skeletal muscle and liver are the two major tissue types where glycogen deposits can be found in abundance. The major difference

between liver and skeletal muscle glycogen metabolism is the utilization of glucose after release from stores. In the fasted state, glucose-1-phosphate produced following the phosphorolysis of glycogen is isomerized to form G6P. The liver expresses glucose-6-phosphatase, which can dephosphorylate G6P to form glucose (27). The free glucose can then be transported into the blood stream and on to other tissues, like brain, which depend on glucose as their primary energy source. Unlike liver, skeletal muscle does not express glucose-6-phosphatase and therefore the G6P formed after glycogenolysis is utilized within the cell. G6P in the skeletal muscle is used for ATP production during muscle contraction by entering into glycolysis. Glycogen metabolism in both liver and skeletal muscle is tightly regulated by hormones which are linked to the nutritional status of the cell (Figure 4).

2. A. Insulin

Insulin is the primary hormone responsible for signaling the conversion of glucose into glycogen. Insulin-stimulated glycogen accumulation accounts for up to 30% in liver and 30-90% in the skeletal muscle of postprandial glucose disposal (1). Type II diabetic patients who are insulin resistant often have lower levels of liver and skeletal muscle glycogen (28). Insulin promotes glycogen accumulation by increasing the activity of GS, the rate-limiting enzyme in glycogenesis (29). In the higher eukaryotes, GS activity is regulated by multiple mechanisms including covalent modifications, allosteric activation and translocations within the cell (4). The binding of insulin to the extracellular α -subunit of the insulin receptor activates its tyrosine kinase domain to initiate a

series of signaling events that are responsible for activating protein phosphatases that dephosphorylate GS and activate the enzyme (30). Insulin also stimulates glucose uptake into the cell by translocating glucose transporters (GLUT4) to the cell membrane. The glucose is then phosphorylated at the C6 position by hexokinases to form G6P. As mentioned previously, G6P has multiple fates, but is also an allosteric activator of GS, capable of activating GS independent of its phosphorylation status (1).

Rising insulin levels in the liver also inhibit GPh, the rate limiting enzyme of glycogenolysis (29). GPh can exist in two different activity states, a more active R state and a less active T state depending on the phosphorylation status of the enzyme. When phosphorylated (phosphorylase a), the enzyme is activated while dephosphorylation (phosphorylase b) inhibits the enzyme, thereby demonstrating a reciprocal relationship with GS in terms of regulation (24). AMP can activate the enzyme through an allosteric mechanism and shift the equilibrium towards a more active R state. Insulin mediated inhibition of GPh primarily occurs through glucose binding to phosphorylase. Glucose binding to an allosteric site causes a conformational change that makes phosphorylase a better substrate for phosphatases. Furthermore, phosphorylase a is an allosteric inhibitor of PP1G/GL, the phosphatase responsible for the dephosphorylation of both GS and GPh (29). Glucose mediated conformation change of GPh from phosphorylase a to b form relaxes PP1G/GL resulting in the dephosphorylation and activation of glycogen synthase (31, 32).

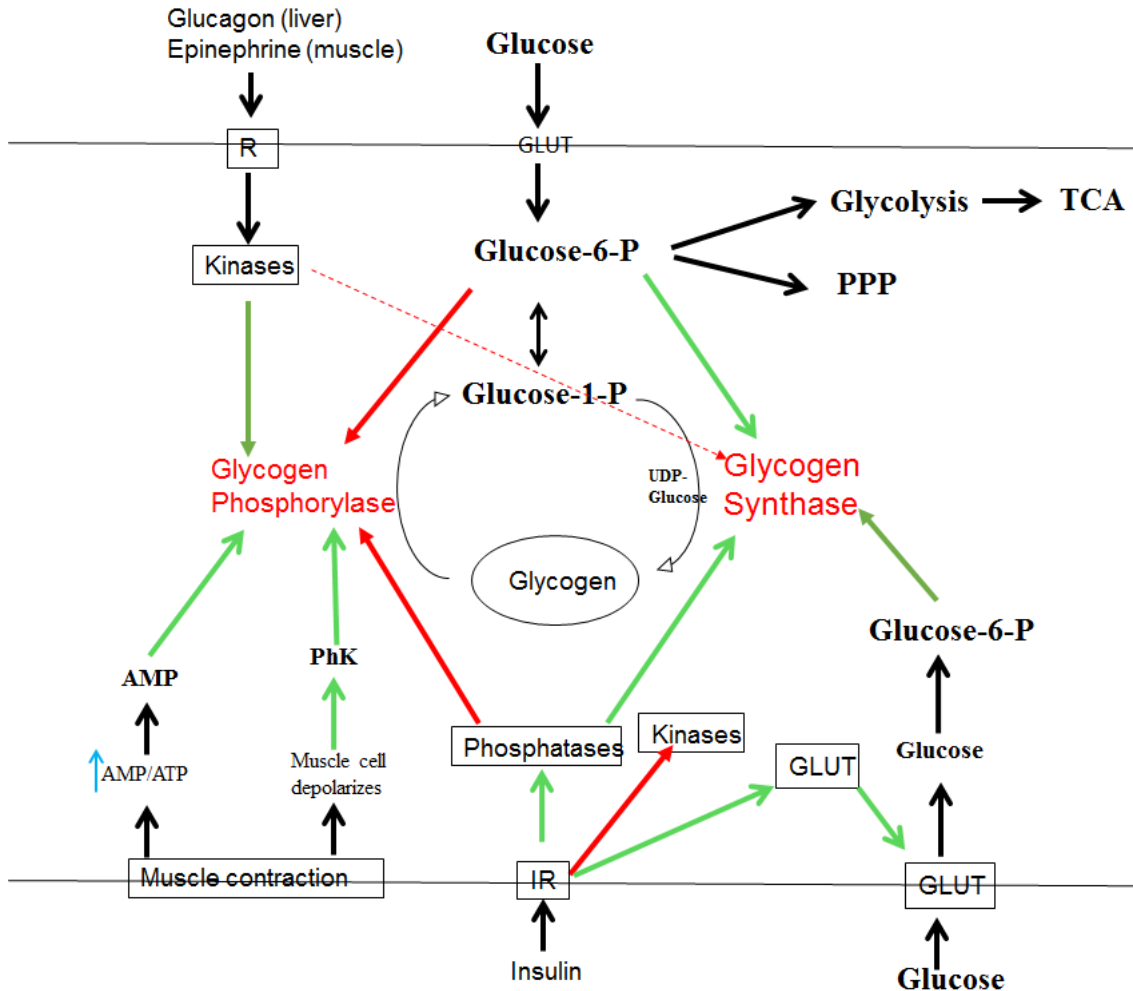


Figure 4. Hormonal regulation of GS.

Schematic representation of the major players in the regulation of glycogen metabolism in the skeletal muscle. The blue open circles are insulin. IR- Insulin receptor, AMP- Adenosine monophosphate, AMPK- AMP dependent protein kinase, B AR- beta adrenergic receptors, PPP- Pentose phosphate pathway, TCA- Tricarboxylic acid cycle, GLUT- Glucose transporters. Red arrows represent inhibition while the green arrows denote activation.

2. B. Glucagon and epinephrine

Muscle contraction and epinephrine stimulate glycogenolysis in the skeletal muscle while glucagon is responsible for glycogen breakdown in the liver. Epinephrine binding to the beta-adrenergic receptor initiates a signaling

cascade through protein kinase A (PKA) that activates phosphorylase kinase (PhK) (33). PhK phosphorylates phosphorylase thereby shifting the equilibrium to the more active R state, promoting glycogenolysis. Both PhK and PKA can inhibit GS by phosphorylating sites on its N-terminus (Biochemistry, Section 21.3). In the case of muscle contraction, release of Ca^{2+} ions from the sarcoplasmic reticulum directly activates PhK and thus increases phosphorylation of GPh (34). As muscle contraction continues, an increase in the AMP/ATP ratio activates AMP kinase that can phosphorylate GPh thereby activating the enzyme. AMP itself can activate GPh allosterically, as mentioned previously. In the liver, glucagon can activate liver adenylyl cyclase which increases cAMP levels which in turn activates PKA (<https://www.ncbi.nlm.nih.gov/books/NBK22429>). The activated PKA can phosphorylate both GS and GPh thereby inhibiting and activating the enzymes, respectively.

3. Glycogen metabolism and regulation in yeast

Glycogen and trehalose are the two major carbohydrate reserves found in yeast. The relative amounts of these macromolecules depend on the changes in the environment indicating a complex regulatory system controlling their metabolism (35, 36). In the budding yeast *Saccharomyces cerevisiae*, glycogen can account for 20% of its dry weight. Glycogen levels in the cell increase with the cell entering the stationary phase and during times of nutritional stress. Yeast has two genes for GS, GSY1 and GSY2, the latter being nutritionally regulated (37). Yeast Gsy2 enzyme (yGsy2) can be inhibited by phosphorylation and can be activated allosterically by G6P. In the yeast cell, Snf1p and PKA are the two

kinases responsible for the phosphorylation of GS (Figure 5) (35). Other kinases like Pcl8/10p and pho85p are also capable of phosphorylating yGsy2p (38).

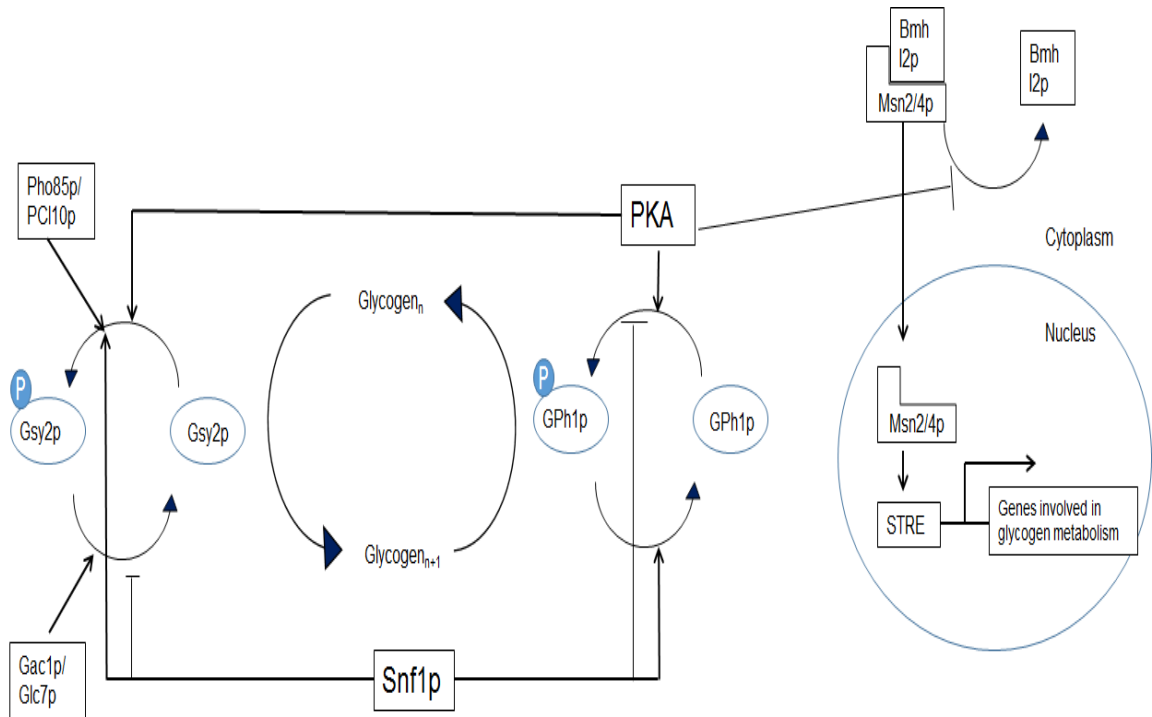


Figure 5. Glycogen regulation in yeast.

Schematic representation of major players in the transcriptional and enzymatic regulation of glycogen metabolism in the budding yeast cell.

Unlike other higher eukaryotes, genes involved in yeast glycogen metabolism can also be transcriptionally regulated depending on the nutrient status of the cell (Figure 5). The activity of the yeast GS enzymes increases as the cell enters the stationary phase of growth. The increase is partly due to the increase in the level of protein expression rather than a simple change in phosphorylation status. This transcriptional regulation of GS and other enzymes depend on the stress response element (STRE), cis-element found upstream of the promoter of glycogen metabolism genes (35). During times of nutritional

sufficiency, the transcriptional activator Msn2/4p is sequestered in the cytosol by Bmh1I2p. Under stress conditions, the trans-activator Msn2/4p dissociates from Bmh1I2p and enters the nucleus where it binds to the STRE and increases the expression of these genes by 2- to 3-fold. Glycogen degradation and utilization is mediated by both c-AMP dependent PKA pathway and a poorly characterized PKA independent pathway (38).

4. Glycogen Synthase

As previously mentioned, GS is responsible for the bulk synthesis of glycogen through formation of α -1,4-glycosidic linkages using UDP-glucose as a glucosyl donor to the non-reducing end of an existing glucose polymer (Figure 6A). Within the glucosyl transferase (GT) super-family, eukaryotic GS is grouped into the GTB-fold family of enzymes (<http://www.cazy.org/GlycosylTransferases.html>). The GTB-fold family is characterized by the presence of two Rossmann fold domains with a deep inter-domain cleft where the substrates bind (39). Within the GTB-fold family, eukaryotic GS enzyme is further divided into GT3 sub-family because of its ability to use UDPG as a donor and its ability to be regulated by covalent phosphorylations and allosteric activation (Figure 6B). The bacterial and archaeal GS enzymes are grouped into the GT5 family and use ADP-glucose as a donor and are not subject to covalent and allosteric regulations (Figure 6B).

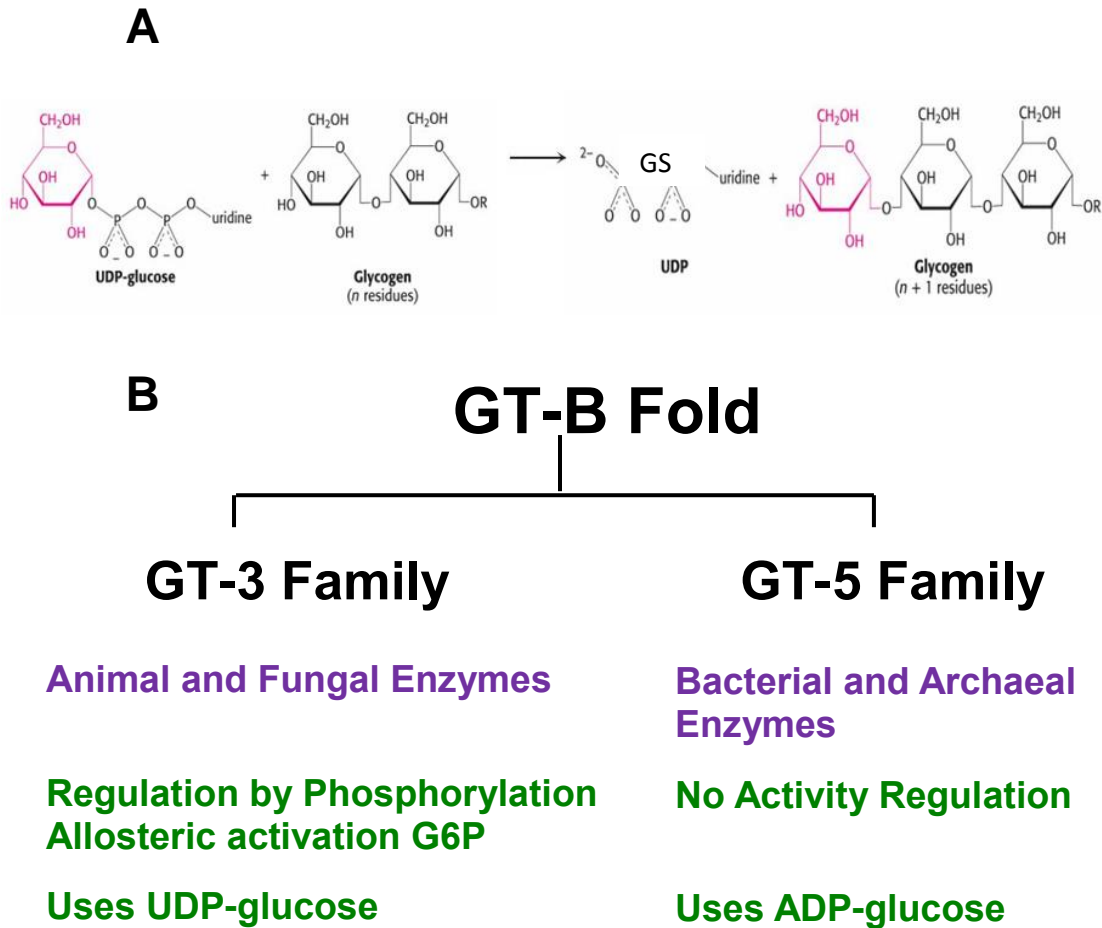


Figure 6. Enzymatic function and classification of glycogen synthase (GS).

A. GS catalyzes the transfer of glucose (shown in brown) from UDP-glucose to an existing glucose polymer giving away UDP as a bi-product. B. Eukaryotic GS is grouped into the GT-3 subfamily of the GT-B fold family of glucosyl-transferases (GT).

4. A. Naturally occurring mutation of the glycogen synthase gene

i. Glycogen storage disease type 0

Glycogen storage disease type 0 (GSD0) is a rare autosomal recessive disorder caused by deficiency in the liver isoform of glycogen synthase. Patients with GSD0 typically experience severe fasting hypoglycemia accompanied by hyperketonemia, hyperlipidemia and elevated transaminase levels(40). To date,

sixteen different mutations have been identified in the *GSY2* gene that leads to GSD0 (Figure 7). Mutations include two splice variants, one deletion mutation, four premature stop codons and nine missense mutations (40) (41). Mice lacking the *GSY2* gene have a 95% reduction in the hepatic glycogen levels and show characteristic symptoms similar to the patients with GSD0 (42).

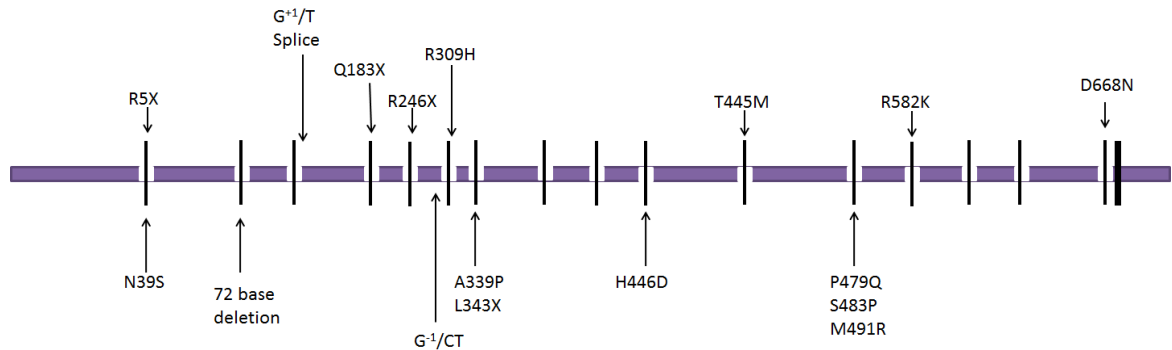


Figure 7. Naturally occurring GS mutations.

Schematic representation of glycogen synthase gene with exons shown in white and the naturally occurring mutants and splice variants that occur in the gene are shown in black lines.

Recent studies have shown that mutations in the muscle isoform of GS can also lead to glycogen storage defects. Three siblings were identified with a premature stop codon at R462 in the *GSY1* gene which led to the death of one of the siblings following cardiac arrest after a bout of exercise (43). Muscle biopsy from the other two siblings showed complete depletion of glycogen, predominance of oxidative fibers and mitochondrial proliferation (43).

ii. Polysaccharide storage myopathy (PSSM)

The R309H mutation found in horses leads to a glycogen storage disorder characterized by abnormal glycogen accumulation in the skeletal muscle and muscle damage with exertion (44, 45). Horses with PSSM show higher GS

activity even in the absence of G6P (45). It is the first known loss/gain of function mutation in the *GSY1* gene leading to glycogenosis. Recent studies have shown that mutating the Arg309 to His result in a constitutively active Gsy1 that has reduced response to the normally inhibitory phosphorylation events (46).

5. B. Covalent regulation of eukaryotic glycogen synthase

Multiple mechanisms, including covalent modifications, allosteric activation and translocations within the cell, regulate the activity of GS. Eukaryotic GS is inhibited by phosphorylation. Mammalian GS is one of the earliest examples of a multiply phosphorylated enzyme. Earlier studies on the rabbit muscle GS showed that the enzyme had 9 discrete sites of phosphorylation: two sites (sites 2, 2a which correspond to serines 8 and 11, respectively) on its N-terminus and seven sites on its C-terminus (sites 3a, 3b, 3c, 4, 5, 1a and 1b which correspond to the serines 641, 645, 649, 653, 657, 698 and 710, respectively) (1). The liver isoform *GSY2*, lacks the extreme C-terminal phosphorylation sites, 1a and 1b. In vitro, several protein kinases are capable of phosphorylating subsets of the nine different phosphorylation sites. Mammalian GS is also one of a number of proteins that shows a hierarchical pattern of phosphorylation where phosphorylation of one site primes for the phosphorylation of the next (Figure 8). For instance, phosphorylation of site 5 by protein kinase CK2 is recognized by GSK3 which then sequentially phosphorylate the sites 4, 3c, 3b and 3a (1). Similar pattern of hierarchal phosphorylations can be seen on the N-terminus where phosphorylation of site 2 primes for the phosphorylation of site 2a by protein kinase CK1 (Figure 8) (1). Elimination of site 2 prevents phosphorylation

of site 2a in COS M9 cells (47). Serine → alanine mutagenesis experiments on rabbit muscle GS had shown that sites 2, 2a, 3a and 3b (serines 8, 11, 641 and 645) had the major effect on GS activity (47). Expression of rabbit muscle GS in COS M9 cells with the sites Ser641 and Ser645 mutated to alanine resulted in a significant increase in glycogen accumulation when compared to the wild type GS expressing cells (47).

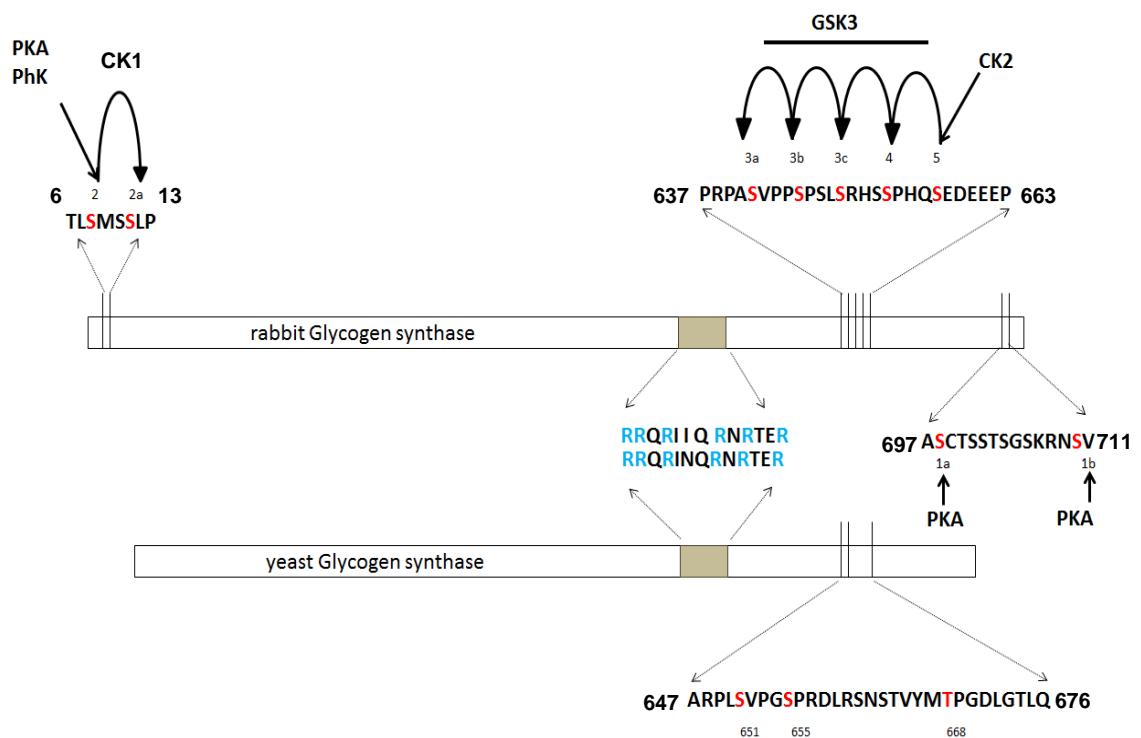


Figure 8. GS regulation by phosphorylation.

Schematic representation of rabbit GS1 and yeast Gsy2 are shown. The phosphorylation sites are shown in black lines and its corresponding serines are color coded in red. The grey box represents the arginine cluster. GSK3-Glycogen synthase 3 Kinase, CK2- Casein Kinase 2, PKA- Protein kinase A, PhK- Phosphorylase kinase.

Dephosphorylating the enzyme can reverse the inhibitory effects of the covalent phosphates. Insulin plays an important role in de-phosphorylating both

the N- and C-terminal phosphorylation sites of GS by activating protein phosphatases 1 (PP1) (48). The phosphatase action of PP1 is regulated by its association with the targeting subunits. There are seven known targeting subunits, of which, the following three are widely studied: R_{GL} (49), G_L (50), PTG (51). The R_{GL} or G_M subunit is restricted to skeletal and heart muscle (52) while the G_L subunit is expressed both in liver and skeletal muscle tissues (53). PTG (protein targeting to glycogen) is more ubiquitously expressed and is proposed to act as a scaffold protein that can interact with GS, GPh and phosphorylase kinase (54). Mice lacking R_{GL}, which is responsible for recruiting PP1 to glycogen in the skeletal muscle, had significantly higher GS phosphorylation which was well correlated with decreased glycogen accumulation in these tissues (55). Loss of hepatic glycogen binding subunit (G_L) in insulin dependent diabetic rats led to 70-80% decrease in liver glycogen deposits when compared to the wildtype rats (56).

Since most of the glucose uptake occurs in the skeletal muscle after a meal through an insulin dependent process, it is speculated that low glycogen levels found in type II diabetes patients are a consequence of inactive forms of GS caused by the inability of insulin to signal the dephosphorylation of GS, as well as the low influx of glucose to form G6P (57). A second covalent modification of GS was recently proposed, an O-linked N-acetyl glucosamine attachment which restrains the enzyme in a G6P dependent state and is unresponsive to insulin dependent de-phosphorylation (58). Other proteomic study identified acetylation of the following lysines in the GS liver isoform:

Lys387, Lys397, Lys694 and Lys695 (59). However, the physiological implication of these acetylations on GS requires further investigation.

The yeast GS enzyme lacks the N-terminal phosphorylation sites found in the higher eukaryotic enzymes and the hierarchical pattern of phosphorylation, but retains the inhibitory effects of C-terminal phosphorylation. There are three phosphorylation sites (Ser651, Ser655 and Thr668) on the C-terminal tail of yeast Gsy2p (60). When yeast cells express an enzyme truncated at residue 644, the cells accumulate four times more glycogen than cells expressing the full-length counterpart (60). In vitro, the Pho85p and Pcl10p complex was shown to directly phosphorylate these sites (61). Of the three phosphorylation sites, Thr668 has the major effect on the enzyme's activity. Studies using aspartate mutants as surrogates for phosphorylation showed that only the T668D mutant decreased the activity of the enzyme despite having no significant effect on the activity ratio, suggesting that aspartate mutants do not behave as true phosphomimics for the yeast enzyme (61, 62). Phosphorylating the double mutant S651A/S655A of yGsy2 with either the Pho85p/Pcl10p or the Pho85p/Pcl8p complex drastically decreased the activity, further demonstrating the effect of T668 phosphorylation. Recombinant yGsy2p truncated at residue 640 (yGsy2p Δ 640) had an activity ratio of 0.5. However, fusing a 49mer peptide containing a phosphorylated T668 to the yGsy2p Δ 640 enzyme decreased the activity ratio to 0.1 and the activity was restored after treating it with the catalytic subunit of the protein phosphatase PP1c γ (63). In vivo, dephosphorylation of yGsy2 occurs via a complex comprised of the type-1 protein phosphatase Glc7p

and its targeting subunit Gac1p (64, 65). Loss of Gac1p in yeast renders Gsy2p inactive and decreases glycogen accumulation in the cells (64).

4. C. Regulation by Cellular translocations

Glycogen metabolizing enzymes are also subjected to regulation by cellular translocations via an insulin dependent process. GS in skeletal muscle and adipocytes is translocated depending on the glucose levels in the cell (66, 67). Tracking muscle GS in C2L2 and COS1 cells with the help of GFP showed that GS is localized near the nucleus when the cellular glucose levels are low and is then translocated to the cytosol when the glucose level rises (68). Studies in rabbit skeletal muscle have shown that phosphorylation at sites 2, 2a and 1b could signal its redistribution within the cell (68). On the other hand, hepatic GS remains distributed throughout the cytosol independent of the glucose levels in cells, although there is a change from the periphery toward the interior of the cytosol as the glucose levels increase within the cell. This translocation of hepatic GS correlates with the increase in glycogen deposits which initiate at the periphery gradually moving inward (69).

The subcellular localization of yeast GS is dependent upon glycogen content (70). When glycogen is abundant, Gsy2p-GFP is uniformly distributed across the cytoplasm which correlates well with the distribution of the glycogen particles. However, under low glycogen conditions, Gsy2p-GFP localizes to discrete spots within the cytoplasm. When there is no glycogen, Gsy2p-GFP translocate into the nucleus. The results suggest that when the cellular glycogen

content is very high, Gsy2p remains anchored to glycogen. However, upon glycogen depletion Gsy2p loses this anchor and can traffic into the nucleus.

6. Allosteric regulation of GS and kinetic model

The allosteric activator, G6P, can override the inhibitory effects of covalent phosphorylation and fully activate GS. In the case of yGsy2p, G6P binding can increase the activity of the enzyme by two-fold even when the enzyme is dephosphorylated (71). The major kinetic effect of G6P binding to yGsy2p is an increase in V_{max} rather than on the K_m for UDP-glucose (71). However, in the case of the mammalian enzymes, G6P binding decreases the K_m values for UDPG from >30 mM to ~50 μ M (72, 73).

The manner in which G6P and covalent phosphorylation regulates GS is controlled by a cluster of six Arginine residues that are conserved across all eukaryotes. A scanning mutagenesis study in the yeast enzyme found that mutating the first three arginine residues (Arg580, Arg581 and Arg583) to alanine resulted in an enzyme that can neither be activated by G6P nor be inhibited by phosphorylation (71). Mutating the second set of three arginine residues (Arg587, Arg589 and Arg592) rendered the enzyme insensitive to G6P mediated activation but allowed it to retain its ability to be inhibited by phosphorylation (71). In the rabbit muscle GS, the same set of mutations similarly led to the loss of G6P activation but their sensitivity to phosphorylation is swapped such that the N-terminal triple mutation retained inhibition by phosphorylation (73).

Based on these kinetic and mutational studies, a three state conformational model was proposed to explain the kinetic behavior of eukaryotic GS (Figure 9)

(71). In this model, the enzyme exists in three different states. When the enzyme is neither phosphorylated nor bound to G6P, it exists in an intermediate state with a V_{max}/K_m value of ~ 6 . Phosphorylating the enzyme decreases the V_{max}/K_m ~ 30 -fold shifting the kinetic equilibrium towards a tense or inhibited state. G6P binding to either state will completely activate the enzyme, resulting in a relaxed state with maximal activity. G6P binding increases the V_{max}/K_m value 2.5-fold over the intermediate state and more than 50-fold over the inhibited state. Phosphorylation of γ Gsy2 increases the AC_{50} for G6P by 20-fold from 0.04 mM to 0.8 mM.

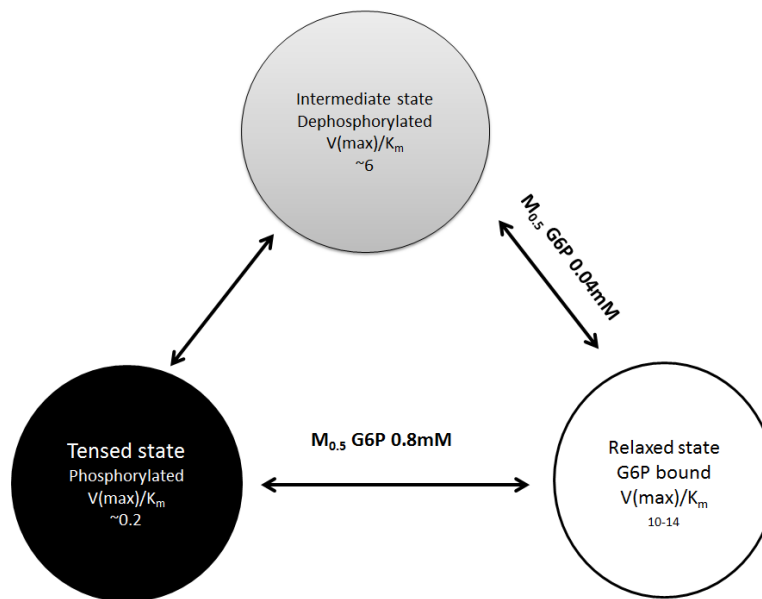


Figure 9. Three state kinetic model for γ Gsy2.

Yeast GS exists in the intermediate state when non-phosphorylated, upon phosphorylation the equilibrium shifts towards the highly inhibited tensed state. G6P binding can fully activate GS to relaxed state. Figure adapted from *J. Biol. Chem.* 275, 27753-61, (2000).

7. Structural studies on eukaryotic glycogen synthase

Crystal structures are available only for two eukaryotic glycogen synthases, *Saccharomyces cerevisiae* (63) and *Caenorhabditis elegans* (74). The crystal structure of the yeast GS isoform 2 was solved for both the intermediate and G-6-P bound activated state (Figure 10A and 10B). In the case of *C. elegans*, the structure was solved in complex with the C-terminal 34 amino acids of human glycogenin (Figure 10C), but the overall structure of CeGS was found to be very similar to the basal or the intermediate state of yeast GS (Figure 10D).

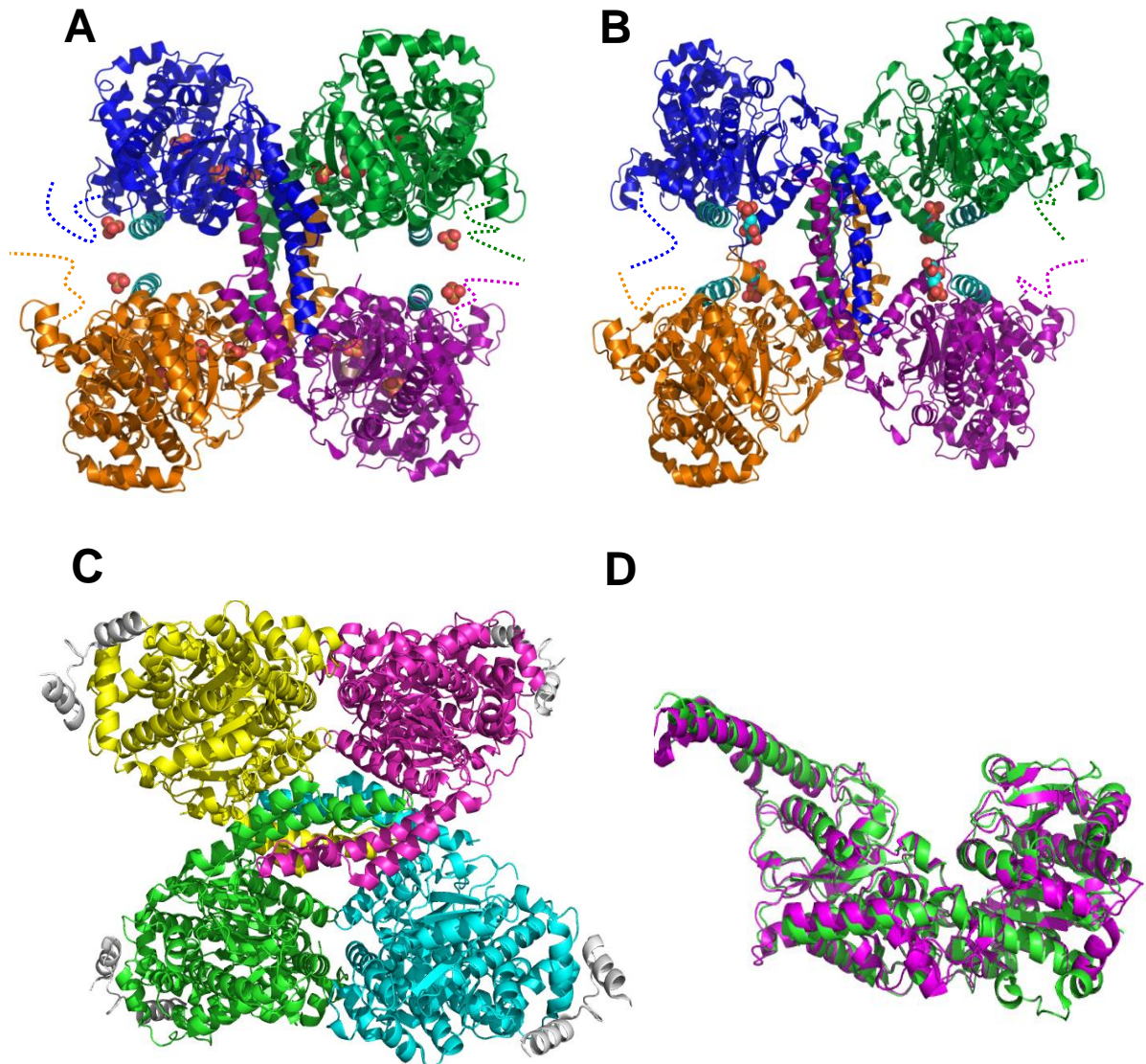


Figure 10. Crystal structures of yeast and Ce GS.

Ribbon representation of the A. basal and B. the activated state of yeast Gsy2. Each monomer is color coded. The regulatory helix carrying the arginine cluster is shown in cyan. G6P and the sulfate ions are shown in space filling atom model. C. Crystal structure of CeGS. The crystal structure of CeGS was solved in complex with the 34mer C-terminal tail of human glycogenin (grey). D. Cartoon representation of the superposed monomers of Sc GS (green) and Ce GS (magenta). Coot was used for super-positioning of both the monomers.

Both the yeast and *C. elegans* GS (CeGS) share more than 50% sequence identity to its mammalian counterparts (~55% when compared to human GS muscle isoform). The major difference between the two species is

that CeGS retains the N-terminal phosphorylation sites (sites 2, 2a) while the yeast enzyme lacks them (Figure 11). Both species lack the extreme C-terminal phosphorylation sites (1a and 1b). GS exists as a tetramer in all the crystal structures. Like the other GTB fold family enzymes, each monomer of GS is made up of two structural domains: an N-terminal Rossmann fold domain and a C-terminal Rossmann fold domain (75). A unique eukaryotic insertion of approximately 100 amino acid residues forms most of the inter-subunit interactions.

The regulatory helices containing the cluster of six arginine residues lie at the end of the C-terminal domain and are situated anti-parallel to each other across one of the molecular 2-fold axes in the tetramer (Figure 10A). It is interesting to note that CeGS lacks the last two arginine residues of the cluster (Arg589 and Arg592). There is a small insertion of around 13 amino acids on the C-terminal domain (from 481-492 in yGSy2p) which provides selectivity to the nucleotide donor UDP-glucose for the eukaryotic forms rather than ADP-glucose, as observed in the bacterial and archaeal forms.

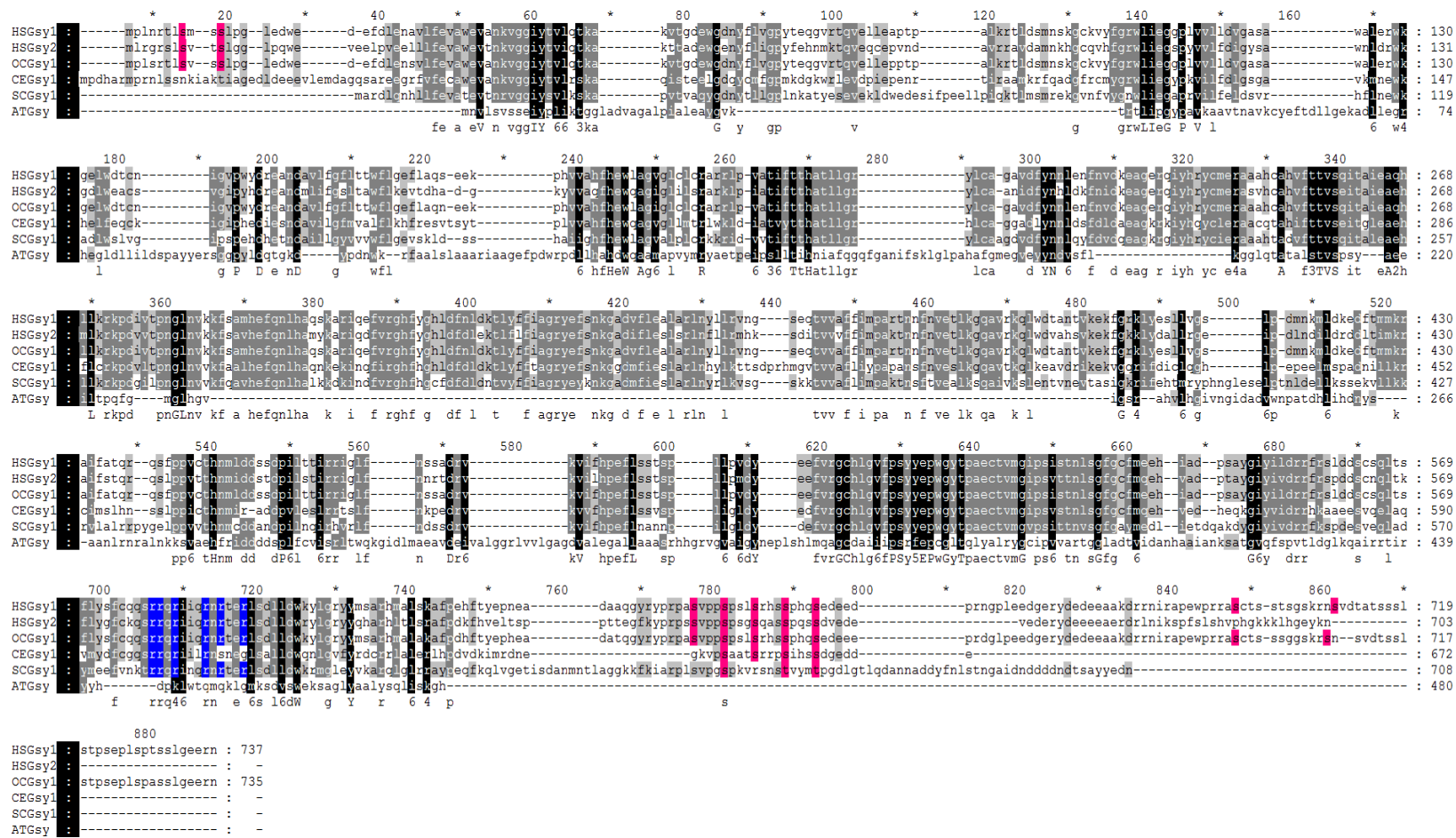


Figure 11. Multiple sequence alignment of various species of GS.

The conserved arginines of the arginine cluster are shown in blue and the phosphorylation sites are shown in red. Clustal omega was used for alignment and the Genedoc software was used for further manipulations.

Glucose-6-phosphate binds to a surface pocket adjacent to the N-terminus of the regulatory helix making extensive interactions involving more than one subunit (Figure 10B). The 6-phosphate binding pocket is composed of five positively charged amino acid residues: His286, Lys290, His500, Arg583 and Arg587 (Figure 12A). The last two amino acids are the third and fourth arginine residues of the arginine cluster. G6P binding to yGsy2p orders a loop (residues from 278 to 284) which was found to be disordered in the basal state structure of the yeast enzyme. Binding of G6P and reordering of residues 278-284 is associated with large scale translational and rotational movements across the regulatory interface.

The large scale structural transitions associated with G6P binding can be better understood if we compare the dimers of the UDP-bound basal state and activated state structures (Figure 12B and 12C). In the basal state structure, the loop connecting the β -strand 16 and helix α 18 are positioned across the molecular 2-fold axes and make contact with each other. The α -helix 16 of one monomer makes contacts with strand β 3 and helix α 2 of the opposing monomer. Upon G6P binding, the subunit contacts are reformed by a subunit translation of more than 15 Å such that α 15, α 16 and the loop connecting β -strand 16 and α -helix 18 are no longer at the molecular axes of the dimer and form new interactions with α -helices 15 and 16 of the adjacent monomer. These altered interactions coupled with a rotational opening of the N-terminal domain by 4.5°, widens the catalytic cleft and affords better acceptor access. The structural findings are consistent with the known kinetic properties which showed that G6P

binding does not affect the binding of the nucleotide donor while it improves the K_m for the acceptor by ~50%.

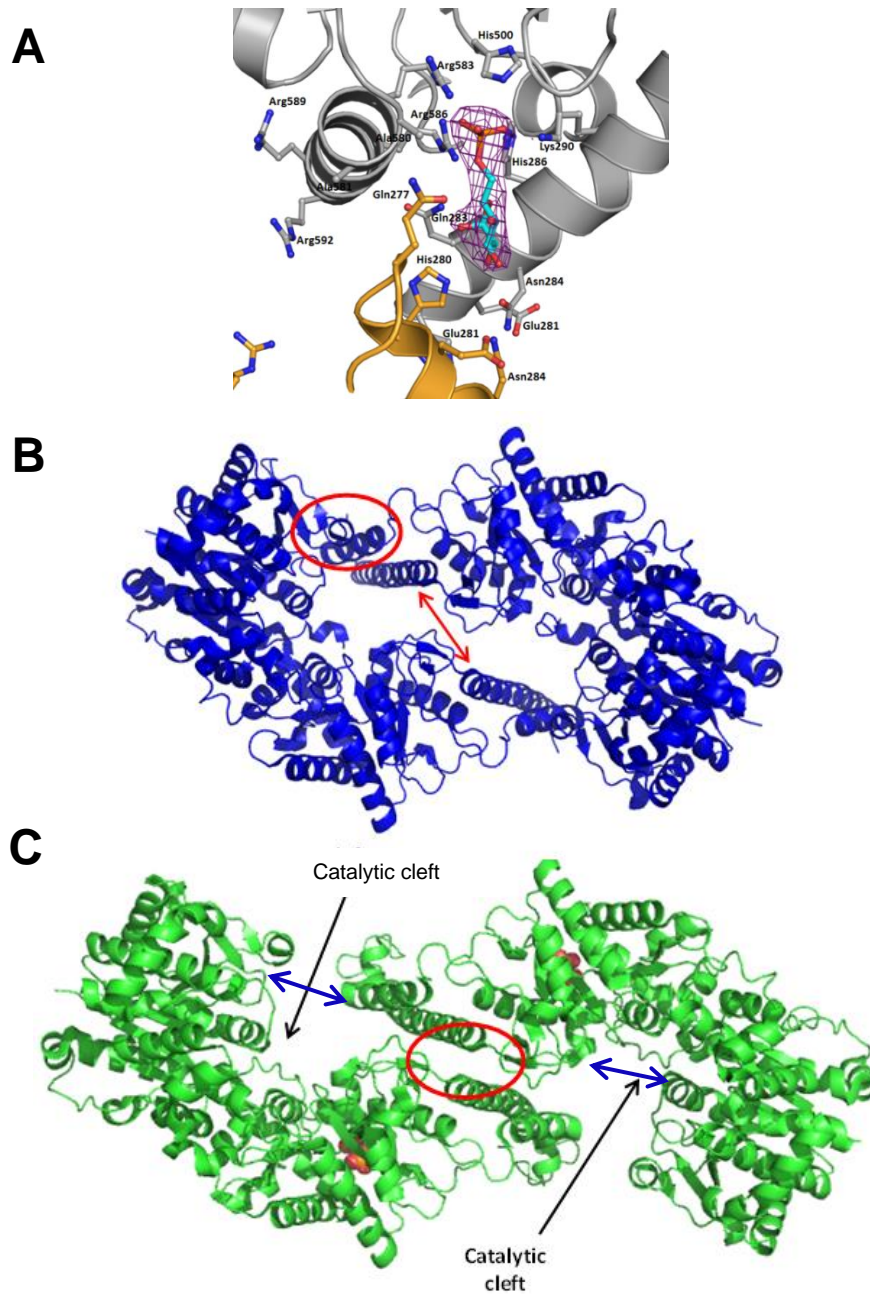


Figure 12. G6P mediated activation of GS.

A. Cartoon representation of the G6P binding pocket. G6P and the surrounding residues with which it interacts are shown in stick model. Ribbon representation of a dimer of Sc GS B. in the absence of G6P and C. in the presence of G6P. Each monomer is color coded separately and the blue arrows are used to show the loss and gain of interaction before and after G6P binding.

7. Role of the regulatory arginines

As mentioned previously, the regulatory helices of adjacent monomers lie at the end of the C-terminal domain and are situated anti-parallel to each other across one of the molecular 2-fold axes in the tetramer. Arg580, Arg583 and Arg587 are adjacent to the G6P binding site and make interactions with the allosteric activator while the other three arginine residues (Arg581, Arg589 and Arg592) lie on the opposing face of the helix and oriented away from the protein surface facing the regulatory helix in the opposing subunit. In the basal state structure, the regulatory helices are separated by a distance of 8 Å. The binding of G6P pushes the regulatory helices apart by an additional 4 Å (Figure 13A and 13B).

In order to delineate the role of each of the six arginine residues, mutational studies were performed (63). The third and fourth arginine residues of the arginine cluster (Arg583 and Arg587) form essential interactions that anchor the phosphate of G6P within its binding pocket. Consequently, mutating either one or both of the arginine residues to alanine created an enzyme insensitive to G6P activation. Mutating the first two arginine residues (Arg580 and Arg581) to alanine did not affect the activity of the dephosphorylated enzyme. However when Arg580 was mutated to alanine phosphorylation at Thr668 did not fully inhibit the enzyme.

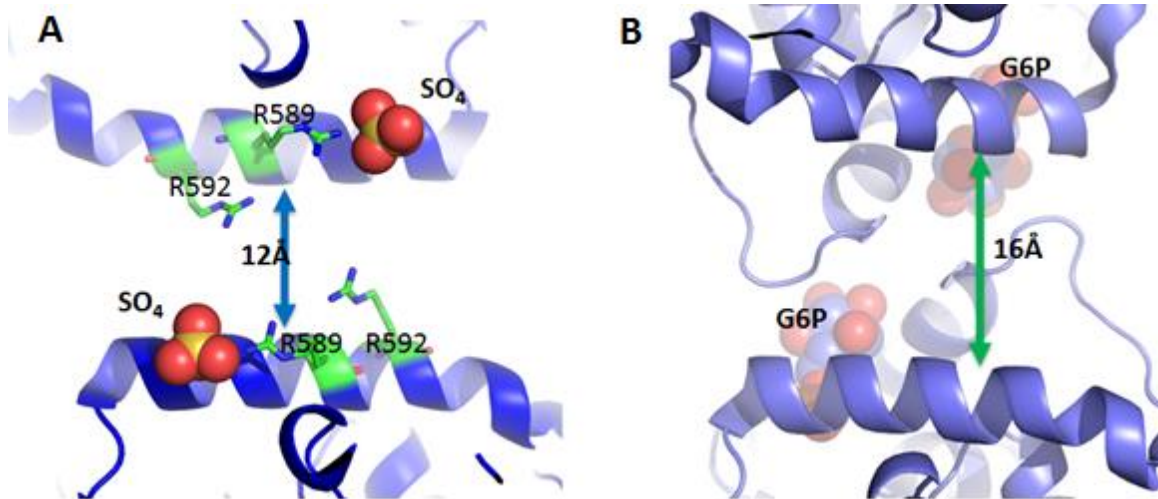


Figure 13. Role of the regulatory helix.

Ribbon representation of the regulatory helix of adjacent monomers in the A. basal and B. G6P bound activated state of Sc GS. The sulfate and G6P molecules are shown in space filling model. The Arg589 and Arg592 of adjacent monomers in the basal state structure are position anti parallel to each other.

Mutating both Arg580 and Arg581 to alanine led to an enzyme whose activity ratio was similar with or without phosphorylation (63). Alternatively, mutating the arginines 589 and 592 to alanine drastically decreased the basal state activity to a level that is similar to the wild-type enzyme phosphorylated at Thr668. However, the double mutant retained its ability to be activated by G6P. Therefore, Baskaran et al. (63) proposed that the first two arginine residues of the cluster stabilize the enzyme in the inhibited state upon phosphorylation while the last two arginine residues keep the enzyme in the basal state. Evidence for Arg589 and Arg592 mediated stabilization of the basal state also comes from the basal state structure where the two arginines of adjacent monomers were positioned across each other. The charge repulsion between the two arginines appears to keep the enzyme in the basal state. Mutating the arginines to alanine

results in charge neutralization at the regulatory interface and leads to an inhibited enzyme.

8. Donor binding at the catalytic site

Eukaryotic GS uses UDP-glucose as the activated sugar donor. Along with glucose, trace amounts of glucosamine were also found in mammalian glycogen (13). Studies demonstrate that rabbit GS was capable of using UDP-glucosamine as the sugar donor (76). The same study showed that glucosamine is incorporated into glycogen at a rate 12-times slower than that for glucose. GS utilization of UDP-galactose/galactosamine, UDP-N-acetyl-glucosamine and UDP-xylose as sugar donors is controversial (77-81). However, structural information only exists for UDP-glucose in complex with yeast GS.

The nucleotide donor UDP-glucose binds in a groove along the surface of the C-terminal Rossmann domain. The positioning of free UDP is unchanged in both the basal (63) and activated state structures (82). However, UDP binding in the activated state structure differs depending on whether the glucose is also bound in the active site (82). The major difference in UDP binding is due to a repositioning of the two phosphates in the binding site (Figure 14A and 14B). When bound productively for transfer, both the α - and β -phosphates of UDP lie parallel to the plane of the glucose residue, in a bent conformation. However, after transfer (UDP product structure), the positioning of the two phosphates changes such that the phosphate interaction with the surrounding amino acid residues is switched.

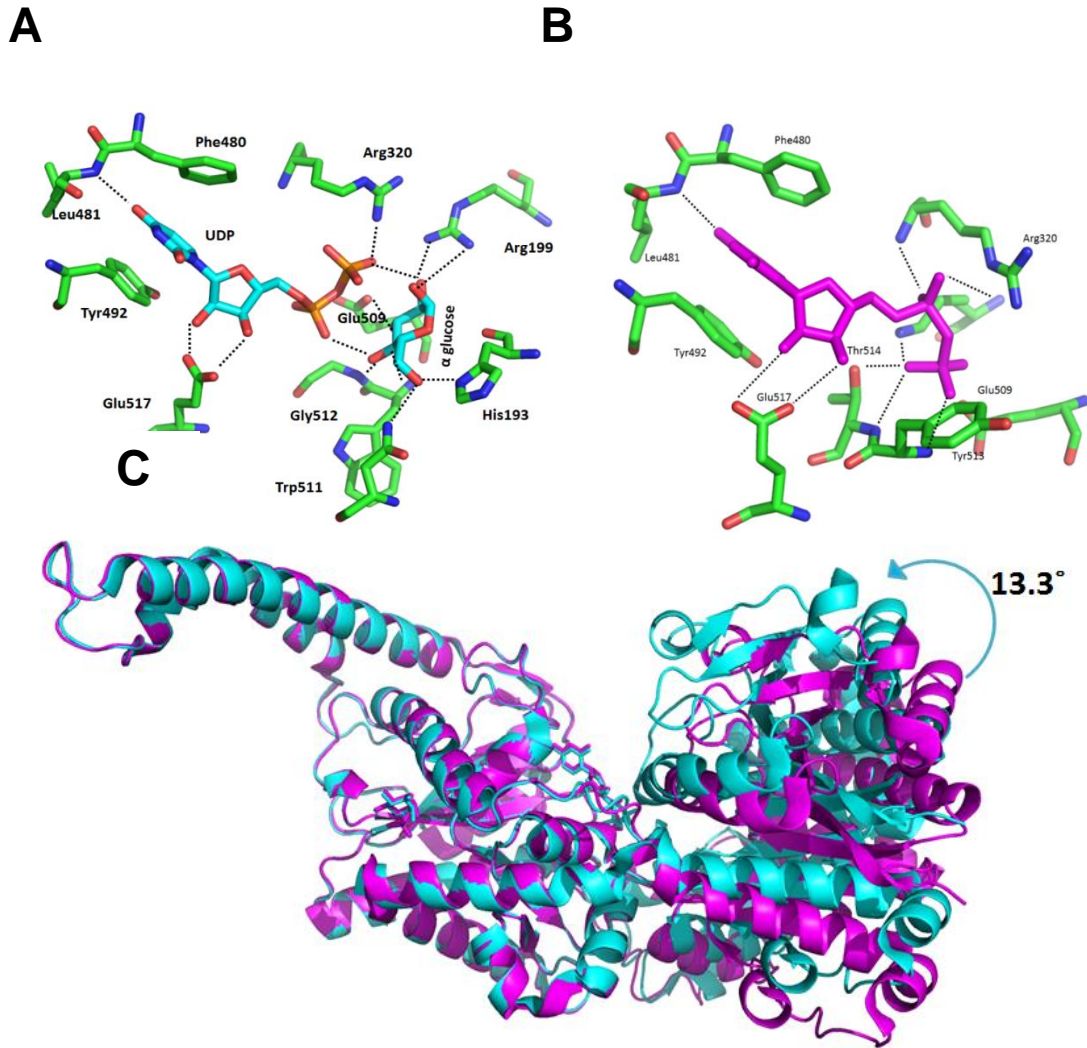


Figure 14. UDP•G binding in yGsy2.

Ribbon representation of the active site of *Sc* GS with A. UDP and glucose (pre-transfer) and B. UDP (post-transfer) only bound structures. The interactions made by the ligands with its surrounding amino acid residues are shown in dotted lines. C. Superpositioning the monomers of UDP only (magenta) and UDP•G (cyan) bound structures. The entire C-terminal domain was used for alignment (300-600). The figure was made using Pymol.

In the productive substrate complex (UDP•G bound), the α -phosphate is in hydrogen bonding distance to Tyr513 and Thr414 and the β -phosphate interacts with the side chains of Lys326 and Arg320. However, in the product transfer, the

α -phosphate that interacts with Lys326 and Arg320 and the β -phosphate is now in hydrogen bonding distance to Tyr513 and Thr514.

The glucose moiety of UDP•G makes several interactions with the surrounding amino acid residues (82). In particular, the 6'-OH group of glucose interacts with the two highly conserved amino acids His193 and Asn269. The 4'-OH group is within hydrogen bonding distance to the peptide nitrogen of Gly512 and one of the phosphate oxygens, while the 3'-OH group interacts with the side chains of Trp511 and the highly conserved Glu509. Lastly, the 2'-OH group of glucose interacts with the side chains of Arg199 and the β -phosphate of UDP. An important feature of glucose binding in the active site is the closure of the N-terminal domain toward the C-terminal domain. The N-terminal domain of UDP•G bound structure is 13.3° more closed when compared to the UDP product complex (Figure14C).

9. Proposed catalytic mechanism

There is considerable debate over the chemical mechanism of retaining glucose transferases where the stereochemistry of the product anomeric carbon is retained with respect to the donor substrate. Both S_N2 or S_N1/S_{Ni} mechanisms have proposed for these retaining glucose transferases (82, 83). Mutational studies have shown that there is no easily identifiable amino acid in the active site of GS that acts as a nucleophile which is a required feature for a S_N2 based reaction mechanism (82). As a result, the S_N1/S_{Ni} mechanism is now gaining more support (82, 84). According to this mechanism, the β -phosphate of the UDP leaving group most likely deprotonates the 4'-OH group of the acceptor so it can

serve as a nucleophile and attack the C1 position of glucose, with the nucleophilic attack and exit of the UDP leaving group occurring from the same face of glucose (Figure 15). This mechanism also requires the formation of an oxo-carbenium ion like intermediate. Unlike glycogenin, GS does not use metal ions during glucose transfer, and therefore, stabilization of the UDP leaving group occurs via hydrogen bond interactions, which include amino acid residues Arg199, Arg320 and Lys326 and the helical dipole contributed by residues 513-521 (Figure 14A).

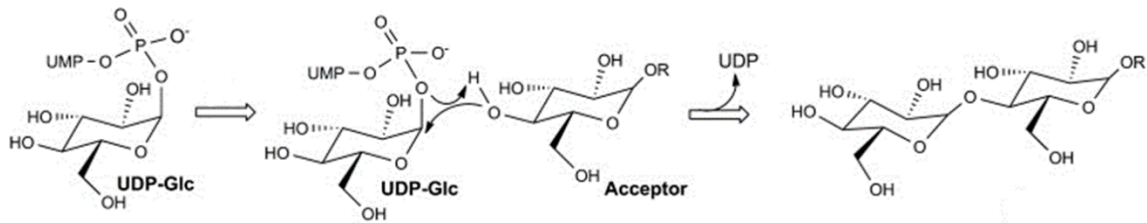


Figure 15. Catalytic mechanism of GS

S_Ni mechanism for catalysis. Deprotonation and the nucleophilic attack is shown using black headed arrows.

RATIONALE AND OVERVIEW OF THE THESIS RESEARCH

The overall aim of this project is to understand the structural basis for the regulated inhibition and appropriate substrate selection in the GT3 family of enzymes. For this, we will use yeast glycogen synthase as a structural model. Yeast GS is ~50% identical to its mammalian counterparts and also shares many of the regulatory and catalytic mechanisms of the higher eukaryotic enzymes.

Despite structural information on the activated and basal states of yeast GS, very little is known about the enzyme's inhibited state. To gain structural insights into the inhibited state, we used the yGsy2-R589A/R592A mutant as a surrogate for the phosphorylated enzyme. This double mutant has basal activity level similar to the Thr668 phosphorylated enzyme but, at the same time, retains the ability to be completely activated by G-6-P. In particular, our laboratory has solved the structure of the activated form of this enzyme. Consequently, to complete our understanding of the transitions between activity states, we aim to determine the three dimensional structure of the low-activity state of the R589A/R592A double mutant enzyme using X-ray crystallography to define the structural features that define the inhibited state.

Apart from UDP-glucose, eukaryotic cells also contain other nucleotide-sugar donors such as UDP-glucosamine, UDP-galactose and UDP-xylose. Yeast, in particular, uses these different UDP-sugar donors in the synthesis of its cell wall and chitin septum (85). Unlike the yeast cell wall, the structural integrity of glycogen has no known functional reason to incorporate different sugars into its structure. In addition, glycogen has a well-defined tertiary structure and the

addition of a sugar other than glucose can be detrimental to its structure and its branching properties. Hence, yGsy2 has to be very selective in choosing the right sugar donor as its substrate. In this project, we used X-ray crystallography and enzyme kinetics to determine the molecular basis by which yGsy2 discriminates between different UDP-sugar donors to be used as substrates by the enzyme.

EXPERIMENTAL PROCEDURES

1. Site directed mutagenesis

The wildtype, R589A/R592A and E169Q mutants of yGsy2 in the pET-28a expression plasmid were prepared previously by other lab members (63, 71).

The other mutant constructs (R581A/R592A and R581C/R592C) were created from the wildtype sequence using PCR-based site directed mutagenesis approach. The following primers were used for amplification for site directed mutagenesis (obtained from Integrated DNA Technologies).

R581C:

Forward primer: 5' GTAAAAAAGACAAGATGCCAAAGAATTAATCAAAG3'

Reverse primer: 5'CTTTGATTAATTCTTTGGCATCTTGTCTTTTTTAC3'

R592C:

Forward primer: 5' GAAATAGAACTGAATGCACTGTCCGACTTACTG3'

Reverse primer: 5' CAGTAAGTCGGACAGGCATTCAGTTCTATTTTC3'

R581A:

Forward primer: 5'GTAAAAAAGACAAGAGCGCAAAGAATTAATCAAAG3'

Reverse primer: 5' CTTTGATTAATTCTTTGCGCTCTTGTCTTTTTTAC3'

R592A:

Forward primer: 5' GAAATAGAACTGAAGCAACTGTCCGACTTACTG3'

Reverse primer: 5' CAGTAAGTCGGACAGTGCTTCAGTTCTATTTTC3'

Pfu Ultra II HS fusion polymerase obtained from Stratagene was used for the amplification of the plasmids. The original parental DNA in the amplified reaction mix was then digested by Dpn I (New England Biolabs). The Dpn I

treated reaction mix was then transformed into DH5- α competent cells. Following transformation, a single colony is inoculated into 10mL of LB media containing 50 μ g/mL of Kanamycin and incubated with shaking overnight. The DNA plasmids from the colonies were isolated using the Qiagen Miniprep kit (27104). The point mutations were confirmed by DNA sequencing of the plasmids either at the DNA sequencing core facility of the IU School of Medicine or at Geneseq.

2. Expression and purification of yGsy2

The protein from each yGsy2 construct was expressed and purified as described below. The cysteine mutant enzyme was purified similarly but no reducing agents were used during purification and storage. The N-terminal His-tagged yGsy2 constructs (pET-28a) were expressed in *E. Coli* BL 21 cells. Following transformation of the plasmid into BL21 competent cells, a single colony was inoculated in 50 mL of LB broth and allowed to grow overnight at 37°C. The overnight culture was diluted to 6 L using the pre-inoculum and allowed to grow at 37° C until an OD₆₀₀ of 0.6 was reached, at which point, the protein expression was induced by the addition of 0.1 mM of IPTG. The cells were incubated at 16° C for an additional 16 hours. Cells were collected by centrifugation and resuspended in lysis buffer containing 20 mM Tris-HCl, pH 7.8, 300 mM NaCl, 2 mM Benzimidazole, 1 mM β -mercaptoethanol (BME) and 0.1% Triton X-100. Cells were then lysed by passing three times through the micro-fluidizer at 12,000 PSI and the lysate was clarified by ultracentrifugation at 35,000 rpm for 35 min. The clarified cell lysate was loaded onto a Ni²⁺-nitrilotriacetic acid-agarose (Qiagen) column that was pre-equilibrated with lysis

buffer. After loading the cell lysate, the column was washed to a baseline absorbance using the lysis buffer. Then two separate wash buffers containing 25 mM and then 50 mM of imidazole in lysis buffer were used to wash the column to elute the non-specifically bound proteins. The bound yGsy2 protein was eluted with a linear gradient of 50-200 mM imidazole added to lysis buffer. The column elution was collected in fractions of 6 mL, and then the fractions were analyzed for yGsy2 protein by running on a 10% SDS-PAGE to visualize the protein levels. Those fractions that had the desired protein were pooled and dialyzed against the Q-Sepharose loading buffer containing 20 mM TRIS-HCl, pH 8.0, 1 mM ethylenediaminetetraacetic acid (EDTA), 2 mM benzamidine and 1mM BME. The dialyzed sample was loaded onto a Q-Sepharose fast flow (GE Healthcare) column which was pre-equilibrated with the loading buffer. The column was washed to baseline absorbance with the loading buffer and the bound protein was eluted using a linear gradient of 0-1 M NaCl in the loading buffer. The eluted fractions were analyzed by running a 10% SDS-PAGE gel and those fractions containing >90% yGsy2 was pooled and dialyzed against the buffer containing 20 mM TRIS-HCl, pH 8.0 and 1mM BME. The dialyzed protein was concentrated to a final concentration of 4 mg/mL using the Amicon Centricon-30 centrifugal concentration devices. The concentrated protein was then filtered using microfuge centrifugal filters, aliquoted to small volumes of 200 μ L, flash frozen in liquid nitrogen and stored at -80° C.

3. Non-reducing SDS PAGE

In order to demonstrate how disulfide bonding might influence subunit associations, the cysteine mutants were analyzed using a non-reducing SDS PAGE. The wildtype and yGsy2-R581A/R592A mutant enzymes were used as controls. The purified proteins were allowed to pass through an 8% non-reducing SDS PAGE gel using standard discontinuous buffer systems. We prepared two different samples for each mutant enzyme, one containing 250 mM BME and another that lacked BME in the sample treatment buffers. 5 µg of the purified recombinant proteins were loaded onto the gel which was developed at 170 V for 80 minutes and stained with Coomassie brilliant blue R-250.

4. Gel filtration

The purified yGsy2-R581C/R581C mutant was loaded onto the size exclusion column; Superpose 6 10/300 GL, at a flow rate of 0.5 ml/min both in the presence and absence of 250 mM BME. A solution containing 100 µg each of thyroglobulin (669 kDa), ferritin (440 kDa), aldolase (160 kDa), conalbumin (73kDa) and ribonuclease (13 kDa) provided molecular weight standards to calibrate the column's elution profile. The apparent molecular weight of yGsy2-R581C/R592C was calculated from the standard curve obtained from these molecular weight standards.

5. Crystallization

5. A. yGsy2 R589A/R592A mutant

Crystallization screening for the yGsy2-R589A/R592A mutant was performed using 96-well plates in the Art Robbins, Inc. Gryphon crystallization robot. We used commercially available crystal screening solutions from Hampton Research and Emerald Biosystems for the screening procedure. The apo enzyme and the crystallization solutions were mixed in 1:1 ratio (200 nL each) and allowed to equilibrate against 50 μ L of the crystallization solution. After 72 hours, clusters of hexagonal crystals formed in one crystallization condition comprising 0.1 M TRIS-HCl, pH 8.0, 200 mM $MgCl_2$ and 20% PEG 8000. This particular condition was chosen for further optimization. After several rounds of optimization, we found that single diffracting crystals can be obtained only after micro-seeding and only in the presence of UDP-glucose.

The conditions for yGsy2-R589A/R592A were scaled up to 2-3 μ L volumes and were incubated using the hanging drop vapor diffusion method. The protein solution was prepared at 2.5 mg/mL and contained 10 mM UDP-glucose. The protein/substrate solution was combined with an equal volume of a crystallization reservoir solution composed of 100 mM TRIS-HCl, pH 8.4-8.9, 200 mM $MgCl_2$, and 5-10% (w/v) PEG 6000. Physically twinned hexagonal crystals were obtained in 5-7 days. These crystals were crushed using the seed bead kit from Hampton research to form the seed stock solutions. The seed stock solutions were made in the mother liquor solution containing 100mM TRIS-HCl, pH 8.9, 200 mM $MgCl_2$ and 10% PEG 6000 and serial dilutions of the seed

stocks were made in the same mother liquor. Two μL of the protein/substrate solution containing 0.2 μL of the seeds were mixed with 2 μL of the reservoir solution described above and allowed to equilibrate against the reservoir solution at room temperature. Single hexagonal crystals of yGsy2-R589A/R592A appeared in about 5-7 days and grew to a maximum length of 200 μm .

Prior to data collection, the crystals were cryo-protected by quickly transferring them to a fresh reservoir solution to which a final concentration of 15% (v/v) ethylene glycol had been added. Crystals treated in this manner were immediately flash frozen at 100 degrees Kelvin directly in the gaseous nitrogen stream for analysis by X-ray diffraction.

5. B. UDP-glucose analogues in the activated state

The crystal complexes of G6P bound yGsy2 mutants (either R589A/R592A or E169Q) and different UDP-sugar donors were obtained using the hanging drop vapor diffusion method using previously determined conditions. The following UDP-glucose analogues were used for the co-crystallization experiment.

1. UDP-glucosamine (synthesized by Dr. Vimbai M. Chikwana)
2. UDP-galactose (Sigma, U4500)
3. UDP-N-acetylglucosamine (Sigma, U4375)
4. UDP-2-deoxy-2-fluro-glucose (synthesized by Dr. Vimbai M. Chikwana)
5. UDP-xylose (Carbosynth, MU07658)

The protein at 2.5 – 3.0 mg/mL was mixed with 25 mM of G-6-P and 10 mM of the respective UDP-sugar donor. Three μL of the protein/G-6-P/donor

complex was then combined with equal volume of the reservoir solution containing 100 mM Bis-Tris, pH 6.2-6.5 and 21 – 26 % PEG 300. The protein/reservoir mixture was then allowed to equilibrate at room temperature against 500 μ L of the reservoir solution in a hanging drop set up. Crystals started forming after 3 days and grew to a full size of 200 μ m after around 3 weeks. The crystals were then dehydrated by sequentially transferring the drops in increments of 5% to a final reservoir solution containing 30% PEG 300. The dehydrated crystals were mounted on to the X-ray machine and frozen at 100 K using the gaseous nitrogen stream.

6. Hydrolysis of UDP-glucose analogues by yGsy2

In order to test whether the different UDP-sugar donors were hydrolyzed by yGsy2, 5 μ M of yGsy2 wildtype enzyme containing 1mM G6P was incubated with 100 μ M of the different UDP-sugars to a final volume of 100 μ L. Fifty μ L of the reaction mix (t_0) was immediately boiled, while the other 50 μ L ($t_{O/N}$) was allowed to incubate overnight at room temperature. Following the overnight incubation, the reaction mix was boiled to terminate the reaction. Both t_0 and $t_{O/N}$ samples were then analyzed by high performance anion exchange chromatography (HPAEC) using a Dionex ICS3000 system and Chromeleon software. All samples were filtered prior to injection. Eluent A consisted of 1 mM sodium hydroxide (NaOH), and Eluent B consisted of 1 mM NaOH containing 1 M sodium acetate (NaOAc). HPLC conditions were based on prior settings (86), and a 2x250-mm CarboPac PA1 column (Dionex) was used at a flow rate of 0.25 ml/min. The elution profile (expressed in terms of percentage of eluent B) was

20-50% from 0 to 10 min, 55-85% from 10 to 35 min and 85-100% from 35 to 40 min with a flow rate of 0.25 ml/min. As a standard, 100 μ M UDP and 10 μ M of UMP were similarly analyzed on the HPAEC column. The hydrolysis products for the UDP-sugars were detected by the decrease in the UV peak size of the donors and the appearance of a new UV signal corresponding to the standard UDP peak.

7. X-ray diffraction, data Collection, processing, structure determination and refinement

7. A. Data collection

The yGsy2-R589A/R592A mutant crystal diffraction data were collected at the beamline 19-BM operated by the Structural Genomics Consortium located at the Argonne National Laboratory. The diffraction data were then indexed, integrated and scaled using the HKL 3000 program suite.

The diffraction data for the G6P bound yGsy2-R589A/R592A and yGsy2-E169Q co-crystallized with UDP-glucose sugar analogues were collected either at the 23-ID or 19-ID beamlines operated by GMCA-CAT and Structural Biology Center at the Advanced Photon Source. The data collected were then indexed, integrated and scaled using either the HKL 3000 program suite or the XDS auto process suite (87).

7. B. Structure determination, model building and refinement

The crystal structure of yGsy2-R589A/R592A was solved by the method of molecular replacement. The program PHASER MR (88) as implemented in the Collaborative Computational Project Number 4 (CCP4) (89) was used for

molecular replacement, using a monomer of the basal state yGsy2-R580A/R581A/R583A (pdb code: 3NAZ) structure as the search model. The structural model was refined using REFMAC5 (90), part of CCP4 program package. The Britton and H-test for twinning were consistent with merohedral twinning with a twin fraction of 0.31. Consequently, all models were refined using amplitude-based twin refinement in REFMAC5 as implemented in the CCP4 program suite. Each refined model was visually inspected and manually adjusted using the molecular display program COOT (v0.7.2.1) (91). The ligands UDP and UMP were manually docked into the active site using the program COOT and the merged models were subjected to further restrained refinements using REFMAC5. The monomer libraries for UDP and UMP were obtained from the structures previously deposited in RCSB protein data bank (PDB) (pdb codes: 4KQ1, 4KQM, respectively).

The different nucleotide bound activated structures of the activated yGsy2-R589A/R592A enzyme and yGsy2-E169Q were solved by molecular replacement using MOLREP as implemented in CCP4 using the G6P bound yGsy2-R589A/R592A structure (pdb code: 3NB0) as the search model. The refinement program REFMAC5 in CCP4 was used for refining the structural models. The monomer libraries for the nucleotides were obtained from the previously deposited crystal structures in RCSB PDB. (pdb codes: UDP-N-acetylglucosamine: 3ST8 ; UDP-xylose: 4WNH; UDP-galactose: 1O0R; UDP-2-fluoro-2-deoxy-glucose: 1UQT). The monomer library for glucosamine was created using the program Sketcher in CCP4. The ligands were manually docked

into the active site and after merging the pdb coordinates; the merged structure was refined again using REFMAC5.

8. Structural alignments and domain motion measurements

Different structures of yGsy2 were aligned/superposed using either the LSQ superpose feature in the molecular display program COOT or the Superpose program, part of the CCP4 program suite. In order to observe the overall structural changes between the yGsy2-R589A/R592A inhibited state structure and the yGsy2-R580A/R581A/R583A basal state structure, the C-terminal domains (298-600) of one state were aligned with the corresponding C-terminal domains of the other state with an additional alignment criterion to fit only those atoms of the moving molecule that are in the spherical radius of 30 Å centered to the reference molecule using the program Superpose in CCP4.

The N-terminal domain motions were obtained by superposing the C-terminal domains of different yGsy2 structures and the rotational matrices required to align the corresponding N-terminal domains were obtained from the aligned structures. The Protein Domain Motion Analysis program, Dyndom (92), was also used to measure the N-terminal domain motions.

9. Glycogen synthase activity measurements

9. A. Glycogen treatment

The glycogen used in the GS activity measurements were first treated with TMD-8 hydrogen and hydroxide form mixed bed resins (Sigma-Aldrich) to remove of any contaminating charged small molecules. The 10-15 mL of the TMD-8 resins was washed with 3 column volumes of Milli-Q purified water in a 50

mL falcon tube. A freshly prepared sample of 10% rabbit liver Glycogen Type III (Sigma-Aldrich) was then mixed with the washed TMD-8 resins and incubated on a rotator shaker for 1 hour at room temperature. The resin was then allowed to settle down, and the supernatant is collected. Ice cold ethanol (95%) was added to a final concentration of 66% ethanol. In order to facilitate precipitation of glycogen, one or two drops of 1M NaCl was added, and the precipitated glycogen was collected by centrifugation at 8000 rpm at 4° C for 20 min. The precipitated glycogen was resuspended in 95% ethanol and precipitated again using the similar centrifugation method. The glycogen pellet was allowed to air dry and ground to a fine powder with the help of a mortar and pestle. For small quantities of glycogen, the precipitated glycogen was resuspended in 0.5 mL of 95 % ethanol and dried using a Speed Vac. The glycogen powder was then dissolved to 10% w/v with distilled water.

9. B. Glycogen synthase assays

i. Standard condition

Glycogen Synthase activity was measured using the standard filter paper assay as described by Thomas et al (93). The assay quantifies the amount of ¹⁴C-glucose that is incorporated from UDP-¹⁴C-glucose into glycogen over a 15 min time period at 30°C. The standard reaction condition uses 4.44 mM of UDP-glucose and 6.7 mg/ml of glycogen as near saturating substrate levels. GS dilution buffer contains 50 mM TRIS-HCl, pH 8.0, 2 mM EDTA, 0.1% treated glycogen and 1 mM DTT. Protein samples were diluted to a final concentration of 0.02-0.05 mg/mL using the GS dilution buffer. Fifty µL of the reaction mix

containing the ^{14}C UDP-glucose, 6.66 mM of cold UDP-glucose and 8 % w/v treated glycogen is pre-warmed in a 30°C water bath for 10 min. 25 μL of GS sample in the dilution buffer is then mixed with 50 μL of the reaction mix and allowed to incubate at 30°C for 15 min. Following the incubation, 65 μL of the reaction mix was spotted on the 31-ET chromatographic filter paper. The filter papers were washed three times in 66% ethanol with the help of the perforated double beaker. The filter papers were then dried under a heat lamp, transferred to a vial and filled with scintillation fluid. The ^{14}C counts were measured with a scintillation counter. For all the yGsy2 mutants, the activity was measured both in the absence and presence 7.2 mM (saturating concentration) of G6P.

For the cysteine mutants, the dilution buffer lacked any reducing agents. In order to measure the activity in the presence of reducing agents, appropriate amounts of DTT/BME/TCEP were added to the reaction mix and the activity measurements were done exactly as described above.

ii. Activity ratio

Activity ratio is the ratio of the activity of GS in the absence of G-6-P to the activity of the enzyme in the presence of saturating amounts of G-6-P. It is a surrogate measure for the activity state of the enzyme even though not all phosphorylation events affect enzyme activity (1).

iii. Reducing agent titrations

Three different reducing agents, DTT, BME and TCEP were used for the reducing agent titration of the cysteine mutants. Initial stocks of the reducing agents were made in degassed water. For these titrations, the activity was measured under standard reaction conditions both in the presence and absence of G-6-P. The concentrations of the reducing agents were varied in the following manner: 1-200 mM BME; 0.1-20 mM DTT and 0.05-5 mM of TCEP.

iv. G-6-P titrations

For the G-6-P titrations, the concentrations of UDP-glucose and glycogen were 4.44 mM and 6.67 mg/mL, respectively and the activity was measured in 8 different concentrations of G-6-P varied in the range of 0.01-10 mM.

v. UDP-glucose titrations

The K_M values for UDP-glucose were determined by varying the concentration of the donor substrate between 0.05 mM and 6 mM with or without saturating amounts of G-6-P. The reaction mix had a fixed concentration of glycogen at 6.67 mg/mL. To examine whether BME can affect the K_M for UDP-glucose, a fixed concentration of 200 mM BME was used across different yGsy2 mutants.

vi. UDP-sugar donor titrations

The activity of yGsy2 wildtype enzyme was measured with varying concentrations of nucleotide sugar donors (UDP-FDG, UDP-galactose, UDP-glucosamine, UDP-GlucNac and UDP-xylose) in the range of 0.01 mM – 20 mM.

For this experiment, saturating amounts of G-6-P (7.2mM) and 0.5 mM of UDP-glucose was used.

10. Kinetic data analysis

All kinetic data analysis was performed using the program package SigmaPlot (version 12.3) by fitting the data to the appropriate binding or kinetic equation. The AC_{50} curves for G-6-P and reducing agents were fit to the four parameter logistic equation. The K_M values for UDP-glucose were obtained following a fit to the standard Michaelis-Menten equation $v = V_{max} * S / (K_m + S)$ where v is the measured reaction velocity, S is the substrate concentration, V_{max} is the maximum rate achieved by the system and K_M is the substrate concentration at half maximum velocity. The values presented in this work is the average \pm the standard error of the mean of three independent experiments (n=3).

RESULTS

1. Expression and purification of yGsy2

His-tagged yGsy2R589A/R592A protein was expressed and purified from the cell lysates of *E. coli* BL21-DE3 cells by Ni²⁺ affinity chromatography followed by anion exchange chromatography. The final elute from the Q-Sepharose column had more than 90% pure yGsy2 protein as estimated after staining the SDS-PAGE gels with Coomassie dye (Figure 16B). A typical prep of 6 L would yield as much as 25-30 mg of protein. There was no significant difference in terms of yield per liter for different yGsy2 mutants when compared to the wildtype enzyme. As described in the methods, expression and purification of the cysteine mutants was done without reducing agents at any point during purification and storage. The protein concentration was estimated by the method of Bradford using bovine serum albumin as the standard.

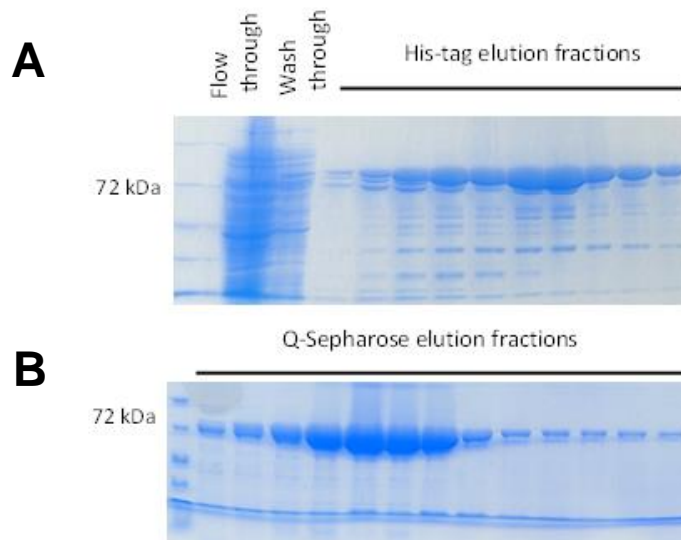


Figure 16. Representative SDS PAGE of ygsy2 purification.

Representative SDS PAGE gel of yGsy2-R589A/R592A. A. Ni-NTA column and B. Q-Sepharose column purification.

2. Crystallization of yGsy2-R589A/R592A

The initial crystals of the double mutant were physically twinned (Figure 17A) and microseeding methods were used to obtain individual crystals. The individual crystals formed did not diffract well but the addition of UDP-glucose to the protein mix improved the observed diffraction. The crystals diffracted to a maximum resolution of 3.6 Å at our home source. The crystals were found to be in the trigonal P3₂21 space group and diffracted to 3.3 Å at the synchrotron (Table 2).

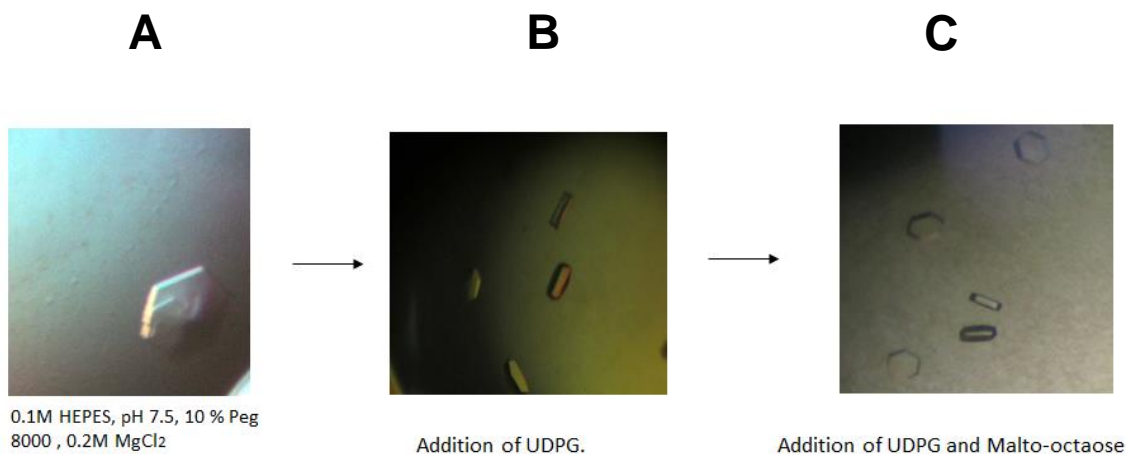


Figure 17. Optimization of yGsy2-R589A/R592A crystals.

A. Initial physically twinned crystals. B & C. Individual crystals obtained after seeding.

The yGsy2-R589A/592A and yGsy2-E169Q co-crystals with both G-6-P and UDP-glucose analogues were orthorhombic in shape and diffracted to a maximum resolutions between 2.7 – 3.2 Å (Table 2).

3. Structure determination and refinement

The crystal structure of the yGsy2-R589A/R592A double mutant was solved by molecular replacement using the monomer of the yGsy2-R580A/R581A/R583A triple mutant structure as the search model. Following molecular replacement, the appropriate amino acid substitutions were made and the structural model was refined using Refmac5 and included NCS restraints for each subunit domain combination. The structure was refined to a maximum resolution of 3.3 Å with a final $R_{\text{work}}/R_{\text{free}}$ of 0.17/0.22.

The crystal structures of the G6P bound UDP sugars were solved by molecular replacement and the structural models were refined using Refmac5 in CCP4 to a final $R_{\text{work}}/R_{\text{free}}$ values reported in Table 3.

Table 2. Data collection statistics.

	yGsy2- R589A/R592A	yGsy2- E169Q+25mM G6P+10mM UDP- Glucosamine	yGsy2- E169Q+25mM G6P+10mM UDPFDG	yGsy2- E169Q+25mM G6P+10mM UDP-Galactose	yGsy2- E169Q+25mM G6P+10mM UDP-GlucNac	yGsy2- wildtype +25mM G6P+10mM UDP-Xylose
Cell Parameters :	a = 124.7Å b = 124.7Å c = 278.1 Å α = 90.00° β = 90.00° γ = 120.00°	a = 193.04Å b = 205.8Å c = 204.6 Å α = 90.00° β = 90.00° γ = 90.00°	a = 193.5Å b = 206.5Å c = 204.7 Å α = 90.00° β = 90.00° γ = 90.00°	a = 193.665Å b = 205.099Å c = 206.446 Å α = 90.00° β = 90.00° γ = 90.00°	a = 192.53Å b = 205.76Å c = 204.44 Å α = 90.00° β = 90.00° γ = 90.00°	a = 192.99Å b = 204.32Å c = 206.67 Å α = 90.00° β = 90.00° γ = 90.00°
Space group	P 3 ₂ 2 1	I222	I222	I222	I222	I222
Twin fraction	0.31	NA	NA	NA	NA	NA
NA-not applicable						
DATA COLLECTION STATISTICS						
Resolution Range	50.0 - 3.3 Å	145-3.03 Å	145-2.73 Å	145-3.26 Å	145-2.9 Å	145-2.69 Å
Unique Reflections	28283	71743	102119	63020	83598	105353
Total Observations	1197984	307031	447683	261516	169710	
Completeness	99.4%	95.2%	99.5%	98.3%	98.08%	98.27%
Redundancy	4.8 (5)	4.27 (1.6)	4.16(4.15)	4.1(3.8)	3.9(3.5)	3.9 (3.4)
R _{pim}	0.069(0.306)	0.073 (2.6)	0.072(0.77)	0.061(0.473)	0.038(0.254)	0.033 (0.27)
CC1/2	0.703	0.997	0.999	0.998	0.999	0.823
R _{merge}	0.134(0.621)	0.079(0.23)	0.05(0.59)	0.072(0.557)	0.108(0.678)	0.093(0.713)
<I> / sigma _{<i>I</i>}	10.28 (2.13)	14.7(2.0)	17.8(2.6)	15.3(2.4)	19.2(2.4)	20.14(2.16)

Table 3. Refinement statistics.

REFINEMENT STATISTICS	yGsy2-R589A/R592A	yGsy2-E169Q+25mM M G6P+10mM UDP-Glucosamine	yGsy2-E169Q+25mM G6P+10mM UDPFDG	yGsy2-E169Q+25mM G6P+10mM UDP-Galactose	yGsy2-E169Q+25mM G6P+10mM UDP-GlucNac	yGsy2-wildtype +25mM G6P + 10mM UDP-Xylose
Resolution Range	108-3.3Å	145-3.03 Å	145-2.73 Å	145- 3.26 Å	145- 2.90 Å	145- 2.69 Å
Number of atoms	9846	20685	20555	20719	20780	20712
R-factors	R _{work} = 17.5% R _{free} =21.9%	R _{work} = 17.7% R _{free} =25.6%	R _{work} = 19.07% R _{free} =24.9%	R _{work} = 17.53 % R _{free} =25.11 %	R _{work} = 18.43% R _{free} =25.29 %	R _{work} = 19.87% R _{free} =25.92 %
R.m.s. deviations from Ideal Values						
Bond angles (°)	0.007	0.01	0.012	0.010	0.012	0.012
Bond lengths (Å)	1.22	1.515	1.62	1.513	1.649	1.691
Ramachandran Plot Preferred/Allowed (%)	98.93	96.8	97.2	95.7	96.7	96.6
Outliers (%)	1.07	3.2	2.8	4.3	3.3	3.4

4. Overall structure of yGsy2-R589A/R592A

The ygsy2-R589A/R592A double mutant enzyme crystallized in the trigonal P3₂21 space group and exhibited diffraction data to a maximum resolution of 3.3 Å. The crystals were merohedrally twinned, with a twin fraction of 0.31. The asymmetric unit for this crystal form contains a dimer (Figure 18A), representing one-half of the functional tetramer (Figure 18B), which is created by one of the crystallographic dyads between asymmetric units in the unit cell. The structure exhibited defined electron density for residues 2-277; 283-401 and 415-639 in one monomer of the dimer and for residues 2-277; 283-401 and 415-626 in the other monomer. Both the monomers lacked interpretable electron density for the C-terminal 60-70 residues.

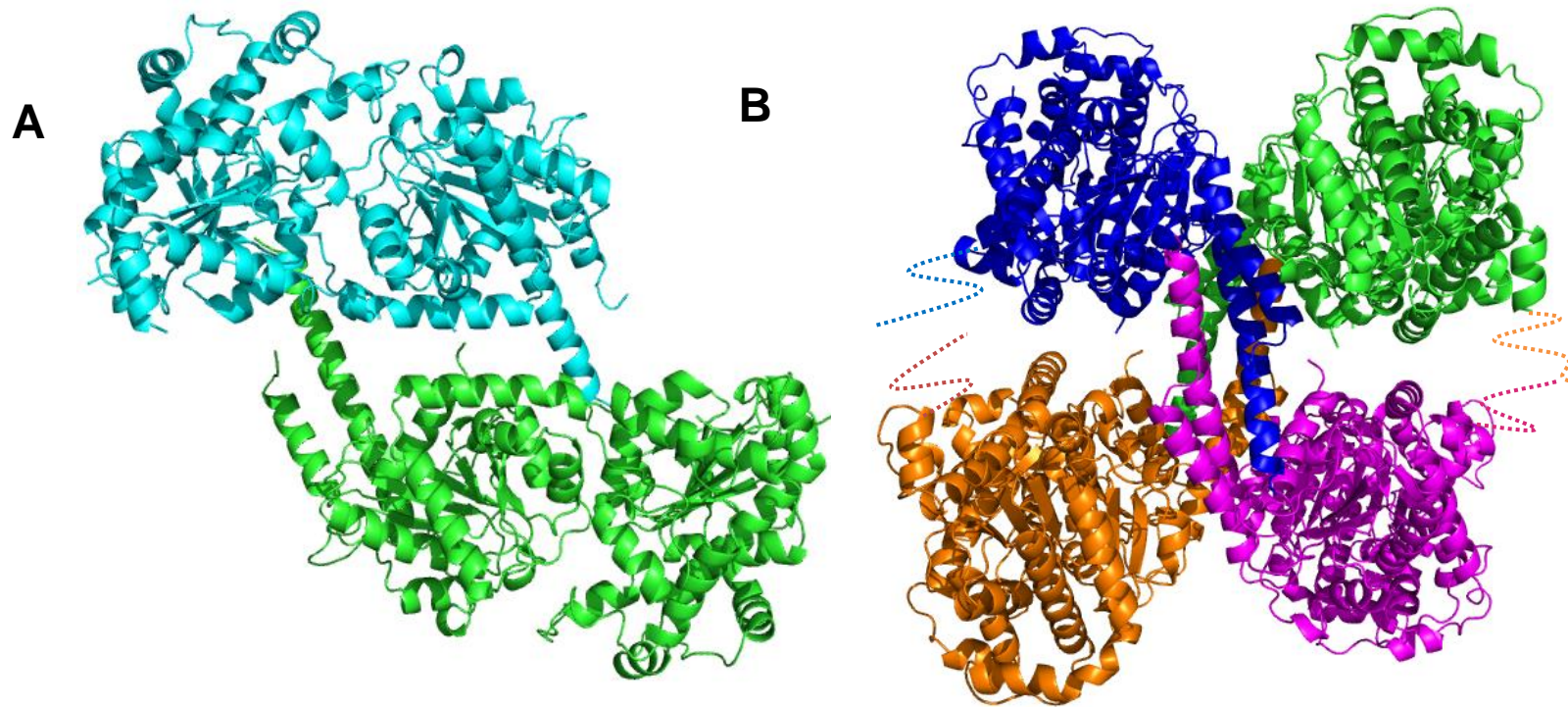


Figure 18. Crystal structure of yGsy2 inhibited state.

A. Crystal structure of yGsy2-R589/R592A as seen in the asymmetric unit and B. Ribbon representation of the double mutant tetramer using the symmetrical co-ordinates of the dimer as the other dimer. The C-terminal tail of each monomer is shown as dotted lines.

The overall structure of the double mutant is very similar to the yGsy2-R580A/R581A/R583A basal state structure in terms of domain and subunit arrangement. As mentioned previously, yGsy2-R589A/R592A like all other yGsy2 structures contains two structural domains; N-terminal domain comprising residues 2-277 and 599-639, and a C-terminal domain comprising residues 283-598. Both of these structural domains contain a Rossmann fold which in turn is characterized by seven beta-sheets flanked by alpha-helices on either side. Most of the subunit interactions occur via two long alpha-helices comprising of residues 366-430. The regulatory helices containing the cluster of six arginine residues lie at the end of the C-terminal domain and are situated anti-parallel to each other across one of the molecular 2-fold axes in the tetramer. The symmetrical co-ordinates of the crystallographic dyad can be used to assemble the biological tetramer.

Since the double mutant was co-crystallized with UDPG, we found electron density for UDP in one subunit (Figure 19A) and UMP in another subunit (Figure 19B). Because of the time frame of the crystallization experiment, it is highly likely that UDPG was hydrolyzed to form the products UDP and UMP and releasing the sugar from the active site (see Figure 29 for more information). The interactions made by UDP and UMP with the surrounding amino acids are very similar to those previously observed (82).

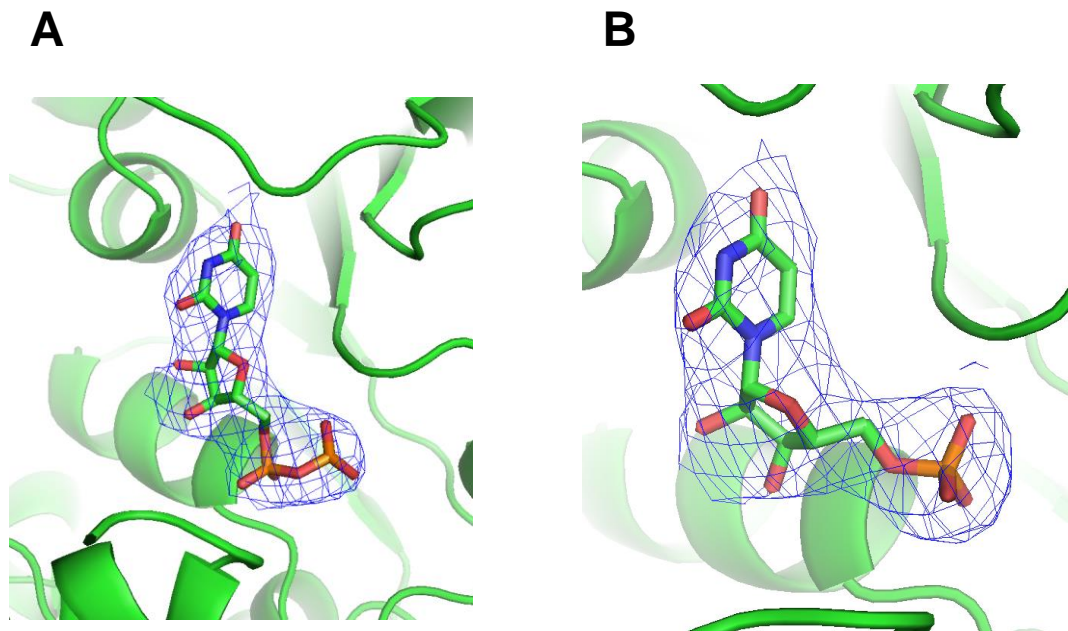


Figure 19. Nucleotide binding in the active site of yGsy2-R589A/R592A.

Ribbon representation of A. UDP and B. UMP bound in the catalytic cleft of each monomer of yGsy2-R589/R592A. The map shown is the original $2F_o - F_c$ electron density map prior to inclusion of the UDP/UMP in the model contoured at 1.0 standard deviation of the map.

Since yGsy2-R589A/R592A was crystallized in the absence of G6P, it showed the characteristic features of a non-activated yGsy2 enzyme. Similar to the basal state structure, the alpha helices 15 and 16 of one monomer interact with $\beta 3$ and helix $\alpha 2$ of the adjacent monomer thereby hindering substrate access to the catalytic cleft (Figure 20A). As previously discussed, G6P binding close to the regulatory helix opens up the active site through the translational motions of alpha helices 15 and 16 which now interact with the corresponding helices of the adjacent monomer (Figure 20B).

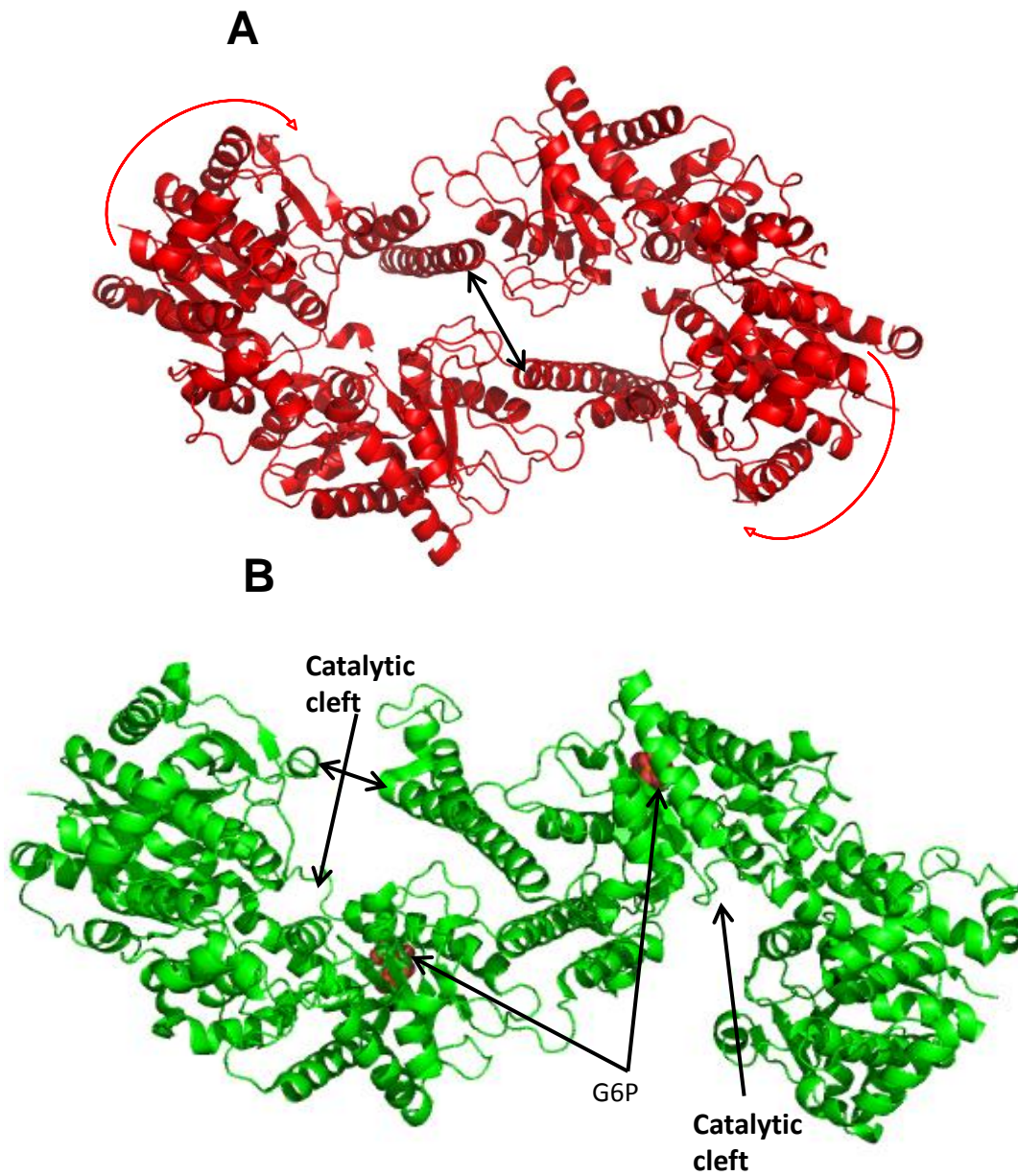


Figure 20. Dimer interface of the inhibited and active state of yGsy2.

A. Closed dimer interface of the inhibited state. Ribbon representation of a dimer of yGsy2 in the A. inhibited state (ygsy2-R589A/R592A) B. G-6-P bound activated state.

5. Structural comparisons with the basal state structure

When compared to the basal state structure, the yGsy2-R589A/R592A structure had a more closed tetrameric interface (Figure 22A). In particular, we found that the N-terminal domain of the inhibited state structure is more closed when compared to the basal state structure. Each monomer of yGsy2 is made up of two structural domains: an N-terminal domain where the acceptor is thought to bind and a C-terminal domain where the donor binds. Superposing the C-terminal domain (283-598) of yGsy2-R589A/R592A with both the basal and activated state structures showed that the N-terminal domain of the double mutant is more closed towards the C-terminal domain when compared to the other two structures. When analyzed by the Dyndom program, the N-terminal Rossmann-fold domain of the Gsy2-R589A/R592A double mutant structure was rotated 5.9° and 10.8° towards a more “closed” domain arrangement compared to the basal and activated state structures (Figure 21), respectively. The r.m.s.d of N-terminal domain α -carbons and C-terminal domain α -carbons of the yGsy2-R589A/R592A inhibited state and the yGsy2-R580A/R581A/R583A basal state structures are 0.51 and 0.42 Å, respectively, suggestive of a global rigid body domain movement. Similar values of 0.62 and 0.71 Å was obtained for the inhibited versus the activated state structures again suggesting global rigid body domain motions. This N-terminal domain closure observed in the inhibited state hinders substrate access, especially the acceptor access to the catalytic cleft (Figure 22B).

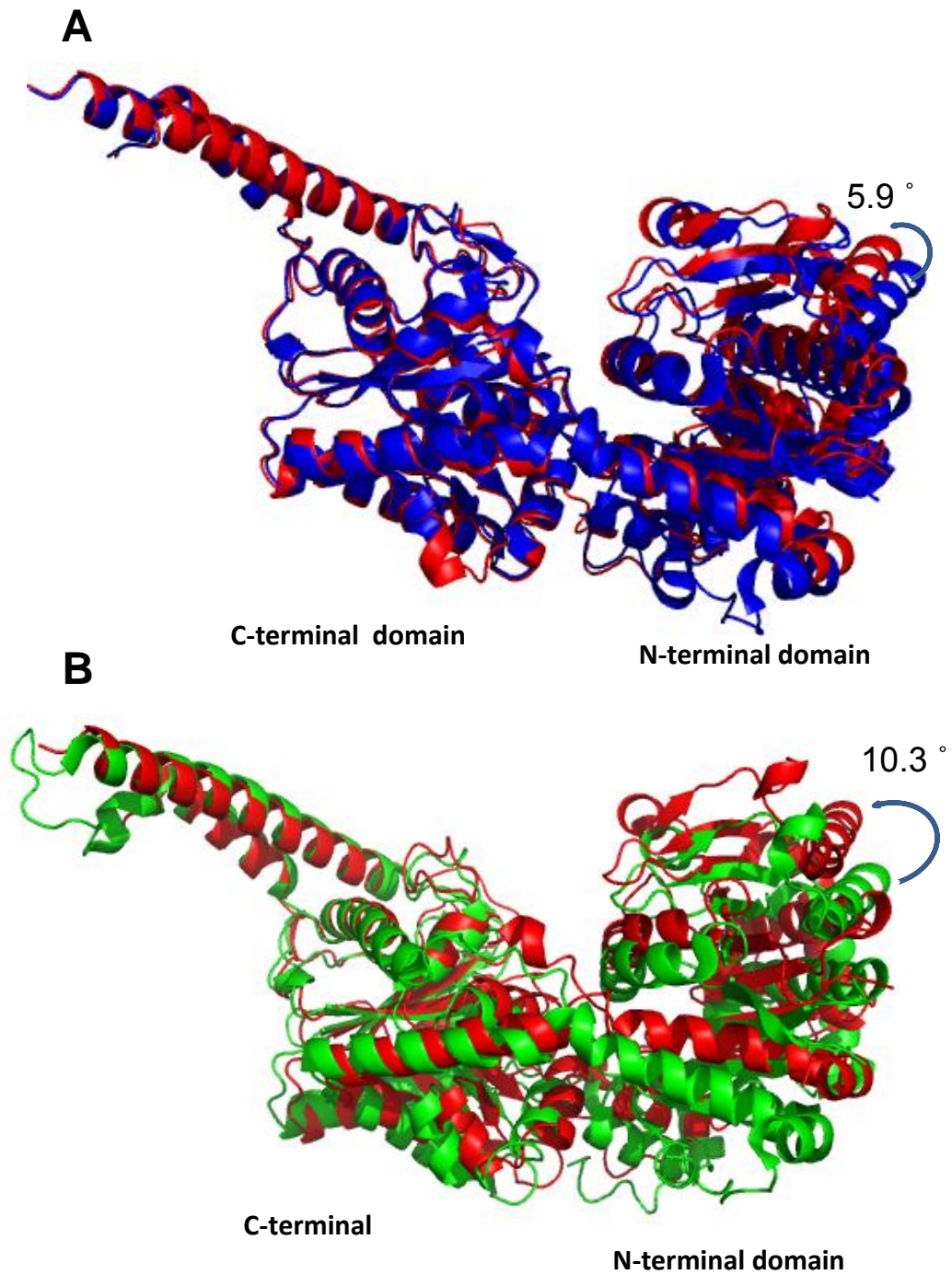


Figure 21. N-terminal domain closure of the inhibited state.

Ribbon representation of the superposed A. basal (blue) and inhibited state (red) structures, B. inhibited (red) and activated (green) state structures. The entire C-terminal domain was used for alignment with the help of CCP4.

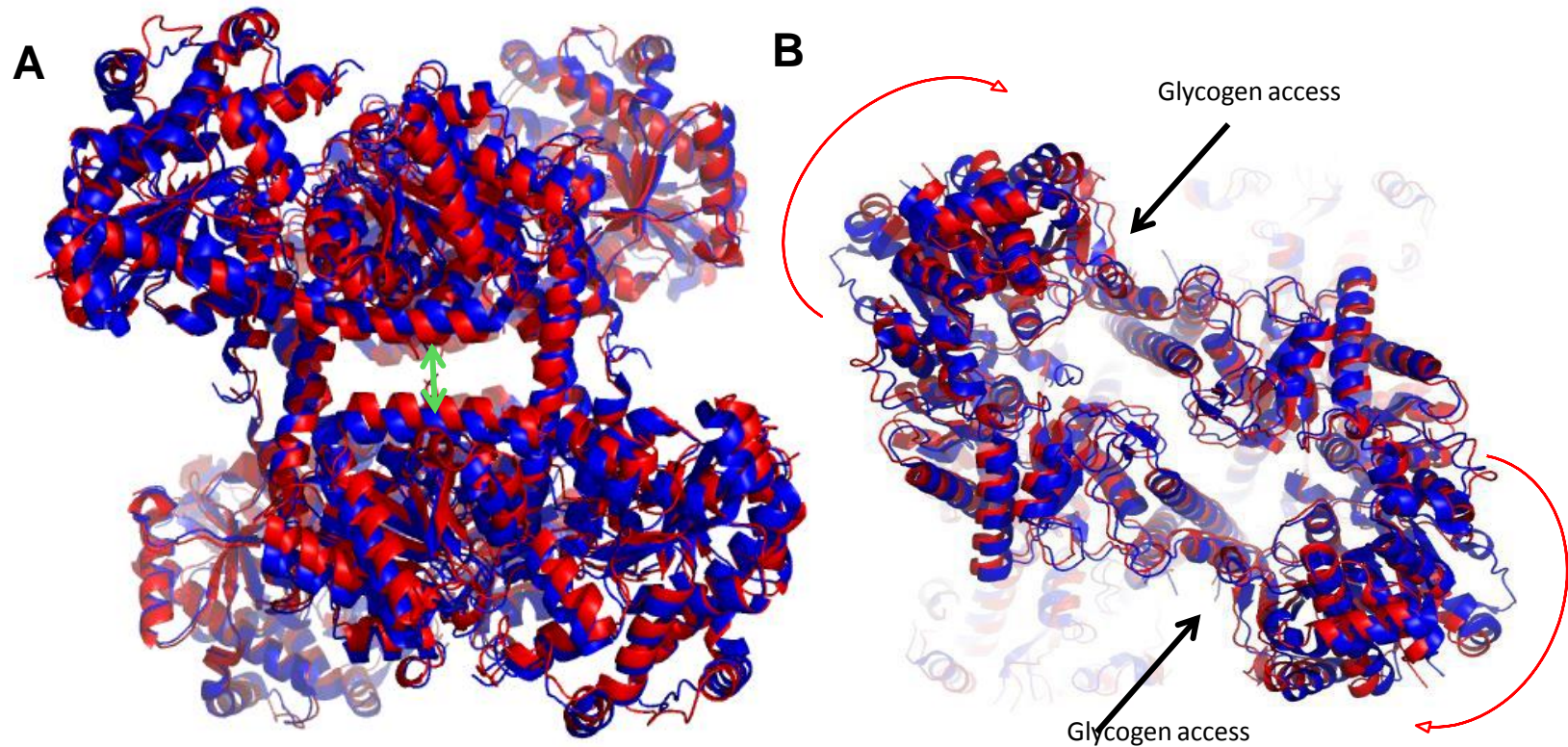


Figure 22. Glycogen access to the inhibited state.

A. Ribbon representation of the superposed basal (blue) and inhibited (red) state tetramers. The entire C-terminal domain of each subunit of the basal state was superposed to the C-terminal domain of the corresponding subunits of the inhibited state using CCP4. B. The same figure rotated 90° showing the glycogen access to the inhibited state is more closed when compared to the basal state.

These domain motions within the monomer impact the relative positioning of the structural elements in the tetramer as well. As mentioned previously, the distance between the regulatory helices of adjacent monomers vary depending on the activity state of the enzyme. Due to differing residue substitutions and differences in the resolution of the structures, we measured the main chain distance between residues Asn585 and Arg589 across the regulatory helical interface. In the basal state structure, this distance is 12 Å (Figure 23B), while in the inhibited state, represented by the Gsy2-R589A/R592A double mutant structure, the regulatory helices are 4 Å closer, at a distance of 8 Å (Figure 23A). In contrast, the binding of G-6-P pushes the regulatory helices apart, to a separation distance of 16 Å (Figure 23C). The structural transitions that impact the positioning of the regulatory helices can be communicated to the N-terminal domain by the fact that the regulatory helices are directly linked to the N-terminal domain by the extension of the helical element composed of residues 600-620 which lies along the back of the N-terminal domain.

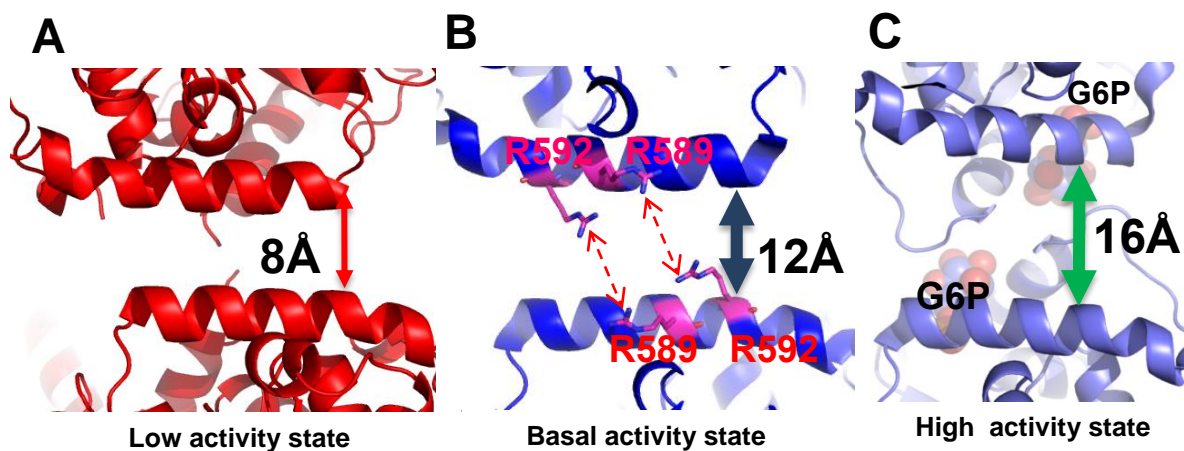


Figure 23. Regulatory interface of the three states of yGsy2.

A, B and C. Ribbon representation of the regulatory helices of adjacent monomers in the yGsy2-R589A/R592A inhibited state, yGsy2-R580A/R581A/R583A basal state and G-6-P bound wild-type activated state, respectively. The Arg589 and Arg592 in the basal state are shown in stick model and the bound sulfate ions are shown in space filling atom model. G-6-P (purple) bound in the activated state is shown in space filling atoms.

6. Redox regulation of yGsy2

Based on the changes in distance between the regulatory helices and the positioning of symmetry-related residues in the tetramer, we hypothesized that we could engineer a reversible redox regulatory feature in the enzyme as a surrogate for regulation by phosphorylation through judicious introduction of cysteine residues. In the inhibited state structure, arginines 581 and 592 lie directly across the dimer interface from each other and their gamma-carbons are separated by a distance of 4 Å (Figure 24A). If the activity state of the enzyme is directly correlated with this separation distance, we hypothesized that upon mutating the two arginines to cysteine residues, the cysteines could form a disulfide bond under oxidized conditions and close the distance between the

regulatory helices by an additional 2 Å to generate a fully inhibited enzyme (Figure 24B). Importantly, these disulfide bridges can be reduced to release the structural constraint and, thus, permit activation.

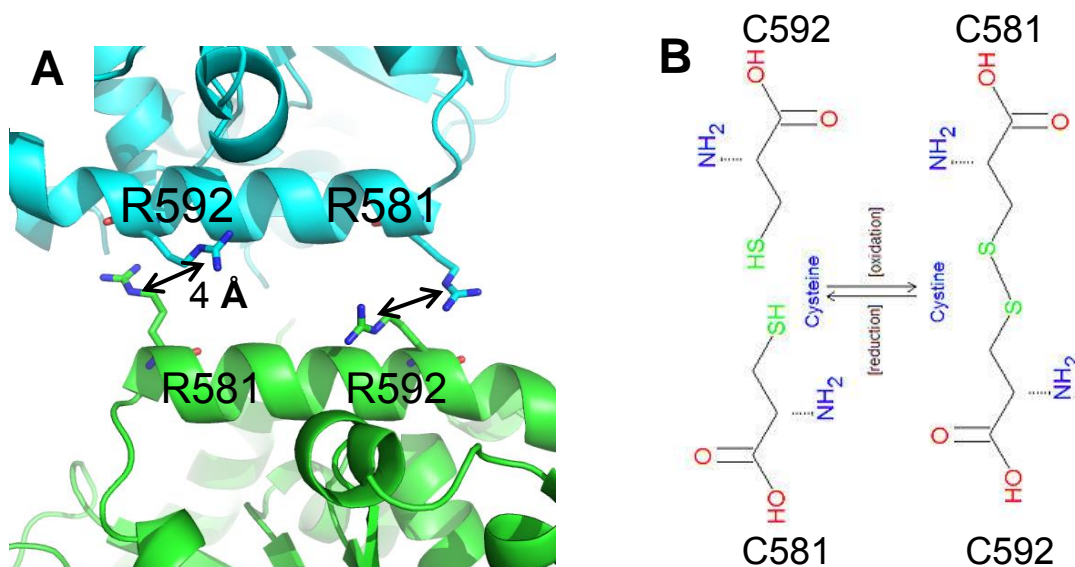


Figure 24. Redox regulation of ygsy2.

A. Ribbon representation of the regulatory interface in the inhibited state. Each monomer is color schemed separately. The arginines 581 and 592 of adjacent monomers are showed in ball and stick model. B. Hypothetical representation of a disulfide bond being formed between the arginines 581 and 592 of the adjacent monomers.

7. Non-reducing SDS-PAGE analysis

We generated two distinct enzymes with mutations at positions 581 and 592, Gsy2-R581C/R592C and Gsy2-R581A/R592A. Both the mutant enzymes were purified similar to the wildtype yGsy2 but without any reducing agents. When the purified enzymes were examined using a non-reducing SDS-PAGE (Figure 25), the cysteine mutants migrated more slowly through the gel when compared to their migration upon treatment with 250 mM BME. Judging from the

molecular weight standards, the non-reduced yGsy2-R581C/R592C mutant enzyme had a molecular weight of >250 kDa, which is consistent with the yGsy2 tetramer, while the reduced form had a molecular weight of ~72 kDa, which is inconsistent with the yGsy2 monomer. Both the wildtype and the yGsy2-R581A/R592A enzyme migrated similar to the reduced form of the yGsy2-R581C/R592C in the presence or absence of BME.

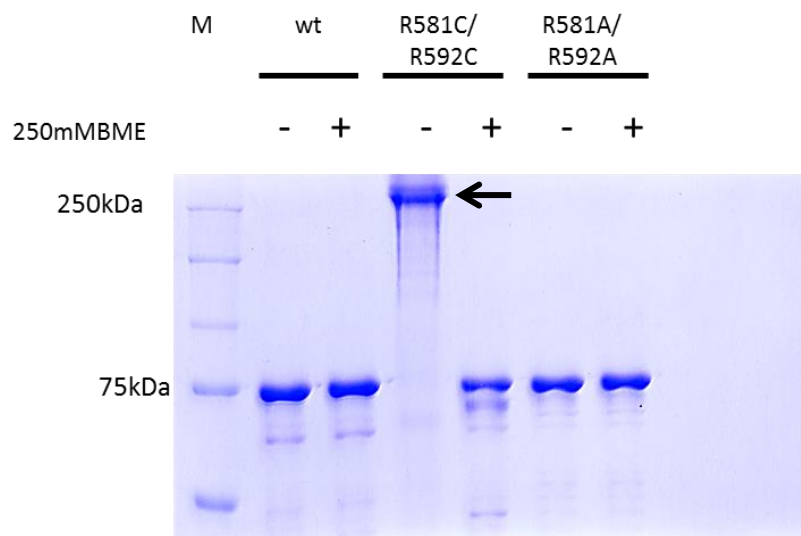


Figure 25. Inter-subunit di-sulfide bond formation.

SDS PAGE gel showing that the non-reduced yGsy2-R581C/R592C mutant migrates as a tetramer while the reduced form migrates as a monomer similar to the wild-type and alanine mutants, irrespective of its oxidative status.

8. Gel filtration

The cysteine mutants with or without 250 mM BME were run through a size exclusion column, Superose 6 10/300 GL. The major portion of the protein in both the cases eluted at around 15 ml with an apparent molecular weight of 313.9 kDa as judged from the standards, consistent with a tetramer (Figure 26).

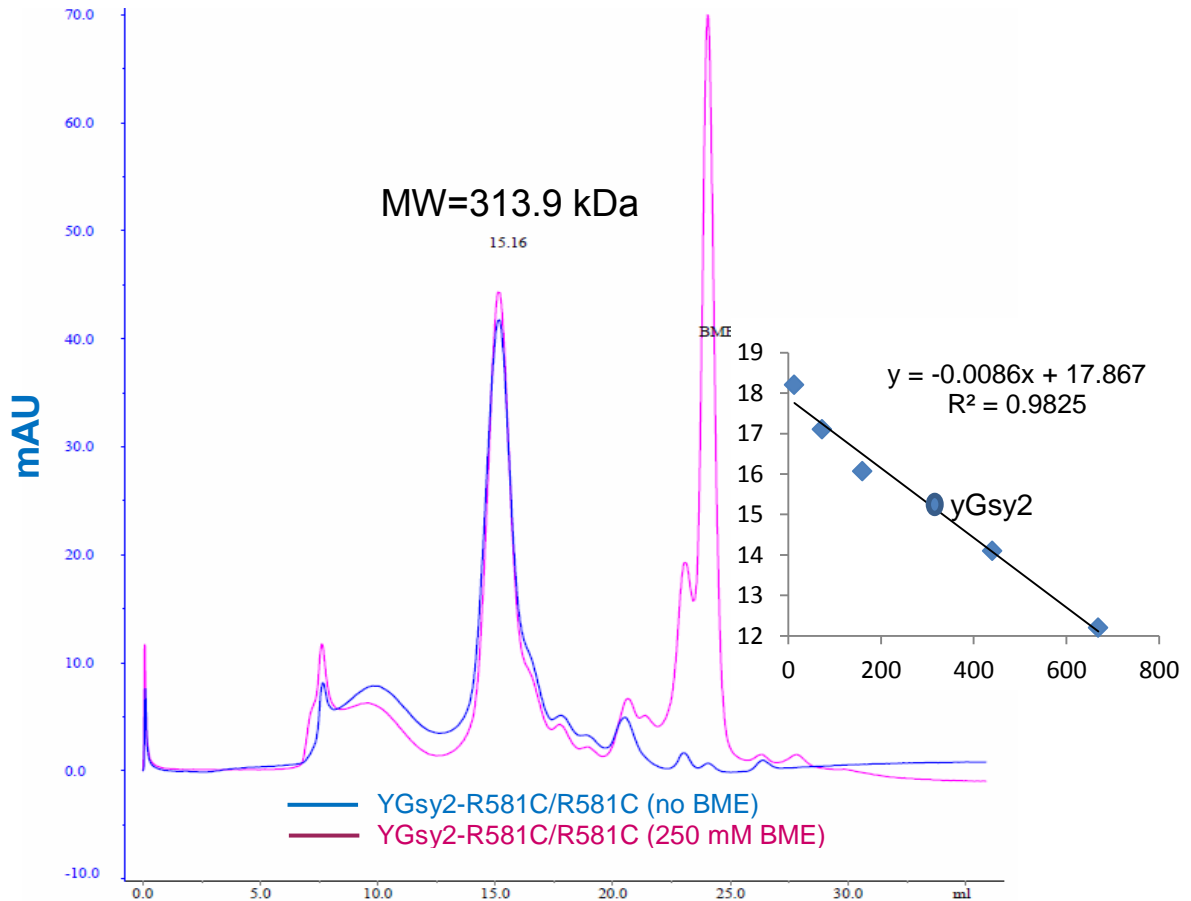


Figure 26. Gel filtration analysis of the cysteine mutants.

Chromatogram showing the elution profile of the yGsy2p-R581C/R592C mutant in the presence and absence of 250 mM BME. The major peak at the end of the column volume (24 mL) is the UV absorbance peak of β -ME. The inner graph shows the standard curve obtained using different molecular weight protein standards.

9. Specific activity measurements

As isolated from *E. coli*, the specific activity of the yGsy2p-R581C/R592C mutant form was decreased 12-fold in the absence of G-6-P and 47-fold in the presence of G-6-P when compared to the yGsy2p-R581A/R592A mutant (Table 4). In particular, the oxidized form of Gsy2-R581C/R592C had a specific activity very similar to the phosphorylated form of Gsy2 and even lower than the Gsy2-R589A/R592A. In fact, the specific activity of Gsy2p-R581C/R592C is most similar to the Gsy2-R589A/R592A enzyme to which the T668 phospho-peptide has been ligated (Table 4). Unlike the Gsy2-R581A/R592A enzyme that demonstrates a robust activation by G-6-P, the oxidized Gsy2-R581C/R592C enzyme cannot be activated by G-6-P at concentrations up to 80 mM. In contrast to the low activity observed for the oxidized form of Gsy2p-R581C/R592C, in the presence of 200 mM BME, the enzyme has activity and responses to G-6-P almost identical to the control Gsy2p-R581A/R592A mutant enzyme (Table 4). It is notable that the activity ratio of yGsy2-R581A/R592A is almost identical to the cysteine mutants in the presence of 200 mM BME (Table 4).

Table 4. Specific activity measurements.

Specific activity measurements for different yGsy2 mutants both in the presence and absence of G-6-P.

	Sp Activity (μ mole/min.mg) (-G-6-P)	Sp activity (μ mole/min.mg) (7.2mM G-6-P)	Activity ratio (-G-6-P/+G-6-P)
	1.03 \pm 0.03	1.73 \pm 0.03	0.6 \pm 0.01
Gsy2-R580A/R581A/R583A*	0.55 \pm 0.02	0.51 \pm 0.03	1.09 \pm 0.02
Gsy2-R587A/R589A/R592A*	0.38 \pm 0.01	0.35 \pm 0.02	1.09 \pm 0.01
Gsy2(1-640) +49mer T668P*	0.1 \pm 0.01	1.9 \pm 0.02	0.05 \pm 0.01
Gsy2-R589A/R592A	0.1 \pm 0.01	1.56 \pm 0.02	0.11 \pm 0.01
Gsy2-R581C/R592C	0.033 \pm 0.001	0.04 \pm 0.001	NA
Gsy2-R581C/R592C +200mM BME	0.58 \pm 0.01	2.1 \pm 0.02	0.27 \pm 0.02
Gsy2-R581A/R592A	0.41 \pm 0.02	1.88 \pm 0.04	0.28 \pm 0.03
Gsy2(1-640)-R589A/R592A* + 49mer T668	0.03 \pm 0.01	0.03 \pm 0.01	NA

*-Results previously published (63).

10. Glucose-6-Phosphate titrations

In the absence of any reducing agents, addition of G6P up to 80 mM did not have any effect on the activity of yGsy2-R581C/R592C. However, in the presence of 200 mM BME, G6P was capable of activating the enzyme with an AC₅₀ value of 0.5 mM (Figure 27). The yGsy2-R581A/R592A mutant can also be

activated by G-6-P with an AC_{50} value of 0.28 mM similar to the cysteine mutants in the presence of BME (Figure 27).

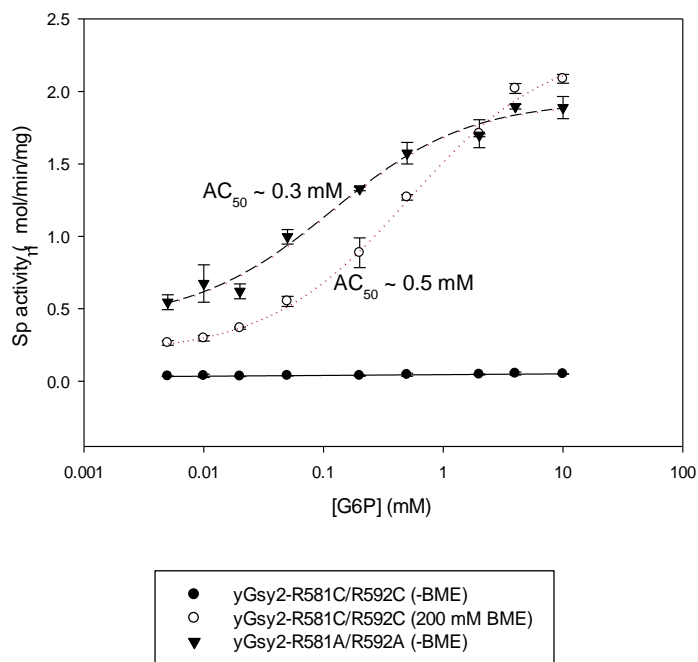


Figure 27. G-6-P activation of the yGsy2 mutants.

G-6-P titration curves for the yGsy2-R581C/R592C mutants both in the presence and absence of 200 mM BME. The G-6-P activation curve of yGsy2-R581A/R592A is shown for comparison.

11. Reducing agent titrations

To examine the relationship between reduction and activity in more detail, we examined the ability of three reducing agents to activate the Gsy2-R581C/R592C enzyme, BME, DTT and TCEP. In keeping with the known redox properties of the reducing agents, we found that the half-maximal activating concentrations (AC_{50}) followed the trend, BME>DTT>TCEP, with AC_{50} values of 15.5 mM, 2.5 mM and 0.29 mM, respectively. It is also interesting to note that the AC_{50} values for these reducing agents were similar in the presence of 10 mM G-

6-P (19.2 mM, 2.3 mM and 0.39 mM for BME, DTT and TCEP, respectively)
 (Figure 28).

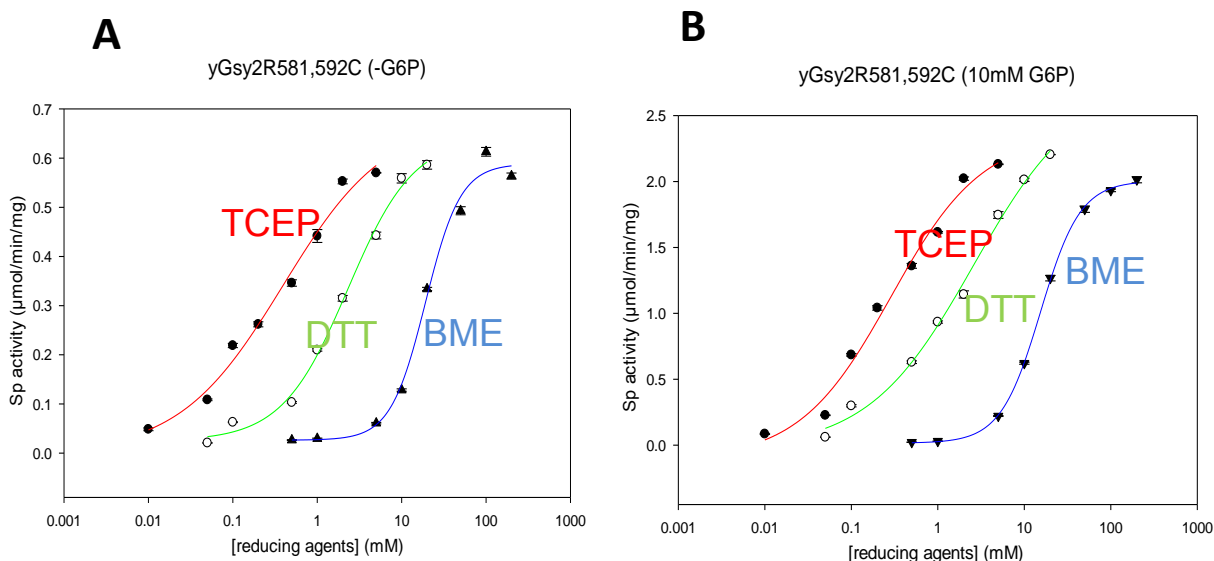


Figure 28. Effect of different reducing agents on the cysteine mutants.

Dose dependent activation of yGsy2-R581C/R592C with increasing concentration of TCEP (red), DTT (green), BME (blue) in the absence of G-6-P. B. Activation of yGsy2-R581C/R592C in the presence of G-6-P. The color scheme is identical to panel A.

12. UDPG titrations

We examined the kinetic parameters for the mutants and, similar to prior work, found that the primary kinetic effect was associated with V_{max} , with minimal effects on K_M or $S_{0.5}$ for G-6-P (Table 5). Using the wild-type Gsy2 enzyme as the basis for comparison, the K_M values vary less than 3-fold between the mutants for any combination of additions (G-6-P or BME), whereas, the V_{max} values vary between 30- to 50-fold in the absence of G-6-P and/or BME to less than 2-fold when both G-6-P and BME are present. For instance, if you compare the V_{max}/K_M values of the wildtype enzyme in the presence and absence of both G-6-P and BME, there is a mere 2-fold increase in activity. However, in the case of the

cysteine mutants, the increase in activity is ~66 fold with the majority (> 90%) of the difference coming from V_{max} alone. Interestingly, the AC_{50} for G-6-P also varied by up to 10-fold, with the wild-type Gsy2 having the lowest AC_{50} at 0.04 mM and the Gsy2-R581C/R592C enzyme the highest at 0.48 mM.

Table 5. UDPG kinetics.

Kinetic parameters for different GSY2 mutants with respect to UDP-glucose (\pm 10mM G-6-P) both in the presence or absence of 200mM BME. Data are represented as mean \pm SEM.

GSY2 Enzyme	V_{max} (-BME, -G-6-P)	V_{max} (-BME, +G-6-P)	V_{max} (+BME, -G-6-P)	V_{max} (+G-6-P, +BME)	$S_{0.5}$ (G-6-P)	V_{max}/K_M (-BME, -G-6-P)	V_{max}/K_M (+BME, +G-6-P)
Wildtype	1.0 \pm 0.1	1.7 \pm 0.1	0.99 \pm 0.1	3.59 \pm 0.1	0.04 \pm 0.01	1.72 \pm 0.05	3.62 \pm 0.1
R589,592A	0.09 \pm 0.01	1.8 \pm 0.1	0.17 \pm 0.006	2.48 \pm 0.11	0.29 \pm 0.03	0.32 \pm 0.06	3.0 \pm 0.14
R581,592C	0.03 \pm 0.001	0.04 \pm 0.003	0.59 \pm 0.02	1.9 \pm 0.04	0.48 \pm 0.02	0.054 \pm 0.001	3.6 \pm 0.12
R581,592A	0.45 \pm 0.02	1.8 \pm 0.04	0.43 \pm 0.007	1.95 \pm 0.01	0.1 \pm 0.01	0.25 \pm 0.03	2.6 \pm 0.07

13. Analysis of yGsy2 activity towards different UDP-sugars

In order to see if yGsy2 hydrolysis activity is limited only to UDP-glucose, we incubated different UDP-sugar donors with the wildtype enzyme for 16 hours and analyzed the products with the help of a HPAEC column using UV absorbance at 262 nm. After overnight incubation, yGsy2 hydrolyzed UDP-glucose and UDP-glucosamine while the other sugar donors (UDP-galactose, UDP-GlucNac and UDP-xylose) were left non-hydrolyzed (Figure 29). From the peak area measurements, we found that yGsy2 prefers UDP-glucose over UDP-glucosamine as a hydrolytic substrate with the former being hydrolyzed 2.5 times faster.

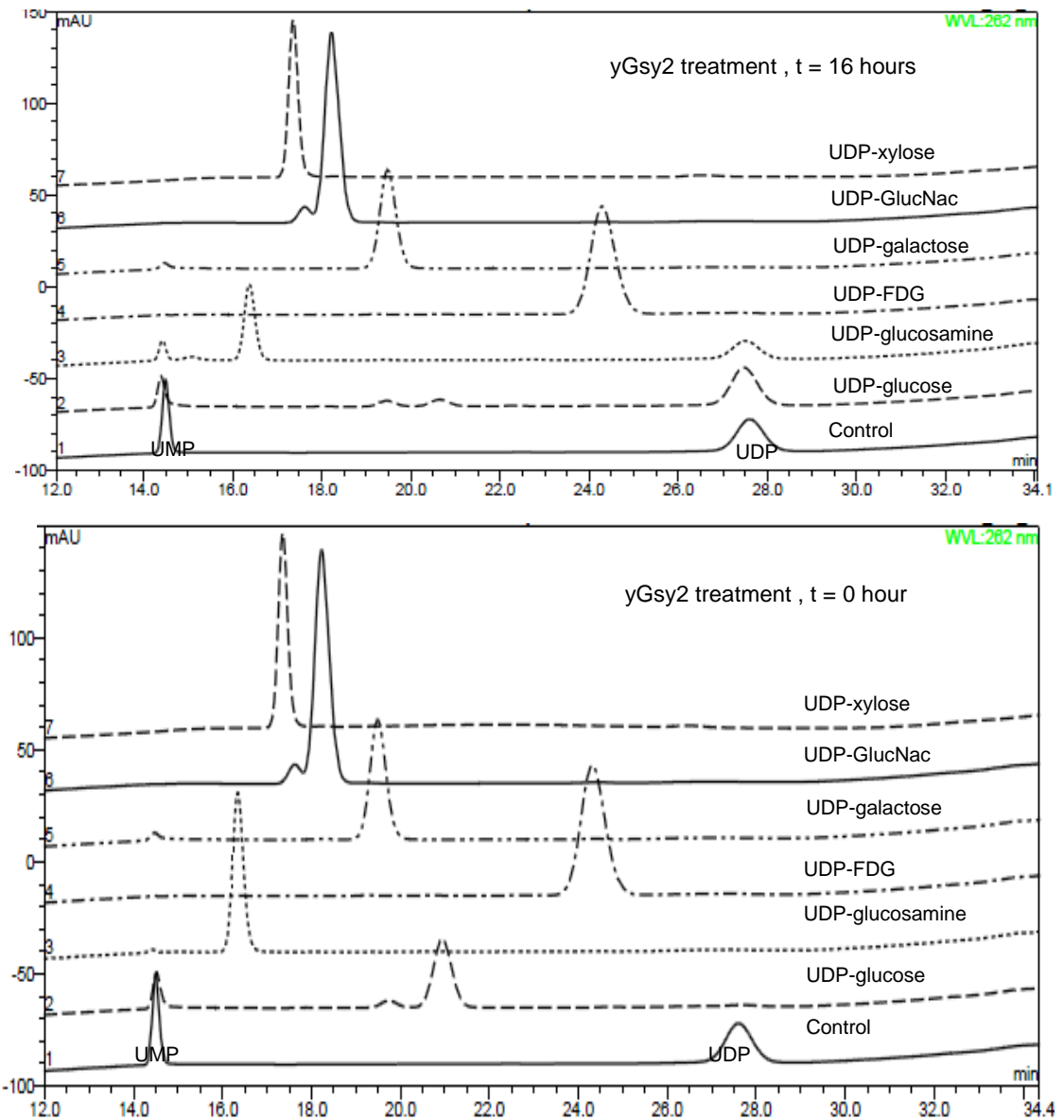


Figure 29. Hydrolysis of different UDP-sugar donor.

Top panel. UV absorbance of the different UDP-glucose analogues after passing them through a HPAEC column. Bottom panel. UV absorbance of the same sugar donors after 16 hour incubation with yGsy2 in the presence of G-6-P.

14. Inhibition of yGsy2 activity by different UDP-sugar donors

The activity of yGsy2-wildtype enzyme was measured using the standard ^{14}C assay in the presence of increasing concentrations of different UDP-glucose analogues.

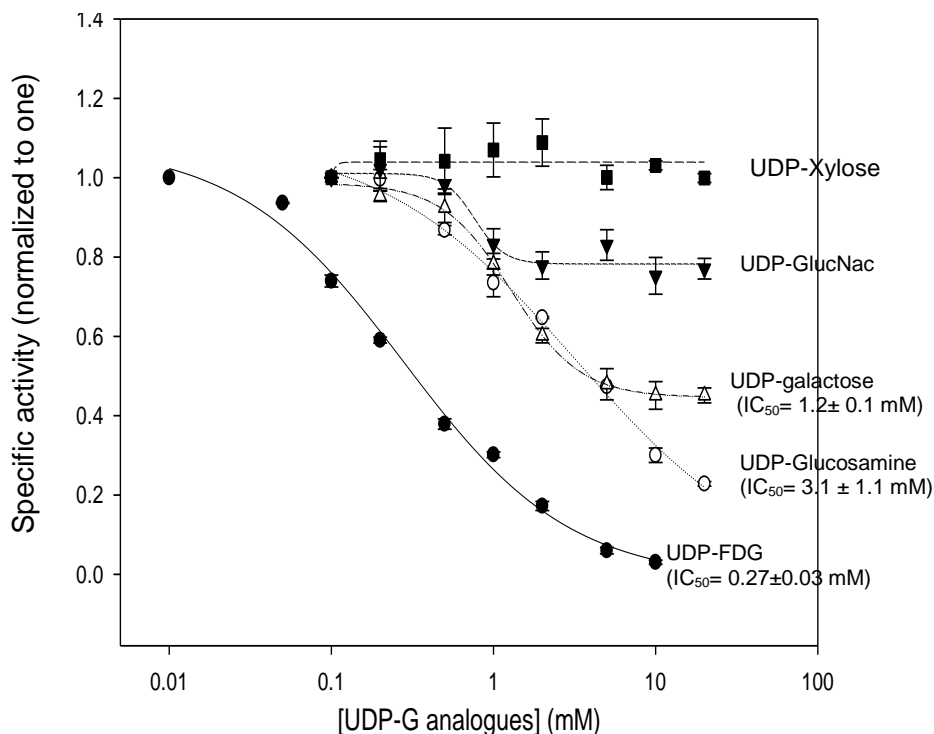


Figure 30. UDP-sugar donor titrations.

The yGsy2 wildtype activity was measured in the presence of increasing concentrations of different UDP-glucose analogues using the standard ^{14}C assay.

Of all the nucleotide sugar donors, only UDP-FDG and UDP-glucosamine were capable of inhibiting the enzyme completely with an IC_{50} value of 0.27 and 3.1 mM, respectively (figure 30). UDP-galactose inhibited the enzyme to only 50% with an IC_{50} value of 1.2 mM. UDP-GlucNac inhibited the enzyme by less than 20% while UDP-xylose up to 20 mM had no significant effect on the enzymes activity (Figure 30).

15. Substrate binding in yGsy2 active site

Based on the HPAEC results, the UDP-sugar donors UDP-glucose, UDP-glucosamine were classified as substrates while UDP-galactose, UDP-N-acetylglucosamine and UDP-xylose were classified as non-substrates for yGsy2. For the sake of simplicity, we have classified UDP-FDG as substrate, since it is a non-hydrolysable molecular mimic of UDP-glucose. In order to understand the structural basis for substrate vs non-substrate selection in yGsy2, we solved the crystal structures of yGsy2 in complex with different UDP-sugar donors to resolutions varying between 2.7-3.3 Å in their respective G6P-activated states.

In the GT-B fold subfamily of glucosyl transferases, donor binding on the C-terminal domain closes the N-terminal domain in order to achieve the catalytically competent donor•acceptor complex (39, 82). We used the activated state of yGsy2 for these studies because upon G-6-P binding, the tetrameric interface of yGsy2 is completely “opened” allowing the individual subunits to form the catalytically competent closed conformation of the N-terminal domain (63). In the case of G-6-P bound activated state of yGsy2, the catalytic complex is captured by closing the N-terminal domain towards the C-terminal domain by 13° (82).

The crystal structure of each nucleotide sugar complex was solved using both the wild-type and E169Q mutant (in the presence of G-6-P) and only those structures that had complete electron density for both the nucleotide and sugar are reported here. The E169Q mutant retains less than 1% of the wild-type activity and it has been successfully used to capture the hydrolyzed glucose of

UDP•G in the catalytic pocket (82). The overall architecture of the activated yGsy2 enzyme is described previously in the G6P bound R589A/R592A mutant structure (pdb: 3NB0) (63).

15. A. UDP-Glucosamine

The crystal structure of UDP-glucosamine bound to the catalytic pocket was solved using the E169Q mutant. Similar to what was observed for the UDP•G complex, only subunit-C of the tetramer showed electron density for both UDP and glucosamine while the other 3 subunits had electron density for only UDP. Modelling UDP-glucosamine into the observed electron density showed that the nucleotide sugar is hydrolyzed (Figure 31). The closest distance between the β -phosphate oxygen and the C1 of glucosamine is too long for a covalent linkage. A dominant negative peak appeared every time a glycosidic bond was modelled and refined, suggesting that the sugar donor is hydrolyzed. The time frame of the crystallization experiment and the absence of an acceptor likely led to the non-productive hydrolysis of UDP-glucosamine to UDP and glucosamine.

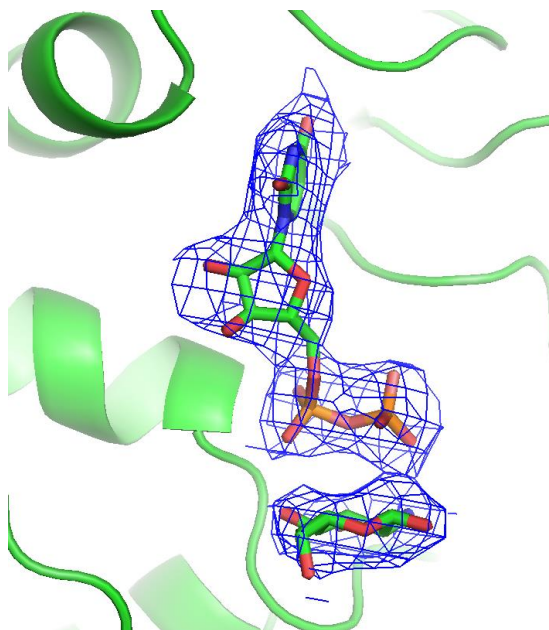


Figure 31. UDP•glucosamine binding to the ygsy2 active site.

Ribbon representation of UDP and glucosamine bound to the active site of yGsy2p E169Q mutant. The map shown is the original $2F_o-F_c$ map contoured at 1.0 standard deviation, prior to the inclusion of the ligand in refinement.

As described in the introduction, the major structural rearrangement following substrate binding in the active site is the closing of the N-terminal Rossmann fold domain. Structural alignment using the program DynDom revealed that the N-terminal domain of the UDP•glucosamine bound subunit is 13.6° more closed towards the C-terminal domain when compared to the subunit A that had only UDP in its active site (Figure 32). The rmsd between the aligned α -carbons of the isolated N-terminal and C-terminal domains were 0.48 and 0.78 Å, respectively, suggestive of a global rigid body domain motion.

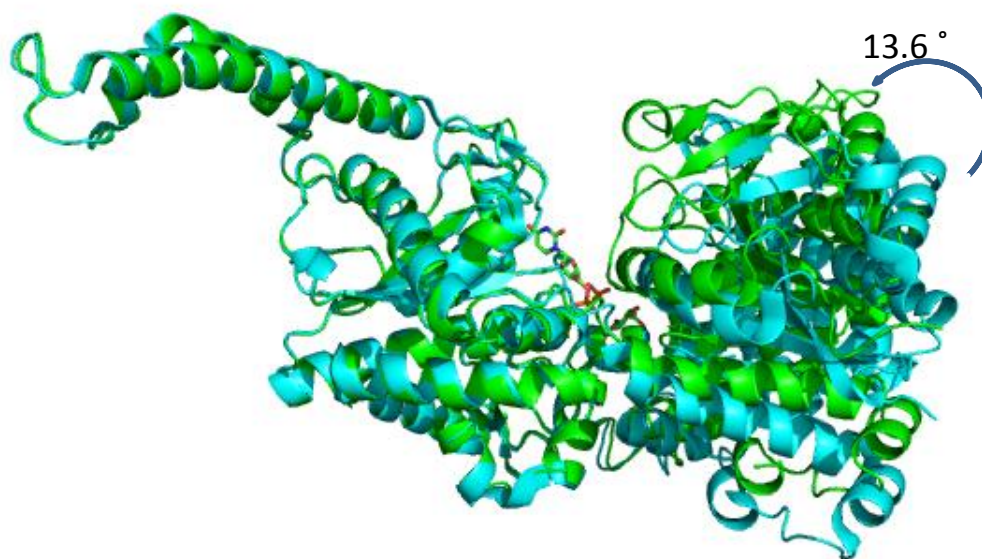


Figure 32. N-terminal domain closure induced by UDP•glucosamine.

Ribbon representation of the superposed monomers containing UDP•glucosamine (shown in green) and UDP (shown in cyan) in the active site. The two subunits were aligned using the entire C-terminal domain (299-600) with the help of Superpose program in CCP4.

UDP•glucosamine was found to be in a 'bent' conformation with the diphosphate group of UDP lying parallel to the plane of glucosamine similar to the UDP•glucose bound structure (Figure 31 and 33A). The overall interaction between yGsy2 and UDP•glucosamine is also very similar to the interaction between yGsy2 and UDP•glucose (Figure 33B). The uridine ring is sandwiched between the aromatic sidechains of Phe480 and Tyr492. The O4 group of the uracil moiety is within hydrogen-bonding distance to the peptide nitrogen of Leu481. The 2'- and 3'-OH groups of the ribosyl moiety are in hydrogen bonding distance to the sidechain of Glu517. Similar to that observed in the the UDP•glucose structure, the di-phosphate of UDP lies parallel to the plane of glucosamine, with the α -phosphate within hydrogen bonding distance to the

peptide nitrogen of Tyr513 and the sidechain hydroxyl group of Thr514. The β -phosphate interacts with the sidechains of Lys326 and Arg320 and the peptide nitrogen of Gly23 which lies across the inter-domain cleft.

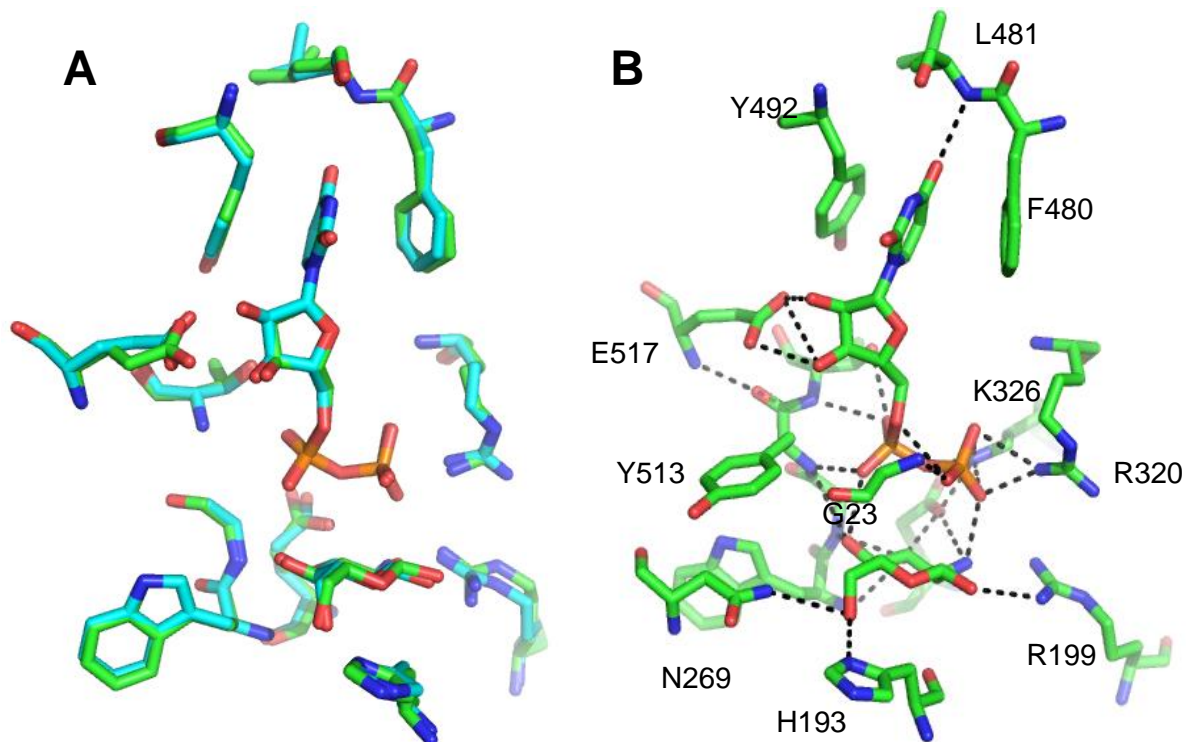


Figure 33. Subunit interactions of UDP•glucosamine.

A. Superposition of UDP•glucosamine (green) and UDP•glucose (cyan) and the surrounding amino acids with which it interacts. B. Subunit interactions made by UDP•glucosamine in the active site.

In the case of glucosamine (Figure 33B), the 6'OH group interacts with the side chains of H193 and N269; 4'OH group interacts with the peptide nitrogen of G512 and to one of the β -phosphate oxygens; 3'OH group interacts with the peptide nitrogen of W511 and the side chain of E509; the 2' amino group interacts with the side chain of R199 and the β -phosphate of UDP.

15. B. UDP-2-fluro-2-deoxy-glucose (UDP-FDG)

The crystal structure of UDP-FDG in complex with G-6-P bound yGsy2-E169Q was solved to a maximum resolution of 2.73 Å. Similar to the UDP•glucose and UDP•glucosamine structures, only subunit C showed electron density for UDP-FDG while the other three subunits exhibited electron density for UDP alone. However, modelling of UDP-FDG into the observed electron density showed that the nucleotide sugar donor was not hydrolyzed (Figure 34A). Structural alignments showed that the N-terminal Rossmann-fold domain of the UDP-FDG bound subunit was more closed when compared to the UDP only bound subunit (Figure 35). The program Dyndom predicted a 13.2 ° domain closure and the rmsd between the α -carbons of the isolated N-terminal and C-terminal domains of the UDP-FDG and UDP bound subunits were found to be 0.45 and 0.64 Å, respectively, suggestive of a global rigid body domain motion.

Replacing the 2'-OH group of glucose with a fluorine atom neither affected the conformation of the nucleotide sugar nor the interactions within the active site. UDP-FDG adopted a 'bent' conformation with the diphosphate group of UDP lying parallel to the plane of 2-fluoro-2-deoxy-glucose (Figure 34A). The 2'-fluoro group interacts with the β -phosphate of UDP and the side chain of Arg199. An interesting observation made in this structure is that, next to the 2'-fluoro group is a well ordered water molecule (Figure 34A and 34C). The water molecule interacts with the 2'-fluorine group of UDP-FDG and the side chain of Arg199.

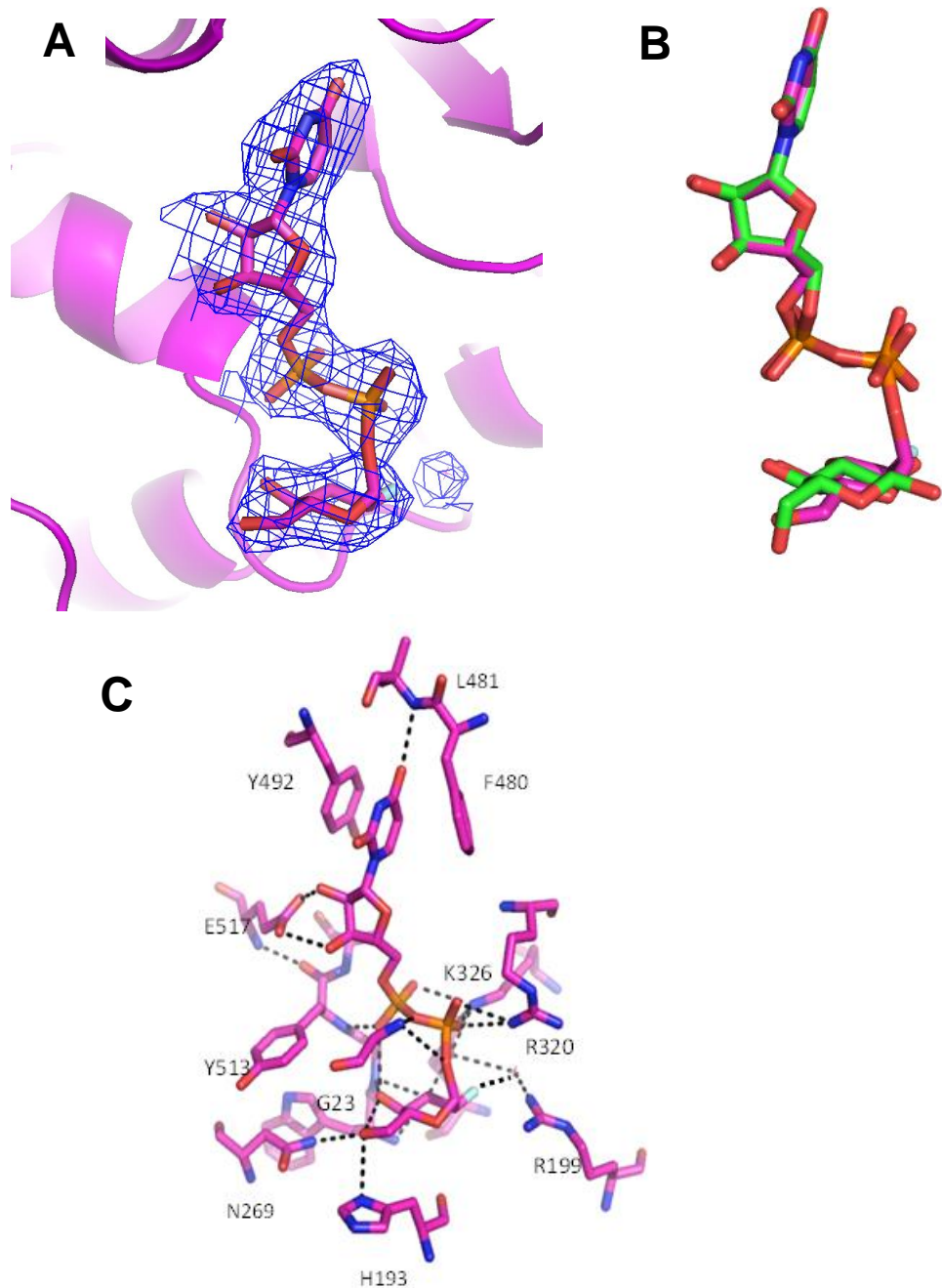


Figure 34. UDP-FDG binding to the yGsy2 active site.

A. UDP-FDG binding to the active site of yeast GS. The map shown is the original 2F_o-F_c map contoured at 1.0 standard deviation, prior to the addition of the ligand. B. Superposition of UDP•glucose (green) and UDP-FDG (magenta) as seen in the active site. C. Interactions made by UDP-FDG with the surrounding aminoacids of the subunit.

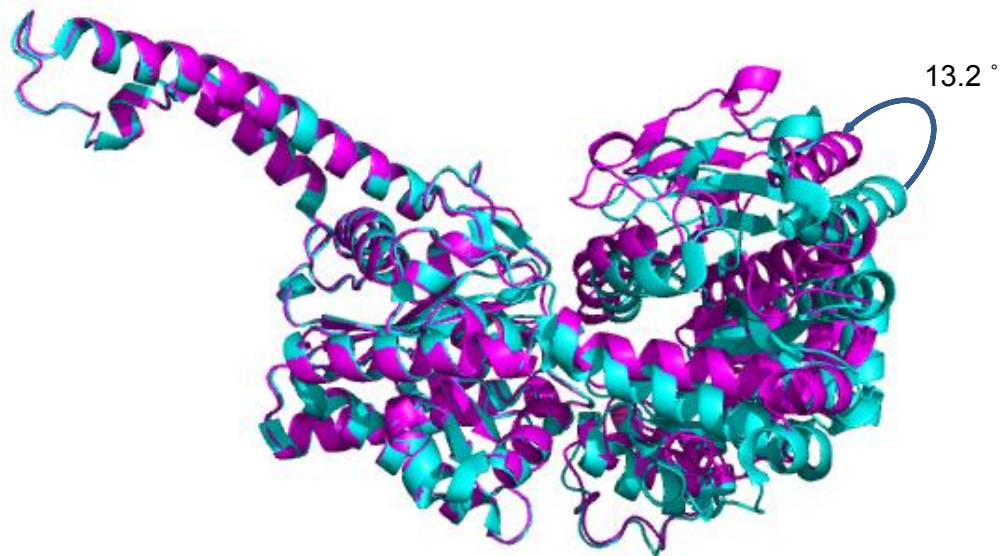


Figure 35. N-terminal domain closure induced by UDP-FDG.

Ribbon representation of the superposed monomers containing UDP-FDG (shown in magenta) and UDP (shown in cyan) in the active site. The two subunits were superposed using the entire C-terminal domain (299-600) with the help of Superpose program in CCP4.

16. Non-substrate binding to the yGsy2 active site

16. A. UDP-galactose

The crystal structure of UDP-galactose bound activated yGsy2 was solved using both the wildtype and E169Q mutant enzyme. In both the cases, UDP-galactose was found to be bound very similarly and the subunit architecture was also unchanged. However, taking into account the resolution of the structures, only the E169Q structure is discussed here.

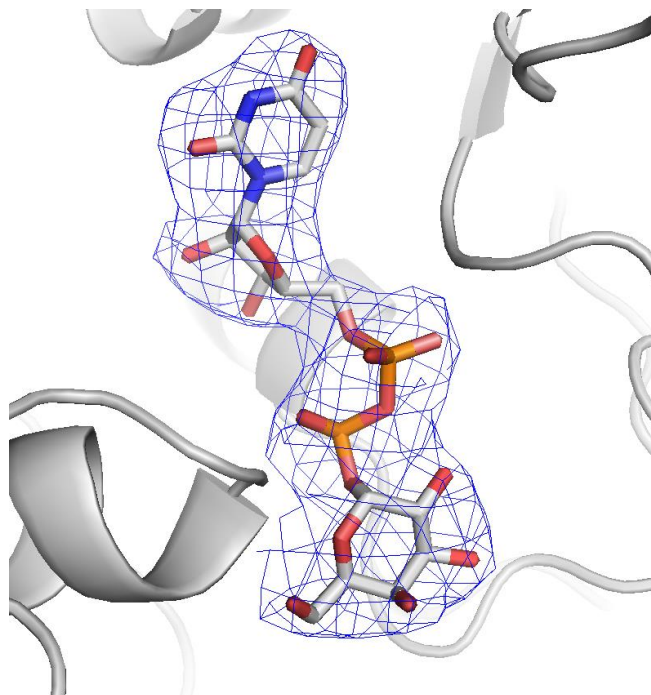


Figure 36. UDP-galactose binding to the active site.

Ribbon representation of UDP-galactose bound to the active site of yGsy2p E169Q mutant. The map shown is the original $2F_o-F_c$ map contoured at 1.0 standard deviation, prior to the addition of the ligand.

The crystal structure of UDP-galactose bound yGsy2-E169Q was solved to a maximum resolution of 3.2 Å. UDP-galactose in its non-hydrolyzed form was found in all the four subunits. However, only subunit C had complete electron density for the ligand and the surrounding amino acid residues (Figure 36). The N-terminal domain of the UDP-galactose subunit was 8.5° more closed when compared to the UDP bound subunit (Figure 38).

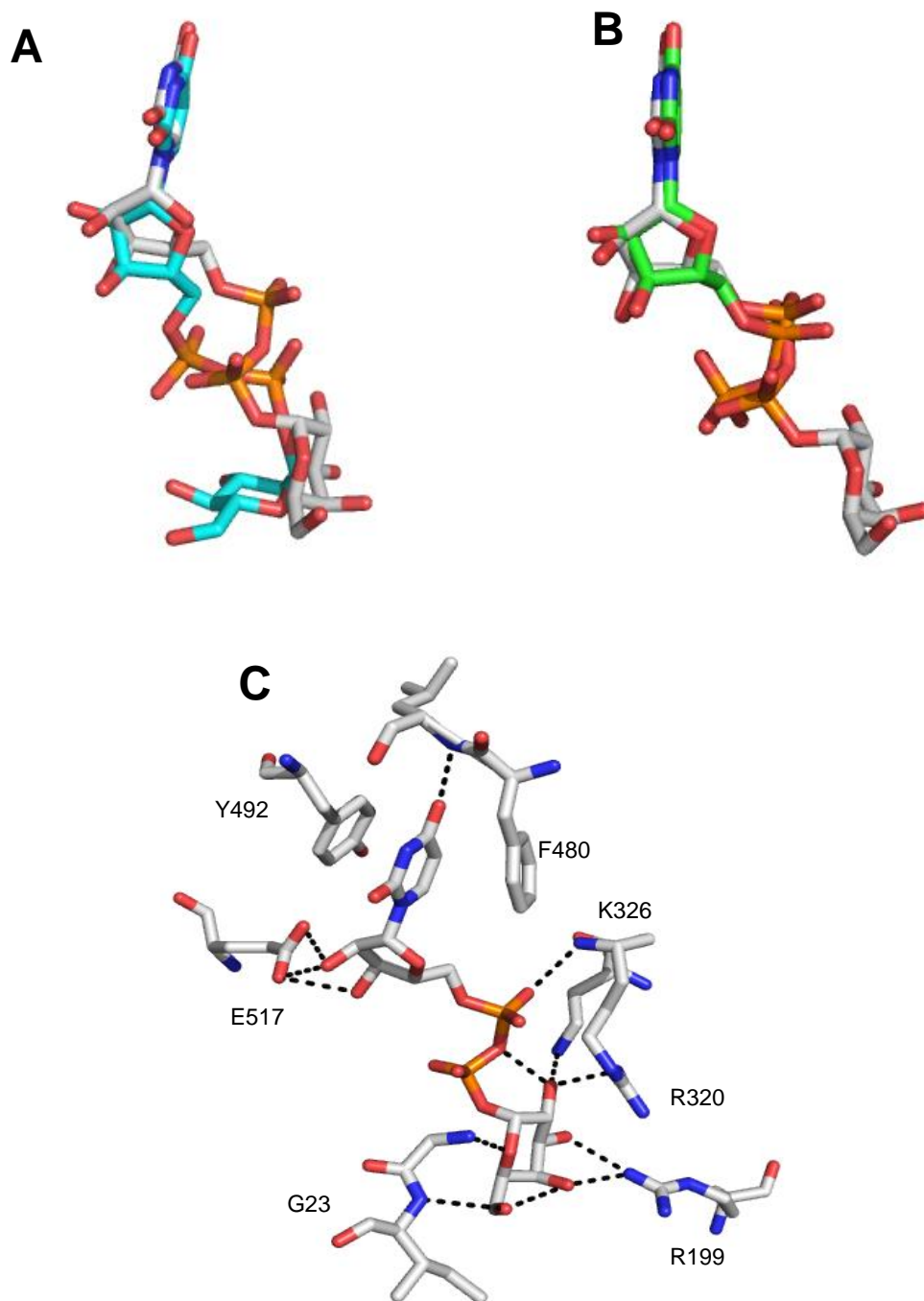


Figure 37. Structural conformation and subunit interactions made by UDP-galactose.

A. Superposition of UDP-galactose (shown in grey) and UDP-FDG (shown in cyan) as observed in the active site. B. Superposition of UDP-galactose (grey) and UDP (green) and C. Interactions made by UDP-galactose with the surrounding amino acids of the subunit.

Unlike the hydrolysable substrates of γ Gsy2 which adopted a 'bent' conformation, UDP-galactose adopted an 'extended' conformation (Figure 36 and 37A). There is no significant change in the conformation of uridine ring of UDP-galactose and its interactions with the surrounding amino acids when compared to the substrates. The major difference was found to be in the conformation of the phosphates and the sugar molecule. The α -phosphate of UDP is within hydrogen bonding distance with the peptide nitrogen of Arg320 and the side chain of Lys326 while the β -phosphate hydrogen bonds to the peptide nitrogen of Gly23. Interestingly, this conformation of UDP in UDP-galactose is very similar to the conformation of UDP in UDP only bound monomers (figure 37B).

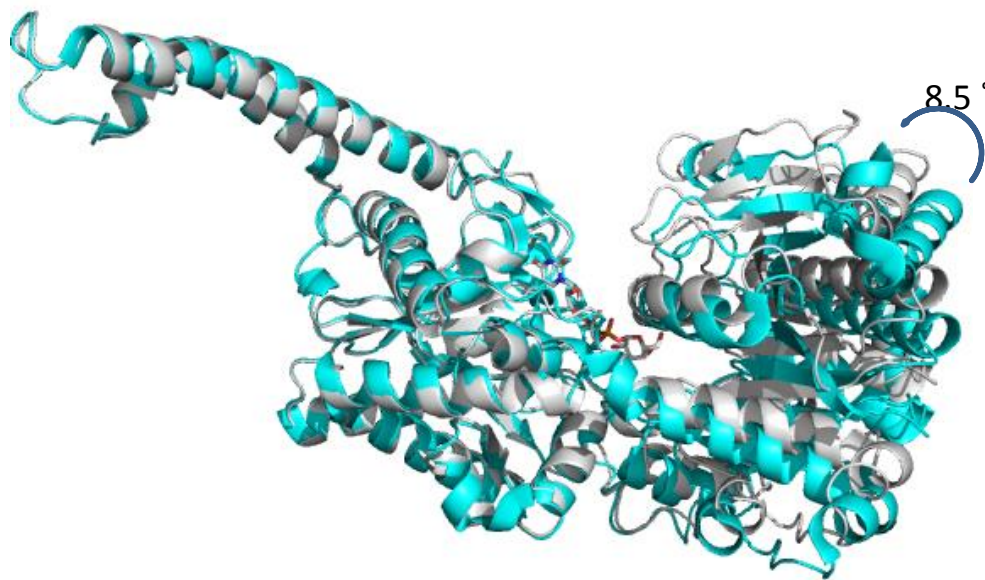


Figure 38. N-terminal domain closure induced by UDP-galactose.

Ribbon representation of the superposed monomers containing UDP-galactose (shown in grey) and UDP (shown in cyan) in the active site. The two subunits were superposed using the entire C-terminal domain (299-600) with the help of superpose program in CCP4.

In the case of galactose (Figure 37C), the 6'-OH group is essentially free without making any subunit interactions. The 3'- and 4'- OH groups are within hydrogen bonding distance to the side chain of Arg199 and the 2'-OH group of galactose interacts with the side chains of Arg 320 and Lys326.

16. B. UDP-N-acetylglucosamine (UDP-GlucNac)

The crystal structure of UDP-GlucNac bound activated yGsy2 was solved using both the wildtype and E169Q mutant enzyme. In both the cases, UDP-GlucNac was found to be bound very similarly and the subunit architecture was also unchanged. For consistency purposes and also taking into account the resolution of the two structures, the crystal structure of the yGsy2-E169Q mutant is discussed here.

The yGsy2-E169Q.G6P complex co-crystallized with UDP-GlucNac diffracted to a maximum resolution of 2.9 Å. The structure showed electron density for UDP-GlucNac in its non-hydrolyzed form in subunits B and D while subunits A and C either had no or incomplete electron density for the sugar molecule. UDP-GlucNac adopted an 'extended' conformation similar to UDP-galactose (Figure 39A). The majority of the subunit interactions come from the UDP group with the N-acetylglucosamine group making minimal contact with the surrounding amino acids (Figure 39B). The subunit interactions of the UDP moiety are essentially the same as the UDP group of UDP-galactose. In the case of N-acetylglucosamine, the following interactions were observed: the 3'-OH group is in hydrogen bonding distance to the peptide nitrogen of Gly23; the 6'-OH

interacts with the peptide nitrogens of Trp511 and Gly512 and the oxygen atom of the acetyl group interacts with the side chain of Arg20 (Figure 39B).

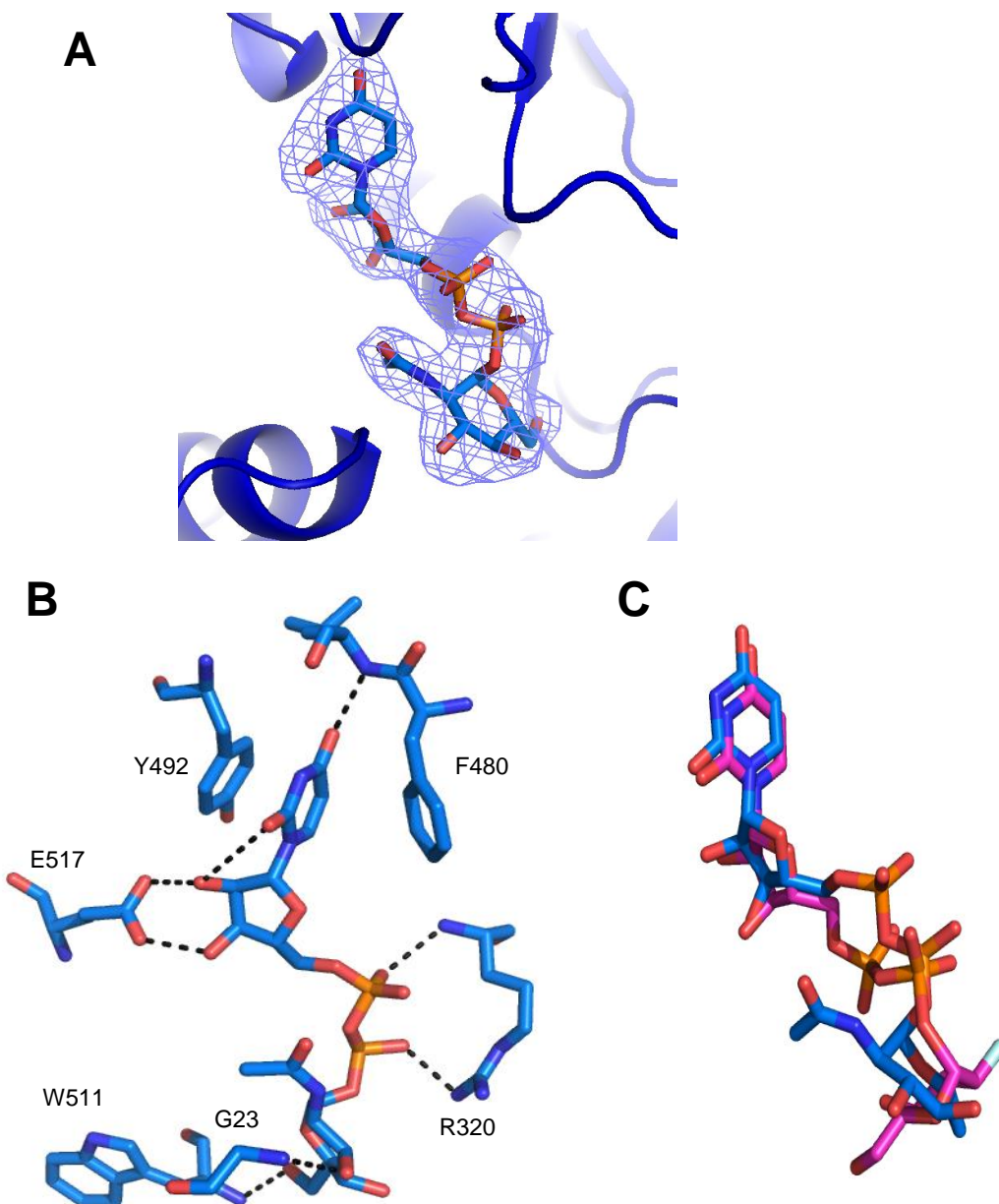


Figure 39. UDP-GlucNac binding to the active site.

A. Ribbon representation of UDP-GlucNac bound to the active site of yGsy2p E169Q mutant. The map shown is the original $2F_o - F_c$ map contoured at 1.0 standard deviation, prior to the addition of the ligand. B. Stick representation of UDP-GlucNac and its interacting amino acids in the active site of yGsy2p. C. Superposition of UDP-GlucNac (blue) and UDP-FDG (magenta) as observed in the active site.

Because of the relatively minimal interactions with the surrounding amino acids, N-acetylglucosamine was not able to close the N-terminal domain (Figure 40). In fact, UDP-N-acetylglucosamine binding to the active site further opened the N-terminal domain of γ Gsy2. The domain motions were quantified using the program Dyndom and it showed that the N-terminal domain of the UDP-GlucNac bound subunit is 6.5° more open when compared to the UDP only bound subunit (Figure 40).

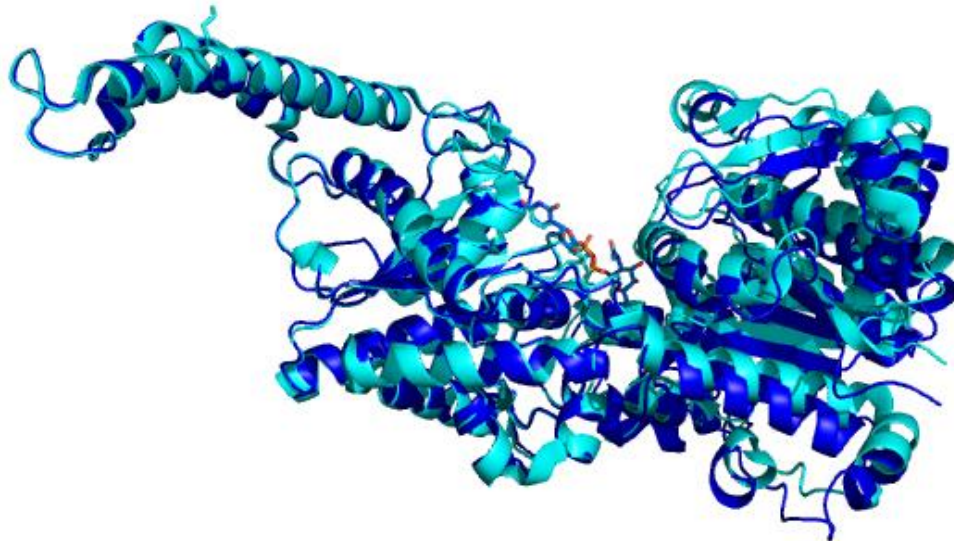


Figure 40. N-terminal domain motions induced by UDP-GlucNac.

Ribbon representation of the superposed monomers containing UDP-GlucNac (shown in blue) and UDP (shown in cyan) in the active site. The two subunits were superposed using the entire C-terminal domain (299-600) with the help of the program superpose in CCP4.

16. C. UDP-Xylose

The crystal structure of UDP-xylose bound G-6-P activated wt-yGsy2 was solved to a maximum resolution of 2.69 Å. Of the four subunits, we observed electron density for UDP-xylose in subunits B and C while subunits A and D had an incomplete electron density for the sugar molecule. UDP-xylose adopted an 'extended' conformation similar to UDP-galactose and UDP-GlucNac (Figure 41). In subunit C, apart from UDP-xylose, we also found electron density for two water molecules on either side of the 2'-OH group that seems to bridge the ligand interaction with the protein molecule (Figure 42A).

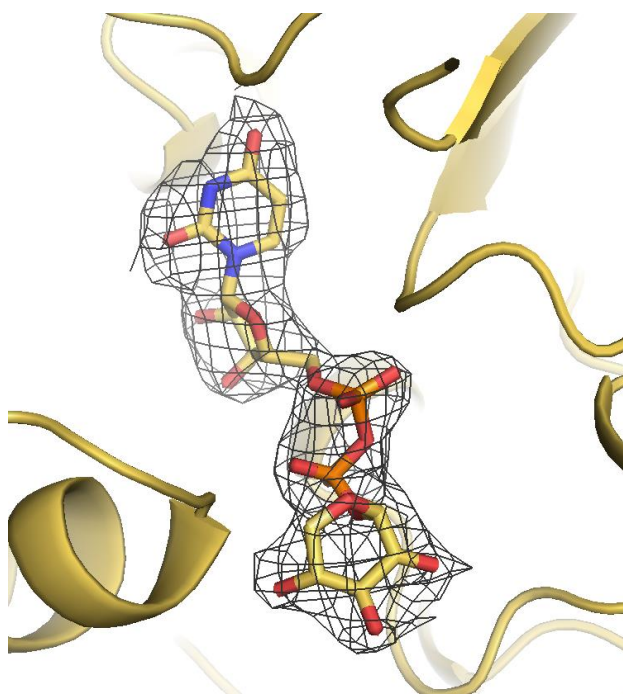


Figure 41. UDP-xylose binding to the yGsy2 active site.

Ribbon representation of UDP-xylose bound to the active site of yGsy2p. The map shown is the original $2F_o - F_c$ map contoured at 1.0 standard deviation, prior to the addition of the ligand.

The uridine interactions found in UDP-xylose are very similar to the other structures. The α -phosphate of UDP is in hydrogen bonding distance to the sidechain and peptide nitrogen of Arg320 while the β -phosphate oxygen hydrogen bonds to the peptide nitrogen of Gly23. The 2'-OH of xylose is within hydrogen bonding distance to the two water molecules and these water molecules in turn interact with the peptide nitrogen of Trp511 and the side chains of Glu509 and Lys326. In addition to these water mediated interactions with the subunit, the 2' and 3'-OH groups of xylose also interacts directly with the sidechain of Arg199. The 4'-OH group and the 5'-oxygen of xylose are within hydrogen bonding distance to the sidechains of Gly23 and Arg320, respectively (Figure 42A). When compared to the UDP only bound subunit, the N-terminal domain of UDP-xylose subunit was only 8.6° more closed towards the C-terminal domain.

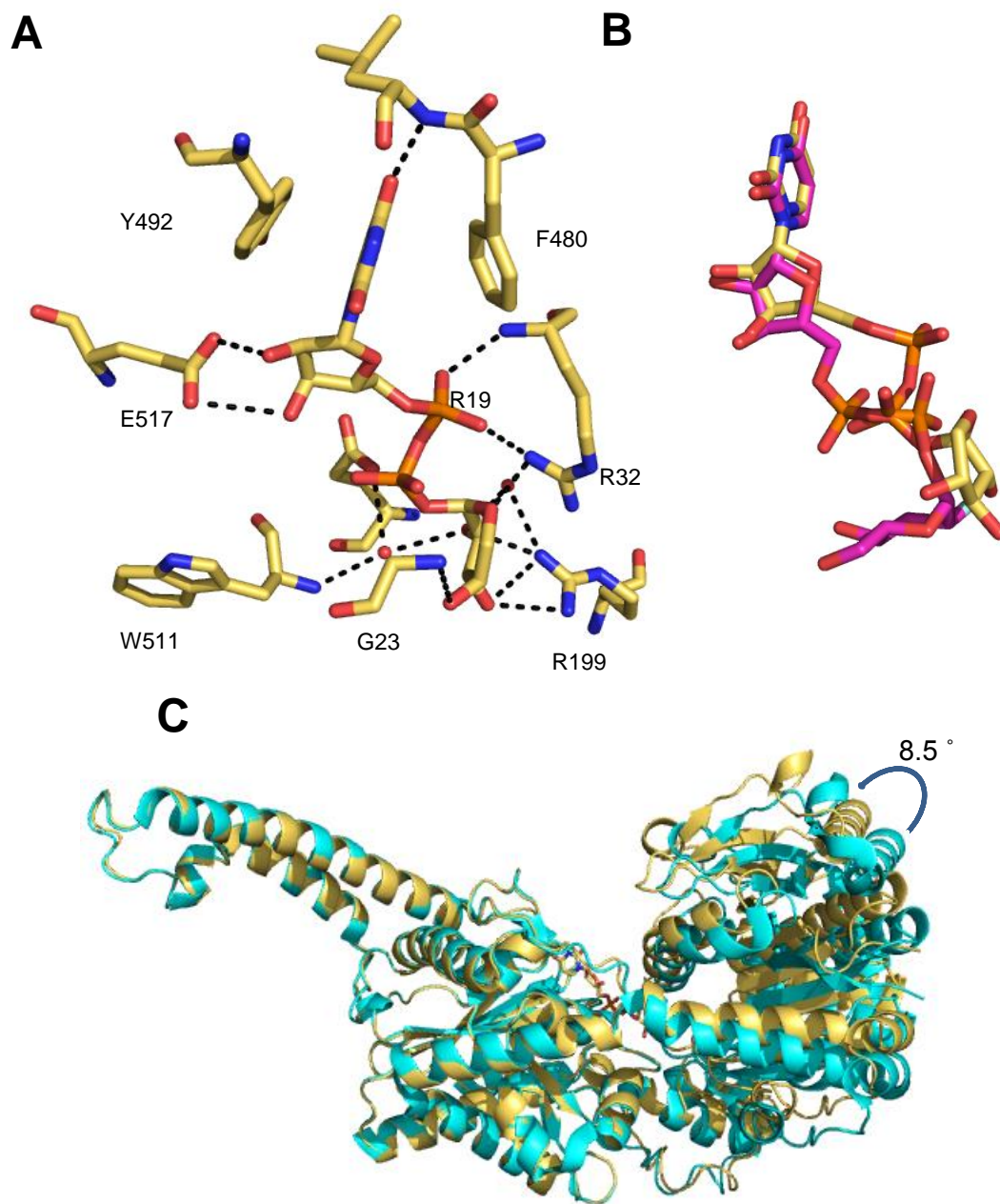


Figure 42. Subunit interactions made by UDP-xylose and the domain motions induced by it.

A. Stick representation of UDP-xylose and the surrounding amino acids with which it interacts. B. Superposition of UDP-xylose (gold) and UDP-FDG (magenta) as observed in the active site. C. Superposition of yGsy2 monomers containing UDP-xylose (shown in gold) and UDP (shown in cyan) in the active site. The two monomers were aligned using the entire C-terminal domain (299-600) using the program in CCP4.

DISCUSSION

Multimeric oligomerization and domain motions provide eukaryotic GS with multiple levels of regulation. Since yGsy2 shares many of the regulatory and catalytic mechanisms with its mammalian counterparts, the yeast enzyme has been extensively studied over the years. Despite a wealth of information on the kinetic and structural functioning of yGsy2, certain key questions remain unanswered. The crystal structures obtained from this work will shed light on the mechanism of substrate selection and regulated inhibition in yeast GS which can be extrapolated to other eukaryotic forms based on their sequence identity and structural homology.

1. Substrate selection in yeast Gsy2

Eukaryotic GS enzymes are grouped into the GT3 family of glucosyl-transferases because of their preference for UDP-glucose as its sugar donor substrate. In addition to UDP-glucose, a eukaryotic cell also contains significant amounts of other nucleotide sugars such as UDP-galactose, UDP-GlucNac, and UDP-xylose. Yeast, in particular, uses these sugar donors to synthesize its cell wall and chitin septum (94). The yeast cell wall is comprised of different sugar moieties like glucose, mannose, galactose and GlucNac while chitin is synthesized exclusively using GlucNac (85, 94). Unlike the yeast cell wall, the incorporation of other sugar residues could be detrimental to the structure of glycogen. Previous crystallographic studies have shown that long polymers of glucose are helical and the intra and inter-molecular hydrogen bonding between the hydroxyl groups of glucose stabilize its helical structure (19). Since glycogen

is made of many such chains of glucose, it is highly likely that glycogen shares similar structural properties. Erroneous addition of an alternative sugar residue that cannot adopt a similar hydrogen bonding pattern into a growing glycogen polymer could adversely affect the three dimensional structure of glycogen.

That GS needs to be very selective in choosing the UDP-sugar donors can be best explained if we look into the impact that different sugar molecules would have on the structure of glycogen and/or the process of catalysis.

Galactose incorporation into glycogen might not affect the glycogen structure significantly but it is highly likely to act as a chain terminator. Placing galactose on the non-reducing end of glycogen will leave an incoming acceptor with the 4'-OH group positioned axially where it will impact formation of the α -1,4-glycosidic bond either because it could not be properly activated for attack or the new stereochemistry of such a glucosyl-galactosyl bond would prevent the resulting acceptor from being productively positioned in the active site, in either case it would result in terminating glycogen chain extension.

On the other hand, GlucNac and xylose additions into glycogen is likely to affect its structure as both lack an OH group required to form the hydrogen bonds that stabilize the helical structure of glycogen. In addition to the detrimental effect xylose can have on the glycogen structure, it can also affect its branching properties. Every time xylose is added into glycogen, it loses a potential branch point. Excessive addition of xylose could result in a glycogen molecule with fewer branches and can lead to the formation of long insoluble polysaccharides.

To identify the mechanism by which yGsy2 discriminates substrates from non-substrates, we performed HPAEC analysis, X-ray crystallographic and kinetic studies on different UDP-sugar donors.

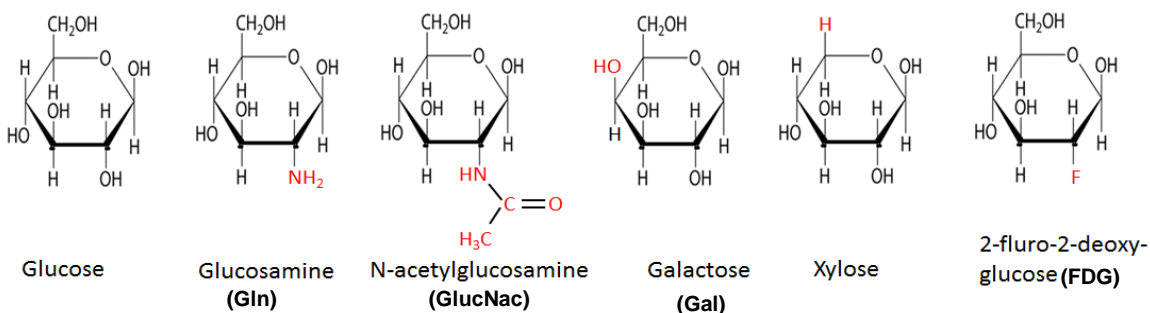


Figure 43. Analysis of glucose and its analogues as potential substrates.

Our HPAEC studies demonstrated that only UDP-glucose and UDP-glucosamine can be captured in the active site of yGsy2 and transferred to water. The ability to utilize UDP-glucosamine is not completely surprising because trace amounts of glucosamine have been detected in glycogen (12, 13). Most importantly, previous studies have also demonstrated that rats can incorporate ¹⁴C-labelled glucosamine into liver glycogen (76). Our crystallographic studies revealed that UDP-glucosamine adopts a “bent” conformation in the active site similar to UDP-glucose and in both cases, the N-terminal domain was completely closed towards the C-terminal domain. Chemically, glucosamine is very similar to glucose but has an amine group on its second carbon instead of the OH group (Figure 44). Both the 2'-amine and -hydroxyl groups are capable of acting as hydrogen bond donors. Therefore, glucosamine incorporation into glycogen is unlikely to affect the hydrogen bonding patterns of the glucose polymer to a large

extent. However, γ Gsy2 transfers UDP-glucosamine to water at a slower rate, compared to UDP-glucose, and animal studies demonstrated glucosamine was incorporated into glycogen at a rate one tenth that of glucose (76). The physical basis for the slower rates associated with glucosamine catalysis are less clear, since the active site hydrogen bonding patterns are very similar between the two sugars. However, if the amine group of glucosamine is charged in the active site, it is possible that stronger interactions with both Glu509 and the beta-phosphate of UDP could slow product release or the charge neutralization of the beta-phosphate could slow the deprotonation of the incoming 4'-OH of the acceptor molecule.

Unlike UDP-glucose and UDP-glucosamine, γ Gsy2 did not hydrolyze UDP-galactose, UDP-xylose or UDP-GlucNac nor do chemical analyses of glycogen detect significant incorporation of these sugars. X-ray crystallographic studies showed that these non-substrates adopted a "stretched" conformation within the active site of γ Gsy2 and the N-terminal domains did not close down and capture the nucleotide sugars for productive transfer.

A common feature of the non-productive complexes with the non-substrate sugars, were interactions between the sugars and Gly23. These interactions do not occur when glucose or glucosamine are productively bound because the main chain nitrogen of Gly23 interacts with the UDP pyrophosphate oxygens. Thus, the non-substrates prevent catalytic closure of the N-terminal domain by engaging Gly23 across the inter-domain cleft and preventing the N-terminal domain from closing further such that Gly23 can bind to the UDP moiety.

In addition to this, the non-substrates also lose interactions with one or more of the N-terminal domain amino-acid residues with which the substrates interact (Arg199, His193 and Asn269).

Galactose is a C-4 epimer of glucose (Figure 43). The chiral configuration of the 4'-OH group is switched between the two sugar molecules. The 4'-OH group of glucose lies in an equatorial position while in galactose, it is positioned axially (Figure 43). Because of the difference in stereochemistry of the two sugar molecules, the 4'-OH group of galactose loses two important hydrogen bonds that stabilize the "folded" conformation of UDP-glucose in the γ Gsy2 active site (Figure 44A). The inability of the 4'-OH to productively engage G512 and the alpha-phosphate of UDP results in the sugar adopting the stretched conformation in the active site of γ Gsy2 where it also fails to interact with residues His193 and Asn269 on the surface of the N-terminal domain across the catalytic cleft (Figure 44B) and instead forms interactions with Gly23, which blocks the ability of the domain cleft to close down upon the nucleotide sugar complex.

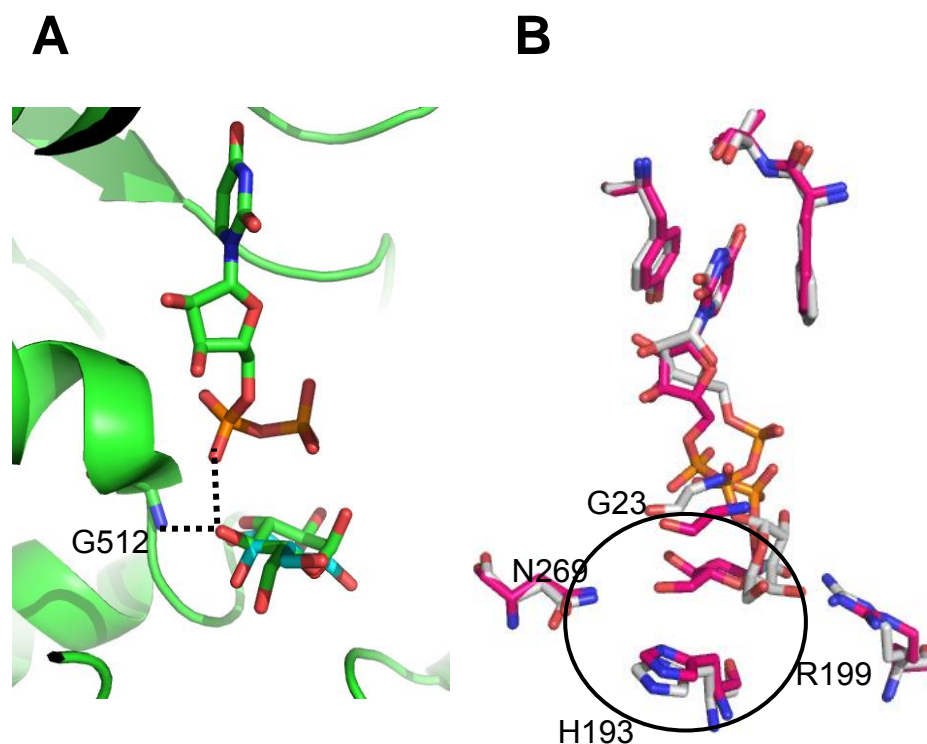


Figure 44. Structural basis for the observed UDP-galactose conformation in the active site of yGsy2.

A. Stick representation of galactose (cyan) superposed on glucose (green) in the UDP•G bound structure. The dotted lines represent the hydrogen bonds made by 4'-OH group of glucose with the peptide nitrogen of Gly512 and the α -phosphate oxygen of UDP. B. Stick representation of the superposed UDP-galactose (grey) and UDP-FDG (magenta) bound structures. The black circle shows the loss of interactions between galactose and the sidechains of His193 and Asn269. The entire C-terminal domain was used for aligning the two structures with the help of CCP4.

Similar to that observed for UDP-Gal, GlucNac (Figure 43) loses all of the interactions made by glucose with the N-terminal domain as a consequence of the 2'-N-acetylamine in its structure (Figure 45B). When the structure of GlucNac is superimposed on the glucose bound structure, the larger N-acetylamine group is likely to sterically hinder interactions with the sidechains of Arg199 and Arg320 if bound in a “bent” conformation (Figure 45A) and also possibly interfere with

acceptor binding. As a result, it adopts a more favorable linear/stretched conformation with minimal subunit interactions and domain motions.

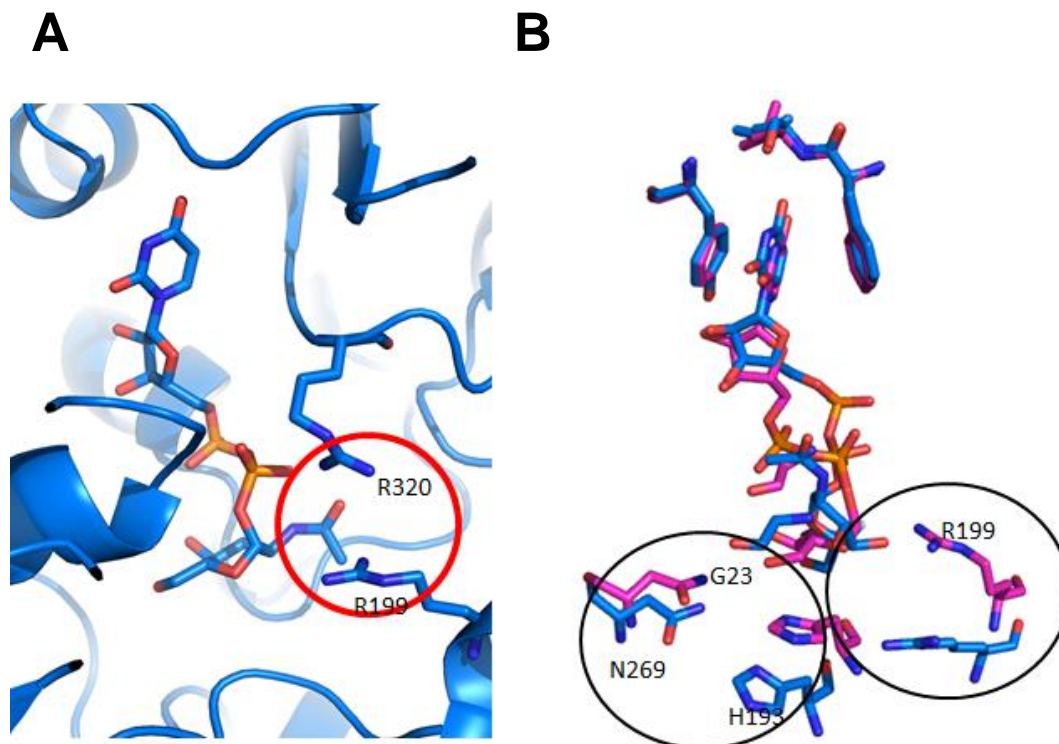


Figure 45. Structural basis for the observed UDP-GlucNac conformation in the active site of yGsy2.

A. Stick representation of UDP-GlucNac (blue) with a bent conformation placed in the active site of the UDP•G bound subunit. The red circle shows the steric hindrance created by the side chains of Arg199 and Arg320. B. Stick representation of the superposed UDP-GlucNac (blue) and UDP-FDG (magenta) bound structures. The black circles show the loss of interactions between GlucNac and the sidechains of His193, Arg199 and Asn269. The entire C-terminal domain was used for aligning the two structures with the help of CCP4.

Unlike galactose and GlucNac, where there are additions or epimeric changes to existing sugar ring substituents, xylose completely lacks the 6'-OH group (Figure 43). In glycogen synthase, the 6'-OH group of glucose hydrogen bonds with the side chains of His193 and Asn269 thereby helps to stabilize the

catalytic productive bent conformation of UDP•G (Figure 46A). Since xylose lacks the 6'-OH group, these interactions cannot be made and likely reduces the stability of the closed N-terminal domain conformation necessary for productive transfer of the sugar.

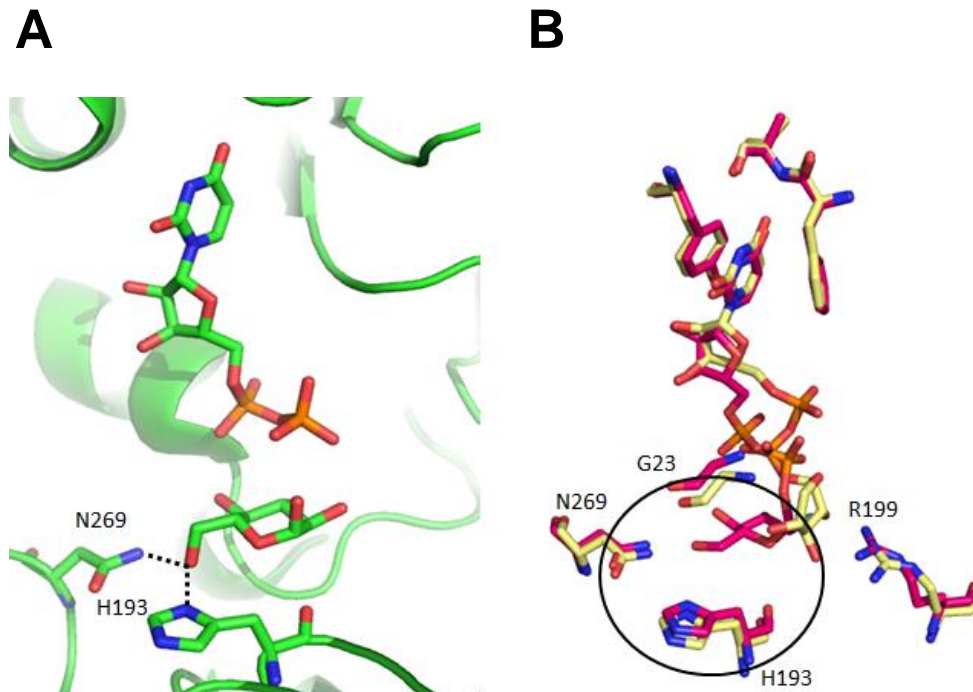


Figure 46. Structural basis for the observed UDP-Xylose conformation in the active site of yGsy2.

A. Stick representation of UDP•G (green) bound in the active site of yGsy2. The dotted lines represent the hydrogen bonding interactions made by the 6'-OH group of glucose with the sidechains of His193 and Asn269. B. Stick representation of the superposed UDP-xylose (gold) and UDP-FDG (magenta) bound structures. The black circle shows the loss of interactions between xylose and the sidechains of His193 and Asn269. The entire C-terminal domain was used for aligning the two structures with the help of CCP4.

2. Catalytic mechanism of yGsy2

Recent crystallographic studies on different retaining type glucosyl-transferases including yGsy2 had shown that these enzymes are likely to use an internal nucleophilic substitution (S_{Ni}) mechanism for catalysis (39, 82, 84). According to this mechanism, the β -phosphate of the UDP leaving group will likely deprotonate the 4'-OH group of the acceptor and the subsequent nucleophilic attack will likely occur from the same face as the departing leaving group. This mechanism also requires the formation of an oxo-carbenium ion-like intermediate state. So far, crystal structures are available only for the hydrolyzed form of UDP•G bound to the active site and only in the absence of an acceptor (82). We used UDP-FDG as a non-hydrolysable UDPG analogue in the hopes of capturing the donor in its non-hydrolyzed state. The fluorine at the 2'-position inductively destabilizes the oxo-carbenium ion-like transition state thereby slowing the reaction dramatically (95). It has been successfully used in several cases as a substitute for UDP-glucose and UDP-galactose (95, 96).

Our crystallization experiment captured UDP-FDG in its non-hydrolyzed form where it adopts a “bent” conformation similar to UDP•G (Figure 47A). UDP-FDG also made subunit interactions similar to UDP•G showing that the sugar donor is likely to exist in a single conformation before and after hydrolysis. The water molecule observed next to the 2-fluoro-2-deoxy-glucose (Figure 47A) is positioned in such a way that is likely to act as a nucleophile in the absence of the glycogen acceptor (Figure 47B). Based on these observations, we propose that the 4'-OH group of the incoming glycogen acceptor is likely to position itself

analogous to the water molecule and proceed with the catalytic reaction as described previously.

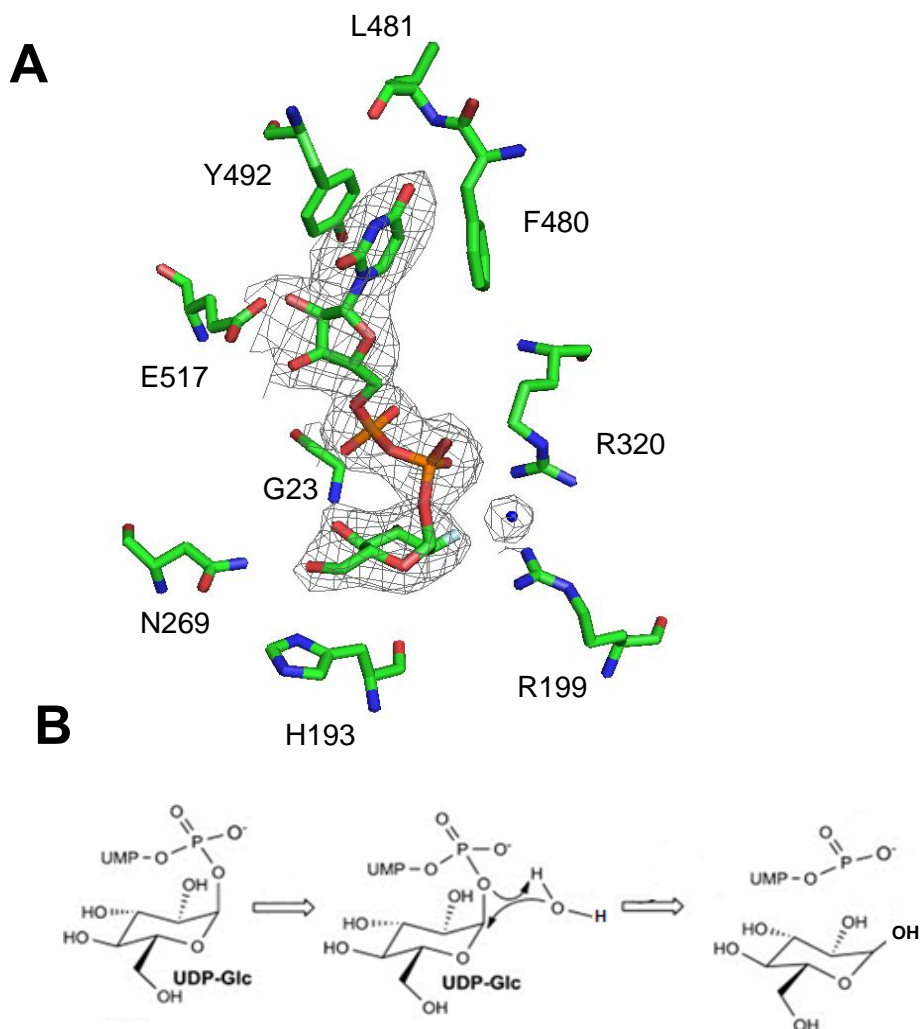


Figure 47. Molecular basis for UDP-glucose hydrolysis.

A. Stick representation of UDP-FDG bound in the active site of yGsy2. The map shown is the original $2F_o-F_c$ electron density map contoured at 1.0 standard deviation, prior to the addition of the ligand and water molecule. The water molecule (blue) is shown in sphere model. B. Proposed catalytic mechanism for UDP•G hydrolysis using water as an acceptor.

The crystal structure of *E. coli* GS was solved in both the apo-form (pdb code: 3D1J) and in the donor•acceptor complex form (pdb code: 2R4T) using ADP-glucose as the donor and HEPPSO as an acceptor analogue (39). It was found that in the donor•acceptor complex structure, the N-terminal domain was 14.5 ° more closed when compared to the apo structure thereby trapping the donor and acceptor in a catalytically competent conformation. It was also found in these structures that the acceptor analogue enters the catalytic cleft by binding along the surface of the N-terminal domain. Similarly, the N-terminal domain closure induced by UDP-glucose and UDP-glucosamine in yeast Gsy2 is likely to bring the 4'-OH group of the acceptor in proximity to the donor-sugar thereby trapping the enzyme in a catalytically competent donor•acceptor complex for efficient sugar transfer (Figure 48A, 48B).

The non-substrates on the other hand are not likely to achieve the catalytically active complex as they adopted a “stretched” conformation that restricted the N-terminal domain closure no greater than 8.5° (Figure 48A). In addition, the position of the C1-carbon and the diphosphate of UDP are less conducive for nucleophilic attack. Our kinetic studies also showed that unlike the substrates, the non-substrates were not capable of completely inhibiting the enzyme’s ability to use ¹⁴C-labelled UDP-glucose as the donor (Figure 30). Taken together, we propose that GS will selectively eliminate UDP-sugars other than UDP-glucose and UDP-glucosamine from remaining in the catalytic cleft as they cannot be catalytically captured in the active site without the ability to induce

active site closure. Without the ability to induce stable closure of the active site, productive transfer to the glycogen is also unlikely.

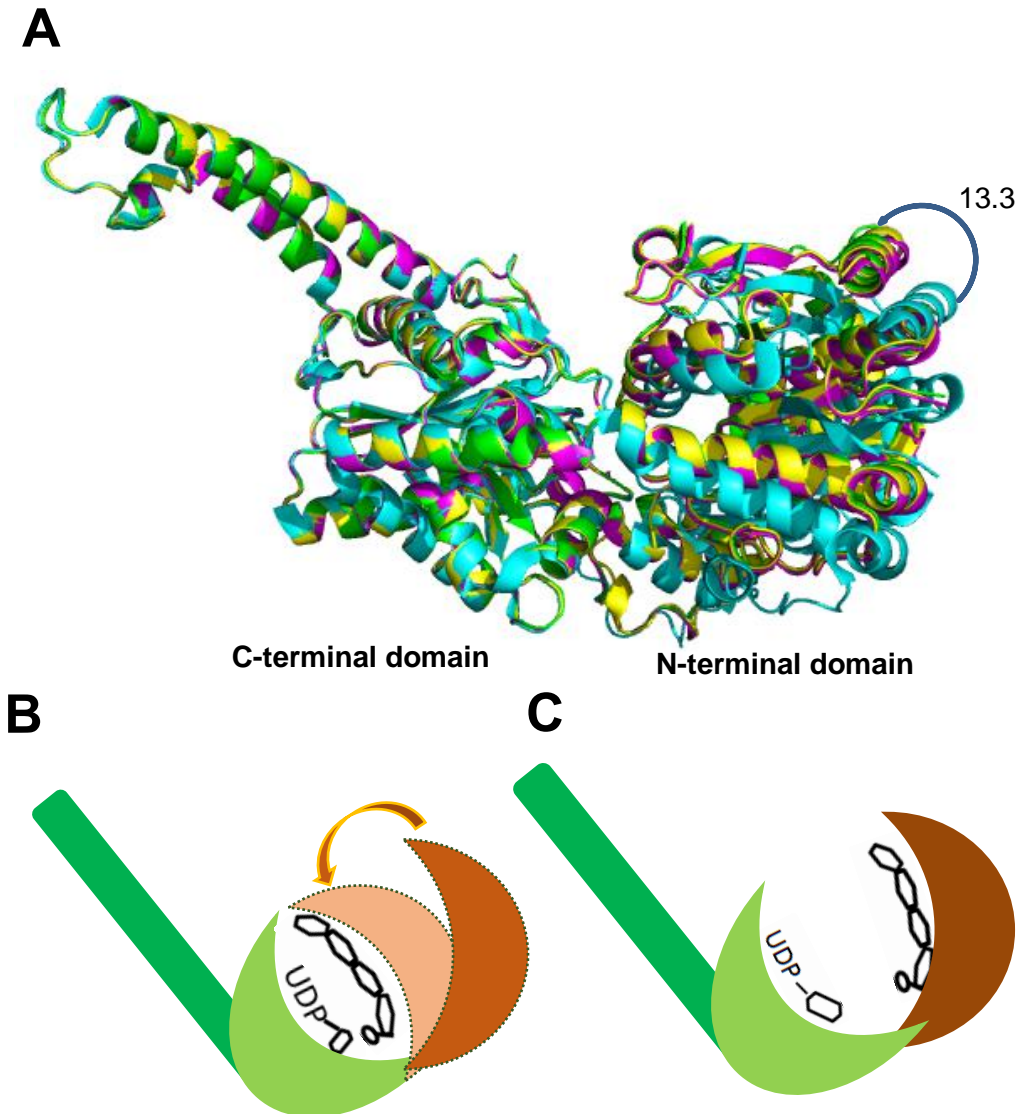


Figure 48. Catalytic role of N-terminal domain closure.

A. Ribbon representation of the superposed monomers of the G6P bound yGsy2 containing UDP•G (yellow), UDP•glucosamine (green), UDP-FDG (magenta) and UDP (cyan) in its active site. Hypothetical cartoon representation of the donor•acceptor complex when B. substrates and C. non-substrates are bound in the catalytic cleft of yGsy2. A monomer of yGsy2 is shown with the C-terminal domain colored green and the N-terminal domain in brown. The N-terminal domain motion following substrate binding on the C-terminal domain is indicated using an arrow.

3. Role of the regulatory helix in the inhibition of GS

Allosteric and covalent regulation of glycogen synthase allows the enzyme to exist in different conformational states. Based on the kinetic studies, a three state model was proposed for γ Gsy2 (71). Dephosphorylated γ Gsy2 in the absence of G-6-P had an intermediate basal activity state. Phosphorylation of the enzyme inhibits its activity to a low level - the tense state - while addition of G-6-P either to the phosphorylated form or to the dephosphorylated form activated the enzyme to a high activity, or relaxed state. Until this study, structural information was available only for the basal and activated states of the enzyme (63). The nature of the inhibited state was an extrapolation from the two known structural models that was supported by kinetic and mutational studies.

Phosphorylation of γ Gsy2 occurs outside of the catalytic core (residues 1-620) on the C-terminal tail. Among the three phosphorylation sites, T668 has the dominant inhibitory effect on the enzyme activity (63, 71). Substituting arginines 589 and 592 of γ Gsy2 with alanine resulted in an enzyme that had a basal activity similar to that of the T668 phosphorylated enzyme. However, this mutant enzyme still retains the ability to be fully activated by G-6-P. It is interesting that while the γ Gsy2-R589A/R592A enzyme can be fully activated by G-6-P, when phosphorylated on T668, the γ Gsy2-R589A/R592A enzyme can no longer be activated by G-6-P at concentrations up to 10 mM.

In order to gain insight into the structural characteristics of the inhibited state of GS, we solved the crystal structure of the low activity γ Gsy2-R589A/R592A enzyme as a surrogate for the phosphorylated form. Despite

sharing the overall oligomeric arrangement with the basal state enzyme, the double mutant demonstrated additional rotational closure of the N-terminal Rossmann-fold domain which was correlated with decreased separation between the regulatory helices of adjacent monomers. These motions created a more compact tetrameric interface than in the basal state. Based on these observations, we propose that the electrostatic repulsion between the opposing arginine residues on the regulatory helix keeps the enzyme “spring-loaded” in the basal state, so it can respond to regulatory inputs more effectively. Supporting this hypothesis is one of our basal state structures where an alternate conformation was observed when a sulfate induced a collapse of the regulatory helices and a more compact interface (pdb code: 3NCH) (Figure 49) (63). Thus, charge neutralization either by mutating the arginines to alanine or through anion binding (sulfate or phosphate) collapses the regulatory helices and induces further tightening of the inter-subunit interfaces.

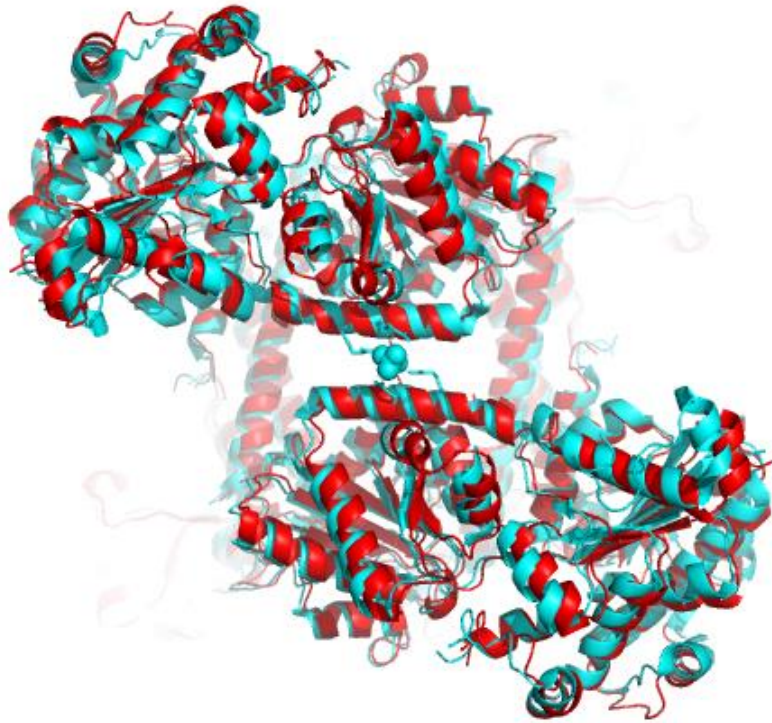


Figure 49. Role of the regulatory interface in inhibiting GS.

Ribbon representation of the superposed yGsy2-R589A/R592A (red) inhibited state structure and the basal state structure (cyan) with a sulfate bound on its regulatory interface. The arginines 589 and 592 are shown in stick model and the sulfate is shown in space filling atom model.

Unlike the yeast enzyme, *Caenorhabditis elegans* GS (*CeGS*) contains the N-terminal phosphorylation sites (sites 2 and 2a) similar to the mammalian enzymes but lacks the last two arginine residues of the arginine cluster. The structure of *CeGS* showed that the N-terminal phospho-sites are positioned in such a way that it can interact with the regulatory helix (Figure 50) (74). The phospho-sites, Ser12 and Thr19 are separated from the cis-regulatory helix by only 6-16 Å. The authors proposed that upon phosphorylation, the N-terminal tail can dissociate itself from its ordered position and can engage with the charged arginine residues. Based on these observations, we propose that the charged

arginine residues in the regulatory helices can act as finely tuned sensor that interacts directly with both G-6-P and the inhibitory phosphorylated residues thereby assisting the structural transition of the enzyme from one state to another.

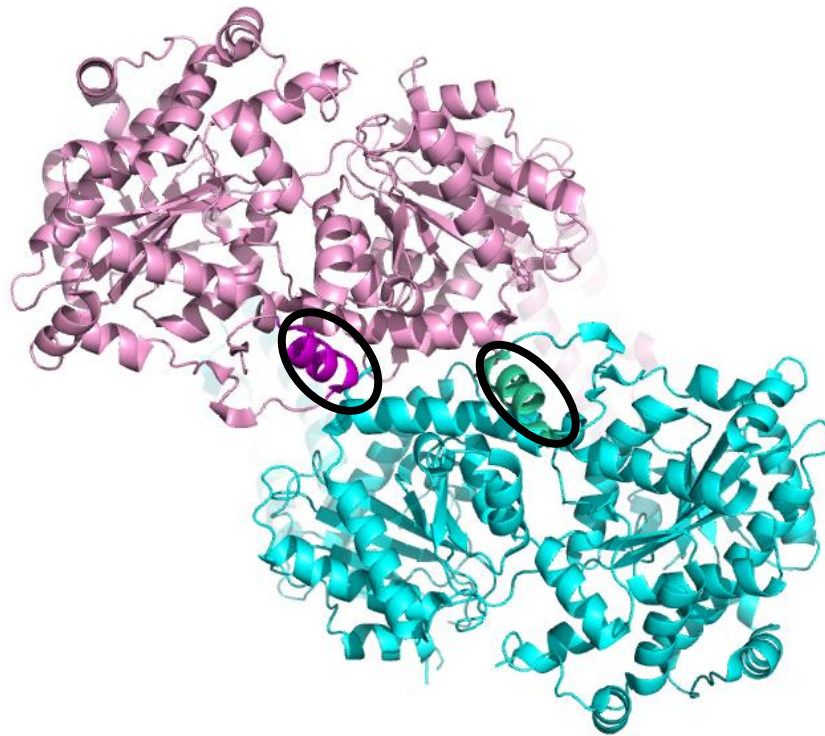


Figure 50. N-terminal phosphorylation.

Ribbon representation of a dimer of CeGS. Each monomer of the dimer is colored separately and the black circle highlights the helix carrying the N-terminal phosphorylation sites.

4. Redox regulation of yeast Gsy2

Reversible redox regulation of enzyme activity via cysteine residues is a commonly occurring natural phenomenon. Upon oxidation, cysteines form disulfide bonds which can be restored to their initial state by reduction. Several studies have taken advantage of this chemistry and engineered di-sulfide bridges to activate/inhibit an enzyme and also to achieve stable structural conformations for the purpose of crystallization (97, 98). We took a similar approach to test the hypothesis that Gsy2 activity is dependent on the dynamics and distance between the regulatory helices of adjacent monomers. Arginines 581 and 592 are positioned on either side of the regulatory helix facing each other across one of the molecular two-fold axes. Because of their proximity, formation of a disulfide bond between directly opposed cysteine residues across the subunit interface should bring the regulatory helices an additional 2 Å closer. An inter-subunit disulfide bond is consistent with the non-reducing SDS-PAGE as the non-reduced cysteine mutant migrated with a mass consistent with a tetramer. That the cysteines do not promote the formation of higher order aggregates is supported by gel-filtration analysis where only tetramers were observed. In addition, no other naturally positioned Cys residues in the GS subunits could form similarly inhibitory interactions with the newly introduced Cys residues at positions 581 and 592 (Figure 51).



Figure 51. Naturally occurring and rationally introduced cysteine residues in yGsy2.

Ribbon representation of a dimer of yGsy2 with the naturally occurring cysteine residues shown in magenta and the newly introduced cysteine mutants on the regulatory helix shown in yellow. The distance between the introduced cysteines and its closest naturally occurring cysteine residue is shown using dashed lines. The figure and the distance measurements were done using Pymol.

The structural constraint on the conformational dynamics of the interface created by these disulfide bridges should not only inhibit the enzyme but will also render it unable to respond to G-6-P activation. The conformational tension can be released by reduction of the disulfide bonds. Consistent with our hypothesis, in the absence of reducing agents, Gsy2-R589C/592C possessed very low activity and the addition of up to 80 mM G-6-P could not activate the enzyme. This result demonstrated that G-6-P mediated activation of Gsy2 requires structural adaptations which are prevented by the engineered covalent restraint. However, addition of reducing agents like TCEP, DTT and BME restored the activity of Gsy2-R581C/R592C in a dose-dependent manner and also rendered the enzyme sensitive to G-6-P. The resulting specific activity and activity ratio of the reduced enzyme is very similar to that of the control Gsy2-R581A/R592A mutant. It should also be noted that both Gsy2-R581A/R592A and Gsy2-R581C/R592C (in the presence of BME) had only ~ 50% of the wild type activity in the absence of G-6-P. This observation is consistent with the fact that both Arg589 and Arg592 are required to keep the enzyme in the basal state, so mutations of one to either alanine or cysteine leads to a partial reduction in basal activity level, by changing the energetics of the conformational set point.

Our kinetic data also suggest that both Gsy2-R589A/R592A and Gsy2-R581C/R592C (oxidized form) share similar kinetic properties with the phosphorylated Gsy2p. In all three cases, the largest changes were observed in the enzyme's V_{max} values with smaller changes to K_M values, showing that UDP-glucose binding is relatively unaffected either in the presence or absence of G-6-

P. Similar observations were made earlier where both G-6-P binding and phosphorylation changed the K_M values for glycogen without significantly changing the K_M values for UDP-glucose. These results are consistent with the available structure evidence where access to the UDP-glucose binding site is much less affected by the conformational transitions, whereas the surface of the N-terminal domain where the acceptor arm of glycogen is thought to bind is impacted by these same structural transitions.

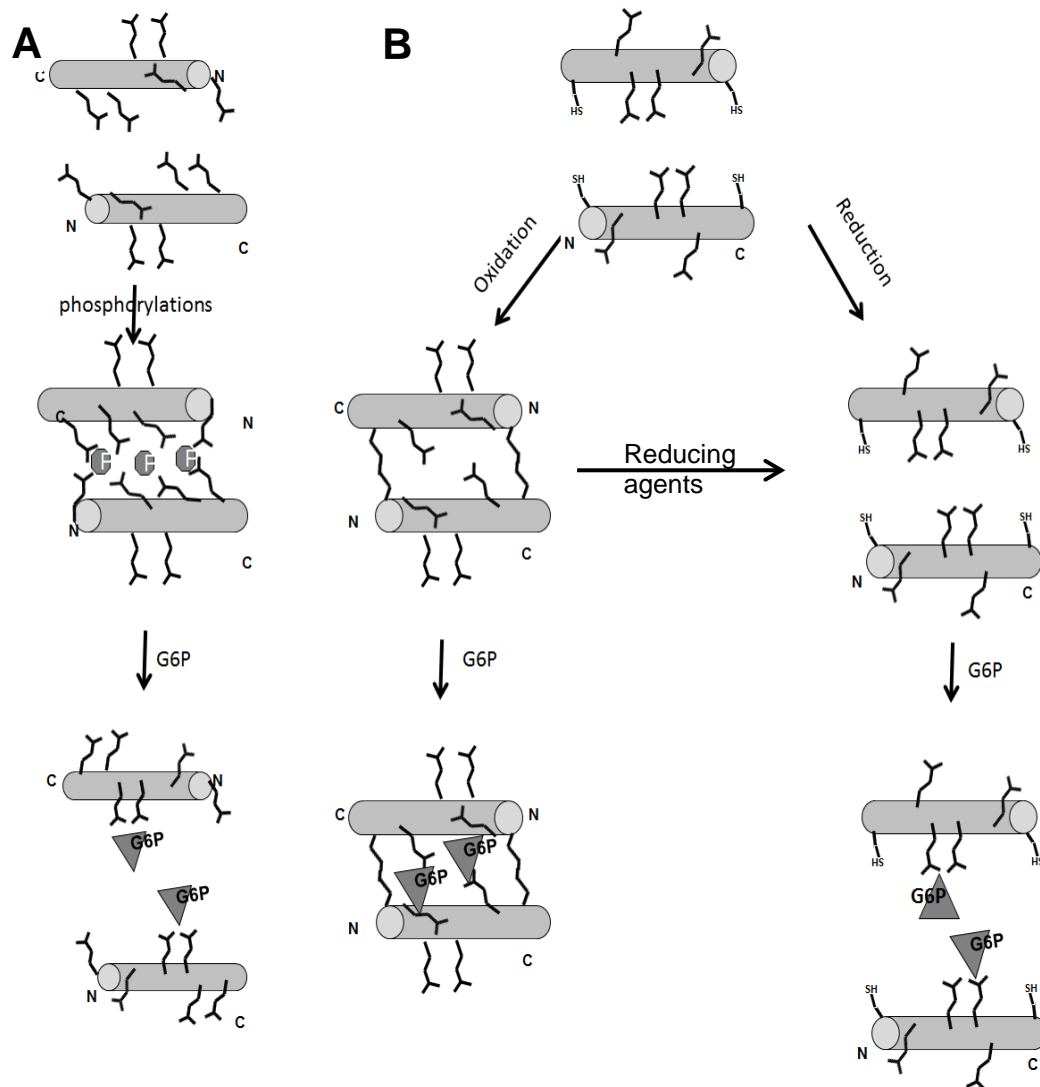


Figure 52. Structural model for the inhibited state and redox regulation of yeast GS.

A. Flowchart showing the changes in the regulatory interface of yGsy2 upon multisite phosphorylation and G-6-P binding. B. Flowchart representation of the redox regulation of yGsy2 using the regulatory interface as the basis for comparison. Here the first and last arginine residues of the arginine cluster are mutated to cysteine residues. The basal activity of the enzyme and its ability to respond to G-6-P depends on the oxidation status of the cysteine residues.

In summary, we propose that redox regulation of Gsy2 serves as a functional model for GS phosphorylations. In our model, the inhibitory phosphoserines/threonines on the C-terminal tail are expected to act as anchor points for a molecular strap by directly interacting with the arginine cluster across the subunit interface. This could promote regulatory helix closure similar to that observed in the Gsy2-R589A/R592A enzyme structure. Multiple phosphorylation sites in the higher eukaryotes on both the C- and N-terminal extensions will provide additional anchoring points for the termini by increasing the effective concentration of these inhibiting interactions and further pushing the conformational equilibrium toward the inhibited state (Figure 51). Our Gsy2-R581C/R592C mutant mimics this effect through disulfide bond formation (Figure 51). G-6-P binding on the regulatory helix can disrupt the inhibitory interactions created by closure of the interface and push the regulatory helices apart, but only if there is an additional repulsive force available in the form of arginines 589 and 592. In the absence of this opposing force or the presence of the disulfide bond in the oxidized form of the Gsy2-R581C/R592C enzyme, G-6-P cannot override the interactions that lock the tetrameric interface closed (Figure 51). These results suggest the key role played by Arg589 and Arg592 in establishing the reversibility of the inhibited state.

CONCLUSION

The crystal structure of yGsy2 in the low activity state and the G-6-P bound activated state structures in complex with different UDP-sugars provide the structural and molecular basis for inhibition and substrate selection in eukaryotic GS and also extend our knowledge of the multiple conformational states of GS. Interestingly, the N-terminal domain motion of yGsy2 plays an important role in both productive catalysis and the activity state of the enzyme. For productive catalysis, the N-terminal domain of yGsy2 has to be able to close down on the substrates toward the C-terminal domain by ~13 degrees so that it can achieve the catalytically competent donor•acceptor complex. When bound to G-6-P, the tetrameric interface of the enzyme is “open” such that the N-terminal domain is free from interactions with the C-terminal domain. Under such circumstances, the subunits carrying the “productively bound” sugar donors in its active site can completely close the N-terminal domain toward the bound nucleotide sugar thereby bringing the acceptor chain in proximity to accept the sugar donor. However, when the enzyme is inhibited, the subunit contacts between the N-terminal domains and helices 15 and 16 in the opposing C-terminal domain act as a wall that prevents domain closure by more than ~6 degrees. Thus, it is not possible for the inhibited state enzyme to fully capture a catalytically competent complex between an acceptor and donor substrate without reorganization of the tetrameric interface. The rate at which the reorganization of the tetrameric interface occurs in the inhibited state is likely to be much slower when compared to the activated state enzyme. To conclude, we

propose that binding of G6P pushes the conformational equilibrium toward a state that is more easily accessible for catalytic capture of the substrates, while phosphorylation or other actions that compact the tetrameric interface, push the conformational equilibrium toward states that cannot easily transition to productively capture the substrates for the transfer reaction.

REFERENCES

1. Roach PJ, Depaoli-Roach AA, Hurley TD, & Tagliabracci VS (2012) Glycogen and its metabolism: some new developments and old themes. *The Biochemical journal* 441(3):763-787.
2. Ball S, *et al.* (1996) From glycogen to amylopectin: a model for the biogenesis of the plant starch granule. *Cell* 86(3):349-352.
3. Zeeman SC, Smith SM, & Smith AM (2007) The diurnal metabolism of leaf starch. *The Biochemical journal* 401(1):13-28.
4. Roach PJ (2002) Glycogen and its metabolism. *Current molecular medicine* 2(2):101-120.
5. Applegarth DA, Toone JR, & Lowry RB (2000) Incidence of inborn errors of metabolism in British Columbia, 1969-1996. *Pediatrics* 105(1):e10.
6. Ausems MG, *et al.* (1999) Glycogen storage disease type II: birth prevalence agrees with predicted genotype frequency. *Community genetics* 2(2-3):91-96.
7. Ausems MG, *et al.* (1999) Frequency of glycogen storage disease type II in The Netherlands: implications for diagnosis and genetic counselling. *European journal of human genetics : EJHG* 7(6):713-716.
8. Goldsmith E, Sprang S, & Fletterick R (1982) Structure of maltoheptaose by difference Fourier methods and a model for glycogen. *Journal of molecular biology* 156(2):411-427.
9. Melendez R, Melendez-Hevia E, & Cascante M (1997) How did glycogen structure evolve to satisfy the requirement for rapid mobilization of glucose? A problem of physical constraints in structure building. *Journal of molecular evolution* 45(4):446-455.
10. Gunja-Smith Z, Marshall JJ, Mercier C, Smith EE, & Whelan WJ (1970) A revision of the Meyer-Bernfeld model of glycogen and amylopectin. *FEBS letters* 12(2):101-104.
11. Geddes R, Harvey JD, & Wills PR (1977) The molecular size and shape of liver glycogen. *The Biochemical journal* 163(2):201-209.
12. Kirkman BR & Whelan WJ (1986) Glucosamine is a normal component of liver glycogen. *FEBS letters* 194(1):6-11.
13. Kirkman BR, Whelan WJ, & Bailey JM (1989) The distribution of glucosamine in mammalian glycogen from different species, organs and tissues. *BioFactors* 2(2):123-126.
14. Fontana JD (1980) The presence of phosphate in glycogen. *FEBS letters* 109(1):85-92.
15. Lomako J, Lomako WM, Kirkman BR, & Whelan WJ (1994) The role of phosphate in muscle glycogen. *BioFactors* 4(3-4):167-171.
16. Lomako J, Lomako WM, Whelan WJ, & Marchase RB (1993) Glycogen contains phosphodiester groups that can be introduced by UDPglucose: glycogen glucose 1-phosphotransferase. *FEBS letters* 329(3):263-267.
17. Gentry MS, Dixon JE, & Worby CA (2009) Lafora disease: insights into neurodegeneration from plant metabolism. *Trends in biochemical sciences* 34(12):628-639.

18. Tagliabracci VS, *et al.* (2011) Phosphate incorporation during glycogen synthesis and Lafora disease. *Cell metabolism* 13(3):274-282.
19. Gessler K, *et al.* (1999) V-Amylose at atomic resolution: X-ray structure of a cycloamylose with 26 glucose residues (cyclomaltohexacosose). *Proceedings of the National Academy of Sciences of the United States of America* 96(8):4246-4251.
20. Wilson JE (2003) Isozymes of mammalian hexokinase: structure, subcellular localization and metabolic function. *The Journal of experimental biology* 206(Pt 12):2049-2057.
21. Dashty M (2013) A quick look at biochemistry: carbohydrate metabolism. *Clinical biochemistry* 46(15):1339-1352.
22. Lomako J, Lomako WM, & Whelan WJ (1988) A self-glucosylating protein is the primer for rabbit muscle glycogen biosynthesis. *FASEB journal : official publication of the Federation of American Societies for Experimental Biology* 2(15):3097-3103.
23. Gibson WB, Illingsworth B, & Brown DH (1971) Studies of glycogen branching enzyme. Preparation and properties of -1,4-glucan- -1,4-glucan 6-glycosyltransferase and its action on the characteristic polysaccharide of the liver of children with Type IV glycogen storage disease. *Biochemistry* 10(23):4253-4262.
24. Titani K, *et al.* (1978) Sequence of the carboxyl-terminal 492 residues of rabbit muscle glycogen phosphorylase including the pyridoxal 5'-phosphate binding site. *Biochemistry* 17(26):5680-5693.
25. Nakayama A, Yamamoto K, & Tabata S (2001) Identification of the catalytic residues of bifunctional glycogen debranching enzyme. *The Journal of biological chemistry* 276(31):28824-28828.
26. Wisselaar HA, Kroos MA, Hermans MM, van Beeumen J, & Reuser AJ (1993) Structural and functional changes of lysosomal acid alpha-glucosidase during intracellular transport and maturation. *The Journal of biological chemistry* 268(3):2223-2231.
27. Swanson MA (1950) Phosphatases of liver. I. Glucose-6-phosphatase. *The Journal of biological chemistry* 184(2):647-659.
28. Beck-Nielsen H (2012) The role of glycogen synthase in the development of hyperglycemia in type 2 diabetes: 'To store or not to store glucose, that's the question'. *Diabetes/metabolism research and reviews* 28(8):635-644.
29. Dent P, *et al.* (1990) The molecular mechanism by which insulin stimulates glycogen synthesis in mammalian skeletal muscle. *Nature* 348(6299):302-308.
30. Siddle K (2011) Signalling by insulin and IGF receptors: supporting acts and new players. *Journal of molecular endocrinology* 47(1):R1-10.
31. Brady MJ & Saltiel AR (2001) The role of protein phosphatase-1 in insulin action. *Recent progress in hormone research* 56:157-173.
32. Cohen P & Cohen PT (1989) Protein phosphatases come of age. *The Journal of biological chemistry* 264(36):21435-21438.

33. Berthet J, Rall TW, & Sutherland EW (1957) The relationship of epinephrine and glucagon to liver phosphorylase. IV. Effect of epinephrine and glucagon on the reactivation of phosphorylase in liver homogenates. *The Journal of biological chemistry* 224(1):463-475.
34. Berchtold MW, Brinkmeier H, & Muntener M (2000) Calcium ion in skeletal muscle: its crucial role for muscle function, plasticity, and disease. *Physiological reviews* 80(3):1215-1265.
35. Wilson WA, *et al.* (2010) Regulation of glycogen metabolism in yeast and bacteria. *FEMS microbiology reviews* 34(6):952-985.
36. Francois J & Parrou JL (2001) Reserve carbohydrates metabolism in the yeast *Saccharomyces cerevisiae*. *FEMS microbiology reviews* 25(1):125-145.
37. Farkas I, Hardy TA, DePaoli-Roach AA, & Roach PJ (1990) Isolation of the GSY1 gene encoding yeast glycogen synthase and evidence for the existence of a second gene. *The Journal of biological chemistry* 265(34):20879-20886.
38. Wilson WA, Wang Z, & Roach PJ (2005) Regulation of yeast glycogen phosphorylase by the cyclin-dependent protein kinase Pho85p. *Biochemical and biophysical research communications* 329(1):161-167.
39. Sheng F, Jia X, Yep A, Preiss J, & Geiger JH (2009) The crystal structures of the open and catalytically competent closed conformation of *Escherichia coli* glycogen synthase. *The Journal of biological chemistry* 284(26):17796-17807.
40. Weinstein DA, Correia CE, Saunders AC, & Wolfsdorf JI (2006) Hepatic glycogen synthase deficiency: an infrequently recognized cause of ketotic hypoglycemia. *Molecular genetics and metabolism* 87(4):284-288.
41. Orho M, *et al.* (1998) Mutations in the liver glycogen synthase gene in children with hypoglycemia due to glycogen storage disease type 0. *The Journal of clinical investigation* 102(3):507-515.
42. Irimia JM, *et al.* (2010) Impaired glucose tolerance and predisposition to the fasted state in liver glycogen synthase knock-out mice. *The Journal of biological chemistry* 285(17):12851-12861.
43. Kollberg G, *et al.* (2007) Cardiomyopathy and exercise intolerance in muscle glycogen storage disease 0. *The New England journal of medicine* 357(15):1507-1514.
44. McCue ME, Valberg SJ, Lucio M, & Mickelson JR (2008) Glycogen synthase 1 (GYS1) mutation in diverse breeds with polysaccharide storage myopathy. *Journal of veterinary internal medicine* 22(5):1228-1233.
45. McCue ME, *et al.* (2008) Glycogen synthase (GYS1) mutation causes a novel skeletal muscle glycogenosis. *Genomics* 91(5):458-466.
46. Maile CA, *et al.* (2016) A highly prevalent equine glycogen storage disease is explained by constitutive activation of a mutant glycogen synthase. *Biochimica et biophysica acta*.
47. Skurat AV, Wang Y, & Roach PJ (1994) Rabbit skeletal muscle glycogen synthase expressed in COS cells. Identification of regulatory

- phosphorylation sites. *The Journal of biological chemistry* 269(41):25534-25542.
48. Skurat AV, Dietrich AD, & Roach PJ (2000) Glycogen synthase sensitivity to insulin and glucose-6-phosphate is mediated by both NH₂- and COOH-terminal phosphorylation sites. *Diabetes* 49(7):1096-1100.
 49. Stralfors P, Hiraga A, & Cohen P (1985) The protein phosphatases involved in cellular regulation. Purification and characterisation of the glycogen-bound form of protein phosphatase-1 from rabbit skeletal muscle. *European journal of biochemistry* 149(2):295-303.
 50. Doherty MJ, Moorhead G, Morrice N, Cohen P, & Cohen PT (1995) Amino acid sequence and expression of the hepatic glycogen-binding (GL)-subunit of protein phosphatase-1. *FEBS letters* 375(3):294-298.
 51. Doherty MJ, Young PR, & Cohen PT (1996) Amino acid sequence of a novel protein phosphatase 1 binding protein (R5) which is related to the liver- and muscle-specific glycogen binding subunits of protein phosphatase 1. *FEBS letters* 399(3):339-343.
 52. Tang PM, Bondor JA, Swiderek KM, & DePaoli-Roach AA (1991) Molecular cloning and expression of the regulatory (RG1) subunit of the glycogen-associated protein phosphatase. *The Journal of biological chemistry* 266(24):15782-15789.
 53. Moorhead G, MacKintosh C, Morrice N, & Cohen P (1995) Purification of the hepatic glycogen-associated form of protein phosphatase-1 by microcystin-Sepharose affinity chromatography. *FEBS letters* 362(2):101-105.
 54. Printen JA, Brady MJ, & Saltiel AR (1997) PTG, a protein phosphatase 1-binding protein with a role in glycogen metabolism. *Science* 275(5305):1475-1478.
 55. Suzuki Y, *et al.* (2001) Insulin control of glycogen metabolism in knockout mice lacking the muscle-specific protein phosphatase PP1G/RGL. *Molecular and cellular biology* 21(8):2683-2694.
 56. Doherty MJ, Cadefau J, Stalmans W, Bollen M, & Cohen PT (1998) Loss of the hepatic glycogen-binding subunit (GL) of protein phosphatase 1 underlies deficient glycogen synthesis in insulin-dependent diabetic rats and in adrenalectomized starved rats. *The Biochemical journal* 333 (Pt 2):253-257.
 57. Hojlund K, *et al.* (2009) Dysregulation of glycogen synthase COOH- and NH₂-terminal phosphorylation by insulin in obesity and type 2 diabetes mellitus. *The Journal of clinical endocrinology and metabolism* 94(11):4547-4556.
 58. Parker GJ, Lund KC, Taylor RP, & McClain DA (2003) Insulin resistance of glycogen synthase mediated by o-linked N-acetylglucosamine. *The Journal of biological chemistry* 278(12):10022-10027.
 59. Zhao S, *et al.* (2010) Regulation of cellular metabolism by protein lysine acetylation. *Science* 327(5968):1000-1004.

60. Hardy TA & Roach PJ (1993) Control of yeast glycogen synthase-2 by COOH-terminal phosphorylation. *The Journal of biological chemistry* 268(32):23799-23805.
61. Huang D, Farkas I, & Roach PJ (1996) Pho85p, a cyclin-dependent protein kinase, and the Snf1p protein kinase act antagonistically to control glycogen accumulation in *Saccharomyces cerevisiae*. *Molecular and cellular biology* 16(8):4357-4365.
62. Huang D, *et al.* (1998) Cyclin partners determine Pho85 protein kinase substrate specificity in vitro and in vivo: control of glycogen biosynthesis by Pcl8 and Pcl10. *Molecular and cellular biology* 18(6):3289-3299.
63. Baskaran S, Roach PJ, DePaoli-Roach AA, & Hurley TD (2010) Structural basis for glucose-6-phosphate activation of glycogen synthase. *Proceedings of the National Academy of Sciences of the United States of America* 107(41):17563-17568.
64. Francois JM, *et al.* (1992) GAC1 may encode a regulatory subunit for protein phosphatase type 1 in *Saccharomyces cerevisiae*. *The EMBO journal* 11(1):87-96.
65. Stuart JS, Frederick DL, Varner CM, & Tatchell K (1994) The mutant type 1 protein phosphatase encoded by *glc7-1* from *Saccharomyces cerevisiae* fails to interact productively with the GAC1-encoded regulatory subunit. *Molecular and cellular biology* 14(2):896-905.
66. Ferrer JC, Baque S, & Guinovart JJ (1997) Muscle glycogen synthase translocates from the cell nucleus to the cytosol in response to glucose. *FEBS letters* 415(3):249-252.
67. Ou H, Yan L, Osmanovic S, Greenberg CC, & Brady MJ (2005) Spatial reorganization of glycogen synthase upon activation in 3T3-L1 adipocytes. *Endocrinology* 146(1):494-502.
68. Prats C, *et al.* (2005) Phosphorylation-dependent translocation of glycogen synthase to a novel structure during glycogen resynthesis. *The Journal of biological chemistry* 280(24):23165-23172.
69. Fernandez-Novell JM, Arino J, Vilaro S, & Guinovart JJ (1992) Glucose induces the translocation and the aggregation of glycogen synthase in rat hepatocytes. *The Biochemical journal* 281 (Pt 2):443-448.
70. Wilson WA, Boyer MP, Davis KD, Burke M, & Roach PJ (2010) The subcellular localization of yeast glycogen synthase is dependent upon glycogen content. *Canadian journal of microbiology* 56(5):408-420.
71. Pederson BA, Cheng C, Wilson WA, & Roach PJ (2000) Regulation of glycogen synthase. Identification of residues involved in regulation by the allosteric ligand glucose-6-P and by phosphorylation. *The Journal of biological chemistry* 275(36):27753-27761.
72. Roach PJ, Takeda Y, & Larner J (1976) Rabbit skeletal muscle glycogen synthase. I. Relationship between phosphorylation state and kinetic properties. *The Journal of biological chemistry* 251(7):1913-1919.
73. Hanashiro I & Roach PJ (2002) Mutations of muscle glycogen synthase that disable activation by glucose 6-phosphate. *Archives of biochemistry and biophysics* 397(2):286-292.

74. Zeqiraj E, *et al.* (2014) Structural basis for the recruitment of glycogen synthase by glycogenin. *Proceedings of the National Academy of Sciences of the United States of America* 111(28):E2831-2840.
75. Coutinho PM, Deleury E, Davies GJ, & Henrissat B (2003) An evolving hierarchical family classification for glycosyltransferases. *Journal of molecular biology* 328(2):307-317.
76. Tarentino AL & Maley F (1976) Direct evidence that D-galactosamine incorporation into glycogen occurs via UDP-glucosamine. *FEBS letters* 69(1):175-178.
77. Maley F, McGarrahan JF, & DelGiaccio R (1966) Galactosamine: a precursor of glycogen glucosamine. *Biochemical and biophysical research communications* 23(1):85-91.
78. Maley F, Tarentino AL, McGarrahan JF, & Delgiaccio R (1968) The metabolism of d-galactosamine and N-acetyl-d-galactosamine in rat liver. *The Biochemical journal* 107(5):637-644.
79. Meezan E, *et al.* (1994) Xylosyl transfer to an endogenous renal acceptor. Characteristics of the reaction and properties of the product. *The Journal of biological chemistry* 269(15):11503-11508.
80. Meszaros K, Antoni F, Mandl J, Hrabak A, & Garzo T (1974) Effects of D-galactosamine on nucleotide metabolism and on microsomal membranes in mouse liver. *FEBS letters* 44(2):141-145.
81. Roden L, Ananth S, Campbell P, Manzella S, & Meezan E (1994) Xylosyl transfer to an endogenous renal acceptor. Purification of the transferase and the acceptor and their identification as glycogenin. *The Journal of biological chemistry* 269(15):11509-11513.
82. Chikwana VM, *et al.* (2013) Structural basis for 2'-phosphate incorporation into glycogen by glycogen synthase. *Proceedings of the National Academy of Sciences of the United States of America* 110(52):20976-20981.
83. Hurley TD, Stout S, Miner E, Zhou J, & Roach PJ (2005) Requirements for catalysis in mammalian glycogenin. *The Journal of biological chemistry* 280(25):23892-23899.
84. Chaikuad A, *et al.* (2011) Conformational plasticity of glycogenin and its maltosaccharide substrate during glycogen biogenesis. *Proceedings of the National Academy of Sciences of the United States of America* 108(52):21028-21033.
85. Cabib E, Roh DH, Schmidt M, Crotti LB, & Varma A (2001) The yeast cell wall and septum as paradigms of cell growth and morphogenesis. *The Journal of biological chemistry* 276(23):19679-19682.
86. Tomiya N, Ailor E, Lawrence SM, Betenbaugh MJ, & Lee YC (2001) Determination of nucleotides and sugar nucleotides involved in protein glycosylation by high-performance anion-exchange chromatography: sugar nucleotide contents in cultured insect cells and mammalian cells. *Analytical biochemistry* 293(1):129-137.
87. Minor W, Cymborowski M, Otwinowski Z, & Chruszcz M (2006) HKL-3000: the integration of data reduction and structure solution--from diffraction

- images to an initial model in minutes. *Acta crystallographica. Section D, Biological crystallography* 62(Pt 8):859-866.
88. Bunkoczi G, *et al.* (2013) Phaser.MRage: automated molecular replacement. *Acta crystallographica. Section D, Biological crystallography* 69(Pt 11):2276-2286.
 89. Collaborative Computational Project (1994) The CCP4 suite: programs for protein crystallography. *Acta Crystallogr D Biol Crystallogr.* 50:760-763.
 90. Murshudov GN, *et al.* (2011) REFMAC5 for the refinement of macromolecular crystal structures. *Acta crystallographica. Section D, Biological crystallography* 67(Pt 4):355-367.
 91. Emsley P & Cowtan K (2004) Coot: model-building tools for molecular graphics. *Acta crystallographica. Section D, Biological crystallography* 60(Pt 12 Pt 1):2126-2132.
 92. Qi G, Lee R, & Hayward S (2005) A comprehensive and non-redundant database of protein domain movements. *Bioinformatics* 21(12):2832-2838.
 93. Thomas JA, Schlender KK, & Lerner J (1968) A rapid filter paper assay for UDPglucose-glycogen glucosyltransferase, including an improved biosynthesis of UDP-14C-glucose. *Analytical biochemistry* 25(1):486-499.
 94. Cabib E & Arroyo J (2013) How carbohydrates sculpt cells: chemical control of morphogenesis in the yeast cell wall. *Nature reviews. Microbiology* 11(9):648-655.
 95. Gibson RP, Tarling CA, Roberts S, Withers SG, & Davies GJ (2004) The donor subsite of trehalose-6-phosphate synthase: binary complexes with UDP-glucose and UDP-2-deoxy-2-fluoro-glucose at 2 Å resolution. *The Journal of biological chemistry* 279(3):1950-1955.
 96. Persson K, *et al.* (2001) Crystal structure of the retaining galactosyltransferase LgtC from *Neisseria meningitidis* in complex with donor and acceptor sugar analogs. *Nature structural biology* 8(2):166-175.
 97. Jung SH, Pastan I, & Lee B (1994) Design of interchain disulfide bonds in the framework region of the Fv fragment of the monoclonal antibody B3. *Proteins* 19(1):35-47.
 98. Kawate T & Gouaux E (2003) Arresting and releasing Staphylococcal alpha-hemolysin at intermediate stages of pore formation by engineered disulfide bonds. *Protein science : a publication of the Protein Society* 12(5):997-1006.

Curriculum Vitae
Krishna Kishore Mahalingan

Education

2017 Indiana University, IN
 PhD in Biochemistry and Molecular Biology

2011 Anna University, Chennai, India
 B. Tech Pharmaceutical Biotechnology

Research Experience

8/11-8/16 PhD student, Prof. Thomas D. Hurley
 Department of Biochemistry and
 Molecular Biology Indiana University
 School of Medicine.

1/11-5/11 International Exchange Student
 Prof. Manjunatha R. Kini, Department of Biological
 Sciences National Univeristy of Singapore.

4/10-6/10 Summer Research Fellow, Indian Academy of Science,
 Prof. H S Savithri, Department of
 Biochemistry, Indian Institute of
 Science, Bengaluru.

Professional Membership

American Crystallographic Association
Graduate student member, American Chemical Society.

Awards and Honors

International exchange student - National University of Singapore.
Summer Research fellow, Indian Academy of Sciences.

Presentations

'Structural basis for the inhibition of yeast Glycogen synthase'. Biochemistry Research Day, 2015 Department of Biochemistry, Indiana University School of Medicine.

Redox switch for the inhibited state of yeast glycogen synthase mimics regulation by phosphorylation. IUPUI Research day, 2016.

Research Skills

Biochemistry, Molecular biology, Enzyme kinetics, X-ray crystallography, High throughput screening of small molecule libraries, Drug discovery, Optimization of lead compounds.

Publications

1. Buchman CD*, **Mahalingan KK***, Hurley TD. Discovery of a series of aromatic lactones as ALDH1/2-directed inhibitors. Chem Biol Interact. 2015 Jun 5; 234: 38-44. Epub 2015 Jan 29.
2. Contreras CJ, Segvich DM, **Mahalingan K**, Chikwana VM, Kirley TL, Hurley TD, DePaoli-Roach AA, Roach PJ. Incorporation of phosphate into glycogen by glycogen synthase. Arch Biochem Biophys. 2016 May 1; 597: 21-9. Epub 2016 Mar 29. PMID: 27036853.
3. Charlotte A Maile; Janne R Hingst; **Krishna K Mahalingan**; Andrias O O'Reilly; Mark E Cleasby; James R Mickelson; Molly E McCue; Shea M Anderson; Thomas D Hurley; Jorgen F Wojtaszewski; Richard Piercy. A highly prevalent equine glycogen storage disease is explained by constitutive activation of a mutant glycogen synthase. Biochimica et Biophysica Acta, 2016, Aug 31 PMID: 27592162.
4. **Mahalingan KK**, Baskaran S, Depaoli-Roach AA, Roach PJ, Hurley TD Redox switch for the inhibited state of yeast glycogen synthase mimics regulation by phosphorylation. Biochemistry, 2016, December 20 PMID: 27935293.
5. **Mahalingan KK**, Chikwana VM, Depaoli-Roach AA, Roach PJ, Hurley TD. Structural basis for substrate selection in yeast Glycogen synthase. (Manuscript in preparation).
6. Morgan CA, **Mahalingan KK**, Terence Kirley, Hurley TD, Depaoli-Roach

AA, Roach PJ. Identification and Characterization of Glycogen Synthase inhibitors. (Manuscript in preparation).